Efficient Control Mechanism Using Data Centers and Electric Vehicles for Grid Frequency Support

*A **Thesis***

submitted in partial fulfillment of the requirements for the award of degree of

Doctor of Philosophy

Submitted by

Kuljeet Kaur

(Registration No.: 901503010)

Under the guidance of

Dr. Neeraj Kumar

Associate Professor

Computer Science and Engineering Department

Dr. Mukesh Singh

Associate Professor

Electrical and Instrumentation Engineering Department

Computer Science and Engineering Department

Thapar Institute of Engineering and Technology (Deemed to be University),

Patiala -147004, India

September 2018

Contents

List of Figures

List of Tables

List of Algorithms

Certificate

I hereby certify that the work which is being presented in this thesis entitled "**Efficient Control Mechanism Using Data Centers and Electric Vehicles for Grid Frequency Support**", in partial fulfillment of the requirement for the award of degree of "Doctor of Philosophy" submitted in Computer Science and Engineering Department of Thapar Institute of Engineering and Technology, Patiala, is an authentic record of my own work carried out under the supervision of *Dr. Neeraj Kumar* and *Dr. Mukesh Singh*.

The matter presented in this thesis has not been submitted for the award of any other degree of this or any other university.

(Kuljeet Kaur)

Regn. No. 901503010

This is to certify that the above statement made by the candidate is correct and true to the best of my knowledge.

(Dr. Neeraj Kumar)
Associate Professor
CSED

(Dr. Mukesh Singh)
Associate Professor
EIED

Acknowledgements

First and foremost, I would like to thank God Almighty for giving me the strength, knowledge, ability and opportunity to undertake this research study and to persevere and complete it satisfactorily. Without his blessings, this achievement would not have been possible.

I would also like to acknowledge my indebtedness and render my warmest thanks to my supervisors, *Dr. Neeraj Kumar* and *Dr. Mukesh Singh*, who made this work possible. Their friendly guidance and expert advice have been invaluable throughout all stages of the work.

I express my sincere gratitude to *Dr. Maninder Singh*, Head, Computer Science and Engineering Department for his extended valuable suggestions which have contributed greatly to the improvement of the thesis. The thesis has also benefited from comments and suggestions made by the Ph.D. committee members *Dr. A. K. Verma*, *Dr. Jhilik Bhattacharya* and *Dr. Ravi Kumar*. I take this opportunity to thank them. I would also like to thank the Director of the institute, *Prof. Prakash Gopalan* for his continuous support and encouragement.

The greatest indirect contribution to this work has been from my mother, *Mrs. Jasmeet Kaur* and my father, *Capt. Manjeet Singh*; who made me capable of reaching this point of life, and for giving me their kind support and love. Special thanks to my husband, *Mr. Sahil Garg*, for his continuous support and understanding. I also want to thank my father-in-law, mother-in-law, as well as my brother and sister-in-laws, for their constant encouragement.

I would like to thank *Tata Consultancy Services (TCS)* for providing me financial support in form of research fellowship to complete my Doctoral studies.

Patiala

September, 2018

(Kuljeet Kaur)

Abstract

Frequency regulation is one of the most crucial ancillary services that strives to maintain the demand and supply balance in Smart Grid (SG) setup. The deviations in grid's frequency can be managed efficiently by adjusting the generation of the supply side against the energy consumption of the demand side. Traditionally, frequency support is provided using conventional generators but their usage leads to the emission of harmful gases, degraded heat rate, and associated wear and tear. Nevertheless, several efforts have been made to manage frequency deviations using flywheels, battery energy storage systems, commercial buildings, and renewable energy resources. However, these agents too have their associated shortcomings such as-heavy installation and maintenance cost; and intermittency issues. Hence, modern frequency regulation agents are required which can strive the delicate balance between demand and supply. Towards this end, the modern Data centers (DCs) and Electric Vehicles (EVs) have emerged as promising solutions for instantaneous frequency support. This can be attributed to their rapid proliferation in the global market accompanied with the large charging and discharging capacities of EVs' batteries. According to a recent survey, the energy consumption of future transportation sector is expected to increase manifold with the penetration of 400 billion EVs by 2020. On the similar lines, the overall energy consumption of cloud DCs is expected to increase up to 1963.74 TWh by 2020. Hence, it is essential to manage their energy interactions with the grid in accordance with the grid's frequency; else risk a blackout. Thus, in this thesis, innovative power management schemes have been proposed to leverage the distributed participation of EVs and DCs for grid frequency support. Consequently, four different schemes have been designed based on hierarchical control structure in lieu of grid frequency stabilization.

The first scheme regulates the charging and discharging rates of fleet of EVs for managing grid frequency fluctuations. It achieves the same using a Colored Petri Net-based controller;

wherein EVs work in close coordination with aggregators and charging stations. The second scheme presents an *"Aggregator-based Hierarchical Control Mechanism"* for frequency regulation using fleet of EVs. In the proposed solution, EVs' scheduling problem has been formulated to provide optimal frequency support, while satisfying EVs' energy demands under battery degradation constraints. This multi-objective primal problem under multiple constraints is solved using an approximation approach. The third scheme also leverages the joint participation of EVs for grid frequency regulation. Additionally, it generates an optimal schedule for EV's charging and discharging needs with reduced battery degradation and maximal revenue generating opportunities. The overall problem has been formulated as a *"Mixed Integer Linear Programming (MILP)"* problem and is solved using Mosek solver. Widely accepted *Pennsylvania-New Jersey-Maryland (PJM)* and *ERCOT* regulation datasets are used to perform extensive simulations. The results obtained demonstrate that the proposed schemes achieve better performance in comparison with the other competing existing schemes.

Last but not the least, the fourth scheme presents an *"Energy-aware and SLA-driven (En-SLA) job scheduling framework"* for cloud DC equipped with MapReduce. The primary aim of the proposed framework is to explore task-to-slot mapping problem as a special case of energy-aware scheduling in deadline-constrained scenario. The designed problem is a complex multi-objective problem comprising of different constraints and is solved using heuristic approaches. The efficacy of the proposed scheme has been validated using real-time data traces acquired from *OpenCloud*. The results obtained prove the efficacy of the proposed scheme in comparison to the other schemes under different workload scenarios.

List of Publications

Refereed Journals

1) Kuljeet Kaur, Neeraj Kumar, and Mukesh Singh, "Coordinated Power Control of Electric Vehicles for Grid Frequency Support: MILP-based Hierarchical Control Design," ***IEEE Transactions on Smart Grid***, 2018, doi:10.1109/TSG.2018.2825322. *(IEEE, SCI/SCIE) (IF: 6.645)*

2) Kuljeet Kaur, Mukesh Singh, and Neeraj Kumar, "Multiobjective Optimization for Frequency Support Using Electric Vehicles: An Aggregator-Based Hierarchical Control Mechanism," ***IEEE Systems Journal***, 2017, doi:10.1109/JSYST.2017.2771948. *(IEEE, SCI/SCIE) (IF: 3.882)*

3) Kuljeet Kaur, Rubi Rana, Neeraj Kumar, Mukesh Singh, and S. Mishra, "A Colored Petri Net Based Frequency Support Scheme Using Fleet of Electric Vehicles in Smart Grid Environment," ***IEEE Transactions on Power Systems***, vol. 31, no. 6, pp. 4638-4649, 2016. *(IEEE, SCI/SCIE) (IF: 5.680)*

4) Kuljeet Kaur, Neeraj Kumar, and Mukesh Singh, "En-SLA: Energy-aware and SLA-driven MapReduce Job Scheduling Framework for Cloud Data Centers," ***Transactions on Parallel and Distributed Systems***, Under Revision, *(IEEE, SCI/SCIE) (IF: 4.181)*

International Conferences

5) Kuljeet Kaur, Mukesh Singh, and Neeraj Kumar, "Fleet of Electric Vehicles for Frequency Support in Smart Grid using 2-layer Hierarchical Control Mechanism," in ***2016 IEEE Power and Energy Society General Meeting (PESGM)***, 17-21 July 2016, Boston, MA, USA, pp. 1-5.

Chapter 1

Introduction

Electricity has become a necessity of modern life and its demand is increasing at a rapid pace. Due to this, the conventional electric grids suffer from frequent power failures and load shedding issues. Thus, their up-gradation is essential to cater these issues and restore grid's stability. Smart Grid (SG) is one such initiative that aims to modernize the conventional grids and make them more efficient, reliable and secure [1–4]. These grids are often referred by different terminologies such as-*"Intelligent networks", "the energy Internet", and "wise wires"*; but the term SG dominates them all [5]. Additionally, many definitions and descriptions of SG are available in the literature. According to [5], SG is defined as follows: *"Smart grids are the set of technology, regulation and market rules that are required to address the challenges to which the electricity network is exposed in a cost-effective way."* Gharavi and Ghafurian [6] define SG as follows: *"The Smart Grid can be defined as an electric system that uses information, two-way, cyber-secure communication technologies, and computational intelligence in an integrated fashion across electricity generation, transmission, substations, distribution and consumption to achieve a system that is clean, safe, secure, reliable, resilient, efficient, and sustainable"*.A typical architecture of SG is depicted in Fig. 1.1.

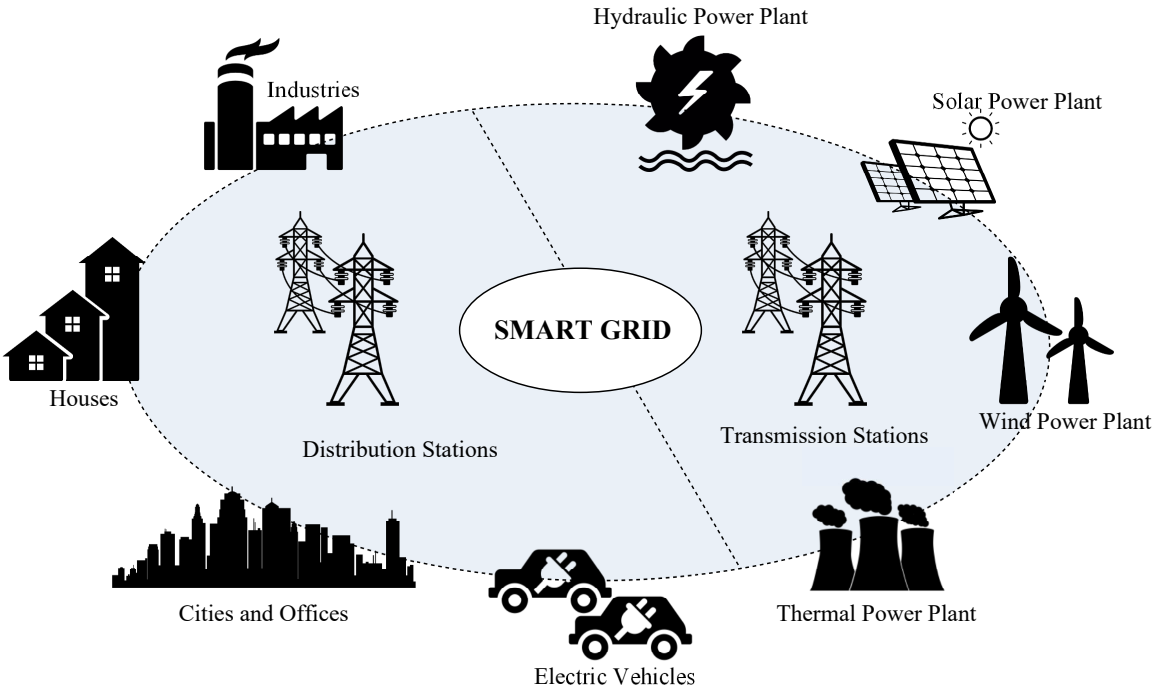

Figure 1.1: Typical architecture of Smart Grid.

In other words, SGs are essentially equipped with two-way links for both communication and flow of power across all the phases namely-electricity generation, transmission and distribution [7]. These grids are often termed as *"Intelligent Grids"* as they can adapt to optimal power consumption or dispatch in accordance with their underlying artificial intelligence techniques, commonly referred to as Energy Management System (EMS) [7]. Moreover, SGs can be accommodated with renewable energy sources (RESs) such as-wind and solar energy to cater consumers' growing power demands [8–11]. Integration of RES with SG not only brings environment benefits in terms of reducing the emission of the Green House Gases (GHG), but also reduces the dependence on non-RES for electricity generation [12]. Unfortunately, these energy sources are characterized by a lot of intermittency issues and may lead to problems such as-frequency and voltage fluctuations [13].

Frequency fluctuations arise due to supply and demand variations. These fluctuations if not regulated properly, may cause series of undesirable events leading to blackouts, severe

brownouts and voltage deviations. Hence, frequency can be visualized as the *"Pulse of SG"* which helps in estimation of its overall health conditions. The delicate balance between demand and supply is generally ensured by the Transmission System Operators (TSO) by leveraging various ancillary services namely-frequency support and voltage regulation. These services help to ensure grid's overall stability and security. One of the most common means to re-balance demand-supply imbalances by TSOs is generally attained using frequency regulation services [14]. The said services can either be provisioned at the generation side or the demand side using different ways as elaborated below.

Fluctuations in grid's operating frequency are usually regulated at two levels, *i.e.*, *primary* and *secondary* (their detailed information is provided in the subsequent sections) [15]. These can further be achieved using two strategies namely-regulation up and regulation down. The former is provided during deficit power supply and high demand. On the other hand, the latter is provided when, supply is more than the demand. Normally, regulation up and down services are achieved by employing generators, which increase or decrease their production in order to match with the demand [15]. However, use of such reserves is accompanied with heavy prices ranging from degraded heat rates to generator's wear and tear. Moreover, their persistent use leads to loss of opportunity to generate more power that would otherwise be available in the electrical market. Additionally, several other inherent issues are also associated with them such as-prolonged start-up time, emission of harmful gases and inadequate response towards huge frequency deviations. Due to these reasons, it becomes difficult to manage frequency variations instantly and effectively. Apart from this, various other non-traditional means have also been explored in the literature. Amongst these, the most sought after frequency support agents are flywheels [16], Battery Energy Storage Systems (BESSs) [17], and commercial buildings [18].

The major drawback associated with flywheels and BESS is that, they impose severe

economic burden in terms of installation and maintenance costs. On the other hand, the commercial buildings consume a lot of time in sustaining their HVAC systems. They fail to provide fast regulation services. Hence, the use of non-traditional reserves may not prove to be beneficial for the service providers in the long run for maintaining grid frequency. Thus, an alternative mechanism is required that not only supports frequency but is economical also.

Thus, this thesis proposes a radically new approach for re-balancing frequency deviations at grid level. The proposed approach leverages the new reserves, *i.e.*, Data Centers (DCs) and Electric Vehicles (EVs) for managing grid frequency fluctuations. Their respective qualities in terms of load management, availability, bi-directional energy exchanges and fast response time make them ideal candidates for grid frequency support [14, 19]. Thus, this thesis presents effective control strategies based on hierarchical structures using both the entities, *i.e.*, DCs and EVs. These entities work in accordance with grid's frequency without effecting either their individual system-specific or user-specific priorities.

But, before we dig deeper into the proposed schemes, the following section presents the preliminary details about grid frequency, associated control services and the need for managing grid's frequency at its nominal value. Along with this, the current status of DCs and EVs in the global market is also explored herewith.

1.1 Background Details about Frequency Control Services

Ancillary services refer to specialized services which support continuous and reliable operations across the electric grid. Among these services, grid frequency stabilization is one of the most prominent which is often referred as the "*pulse of grid*". Even minor frequency deviations can disrupt the normal functionality of the grid. In technical terms, grid frequency refers to the oscillations of the Alternating Current (AC) that is transmitted from the generation unit

to distribution unit. Frequency is expressed in number of cycles per second or Hertz (Hz) and is a variable entity that varies with respect to the demand-supply imbalances.

In case the demand increases, the grid frequency tends to reduce; whereas it increases if the supply exceeds the demand. In both the scenarios, the frequency deviations need to be balanced by either pumping extra energy to the grid or by reducing the overall generation as depicted in Fig. 1.2. The demand-supply balance and its effect on frequency has been depicted in the Fig. 1.3.

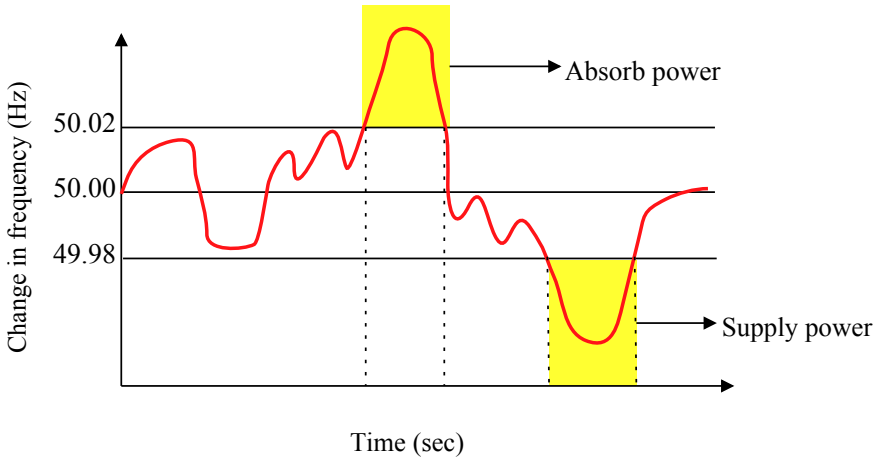

Figure 1.2: Frequency deviations v/s time.

Frequency fluctuations are generally managed through two techniques namely, primary and secondary. These techniques are generally referred to as regulation or control services and their detailed description is mentioned below.

1.1.1 Primary frequency control

It is one of the most commonly used frequency control technique and referred to as "frequency response". It is generally achieved by adjusting the generator's response with respect to frequency deviations. This is mandatory provision for all generators with the installed capacity of more than 50MW with droop of 3-5%. This technique is the faster than the

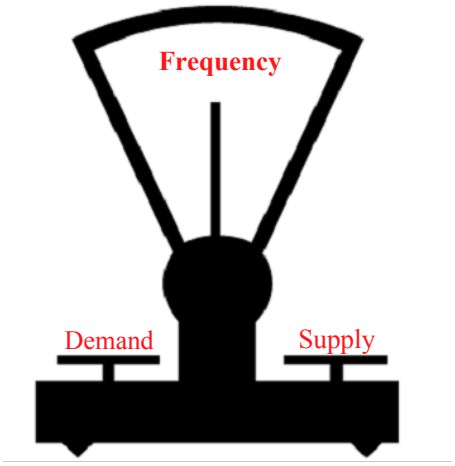

Figure 1.3: Demand-supply balance with respect to grid frequency.

secondary frequency control and provides regulation within a few seconds (5-10 seconds). However, the major disadvantage of this approach is that it can stabilize frequency fluctuations only upto to some extent and cannot exactly return the frequency to its nominal value.

1.1.2 Secondary frequency control

This control technique involves coordinated signals to bring the grid frequency back to its nominal value. However, this technique is much slower than the primary frequency control technique and takes minutes time-scale for regulating frequency imbalances (10s to 15 minutes). These are often utilized once the primary frequency control resources fail to provide the necessary regulation. These regulations are achieved by controllable load shedding and energy interchanges. Essentially, these regulation services are considered as commercial services unlike mandatory provisions of primary frequency control.

The next section reviews the major grid disturbances witnessed by the world and that were triggered due to skewed frequency deviations. In addition to this, it also highlights the current and expected developments of DCs and EVs both nationally and internationally.

1.2 Need for Grid Frequency Support

One of the most severe and largest power disturbances at international level was reported in Europe on 4^{th} November, 2006 [20]. This power outage plunged nearly 15 million Europeans households into darkness. The blackout initially originated from north-west Germany and affected Paris including 15 French regions. The effects of the severity of this blackout were also experienced in Austria, Belgium, Italy, and Spain. Another critical power outage issue was reported in Indonesia (Java Island) on 18^{th} August, 2005. Due to this outage, power failures were observed in Java and Bali. This in turn led to cascading failures, which eventually caused the shutdown of several units of Paiton and Suralaya plants in east and west Java respectively.

Power deficient India has had a history of the frequency deviations ranging from 48Hz to 52Hz [21]. The most significant amongst these was on 30^{th} and 31^{st} July, 2012. During this time, the nation witnessed major grid imbalance. It was caused due to skewed imbalance between demand and supply on the northern, western, and eastern regional grids. Thus, affecting almost 21 states and 3 union territories which caused more than $ 2 billion losses [22]. Apart from this, India has also witnessed another blackout on 2^{nd} January, 2001 [23]. This blackout was caused due to collapsing of Northern regional grid due to technical failure. The impacts of this massive failures were seen across various sectors including hospitals, telecoms, railway stations, airports, traffic light systems etc.

These power failures are just an indication that supply and demand gaps are observed across the nations, and is a growing global concern. Although many nations are striving for RESs to manage the growing energy demands but frequency fluctuations arise in power systems from time to time. In such scenarios, electric grids must keep frequency at nominal value else risk a blackout. Hence, this thesis explores the potential use of DCs and EVs to restore the grid frequency deviations while satisfying the end user's requirements.

1.3 Current Status of Data Centers

Technological advancements and the need to process real-time information seamlessly, have paved way to the Cloud Computing platform. It is the next most vital paradigm shift for Information and Communications Technology (ICT). It comprises of several DCs that form its structural and operational foundation. However, its rapid popularity has brought numerous challenges for the research community. The major challenge being that of energy-efficiency. According to [24], the cloud computing infrastructure alone consumed approximately 623 TWh of energy in 2007. Furthermore, this consumption is expected to rise as high as 1963.74 TWh by 2020 [24].

India being the nerve center for all IT activities and the outsourcing activities demands high data storage; resulting in phenomenal growth of DCs in India. With the increase in business volume, the Indian DC service market is poised to witness rapid growth in the coming years. The total DC capacity in India grew from 2.3 million square feet in the year 2008 to 5.1 million square feet by the year 2012; and an overall growth of almost 31% from 2007 to 2012 [25]. The storage demand which has increased from one petabyte in 2001 to almost 34 petabytes in 2007 [25], has resulted in existing DC capabilities being fully utilized and, consequently, the need has arisen to build more capacity.

It is evident from the above figures, that DCs would be the major consumers of electricity in the near future. These bulk consumers of electricity are liable to cause significant electricity disturbances in the near future; if left unmanaged. Hence, an efficient control mechanism focusing on scheduling of jobs at DC level is of paramount importance. Keeping these issues in mind, this thesis exploits DCs for overall frequency support at the grid level while catering the energy requirements and required QoS parameters.

1.4 Current Status of Electric Vehicles

Increasing fuel prices and concerns about environmental degradation, have led to the electrification of vehicles and emergence of Vehicle-to-Grid (V2G) [26]. EVs are being widely accepted due to their greater fuel efficiency, and ability to discharge and charge to and fro the grid using V2G, whenever required. The global penetration of EVs has reached over 2 million in accordance with the International Energy Agency's report released in the year 2017 [27], and the count is expected to further expedite with an astonishing speed. For instance, according to a recent report, it is expected that there would about 400 million EVs on roads worldwide by 2020 [28]. However, the literature suggests the current number of EVs available on road is still not significant to cause prominent changes in the SG setup, but their massive deployment in the near future can lead to significant harmful effects on the grid [12]. Thus, their huge infiltration, would surely require a dedicated scheduling policy such that the grid is left undisturbed at all times. For instance, in Greater Britain alone by the year 2030, an additional power demand of almost 8 GW would arise (that too during the peak hours) if EV's energy demands are not controlled in an efficient manner [29]. On the contrary, if this wide-scale penetration of EVs can be controlled in an effective manner; then these distributed energy sources have the potential to benefit the power systems operations at large, i.e., improve grid's overall stability, provide ancillary support and fast active power [30].

Further, the electric automobile industry in India is expected to flourish at a rapid pace in the coming years. The initiatives of Government of India in nation-wide adoption of EVs is also remarkable in this regard. Recently, Union Minister of Heavy Industries and Public Enterprises has launched a scheme for Faster Adoption and Manufacturing of (Hybrid &) EVs in India, better known as FAME India [31]. Consequently, National Electric Mobility Plan (NEMMP-2020) has been released in 2013, which targets to release 6-7 million EVs per year by 2020.

With such a huge proliferation of EVs around the world, the proposed theme of this thesis seems to be more feasible and appropriate for grid frequency support in the near future. Other prominent reasons to use EVs for frequency support are illustrated as under. EVs' aggregated regulation capacities are helpful in tracking the regulation signal. Additionally, EVs' owners can attain financial benefits by selling their regulation capacities to the independent system operator [32]. According to [33], an EV can earn almost $1.71 on daily basis for participating in the regulation market. Consequently, in Germany, the average revenue earned by an EV in one month varies between 30€ to 80€. Thus, it can been inferred from these facts that V2G energy trading would become a common phenomenon in the near future; wherein bidirectional V2G support is an inevitable outcome [34, 35].

1.5 Summary

With the growing concerns of environmental degradation and prominent hike in fuel prices, the penetration of EVs and DCs in the market is inevitable. However, with their increasing penetration, the demands on the existing grids would further increase manifold. Thus, there arises an essential need to develop a comprehensive solution to cater the growing demands while maintaining SG's stability in terms of frequency fluctuations. Currently, frequency regulation services are supplied through partially loaded power plants. However, with the growing global environmental concerns, such inefficient and environmentally hazardous means of regulation are difficult to ignore. Thus, an alternative mechanism is need of the present era which would not only be at par with the current regulation techniques in terms of efficiency but is environmentally friendly too. Integration of DCs and EVs into the electricity market as primary source of frequency support, can act as a catalyst for provisioning fast and reliable frequency support to the electrical power system network. Moreover, with higher

penetration of EVs and DCs, this approach seams to be more feasible and reliable in the times to come.

1.6 Thesis Organization

The thesis has been organized and the objectives stated above have been accomplished as per the following chapters.

Chapter 1: Introduction: This chapter provides an overview of grid frequency regulation and the need for its regulation. Additionally, it also highlights the different techniques for bringing the grid's frequency to its nominal value.

Chapter 2: Literature Review: This chapter provides a comprehensive literature review pertaining to the current state-of-the-art techniques used for frequency support. This is in line with the techniques and strategies proposed by the researchers for implementing control mechanism specifically for EVs and DCs for grid frequency support.

Chapter 3: Frequency Support Scheme using Fleet of Electric Vehicles: This chapter proposes a novel scheme for efficient frequency support in SG environment by utilizing fleet of EVs; in which EVs act as controllable loads and work in close coordination with aggregators and charging stations.

Chapter 4: Frequency Support using Electric Vehicles with an Aggregator-based Hierarchical Control Mechanism: In this chapter, an *"Aggregator-based Hierarchical Control Mechanism"* for Secondary Frequency Regulation (SFR) using a fleet of EVs has been proposed.

Chapter 5: Coordinated Power Control of Electric Vehicles for Grid Frequency Support: In this chapter, a coordinated and manageable strategy to leverage the consolidated participation of EVs for SFR has been designed, based on Mixed Integer Linear Programming.

Chapter 6: Energy-aware and SLA-driven MapReduce Job Scheduling Framework for Cloud Data Centers: In this chapter, an *"Energy-aware and SLA-driven (En-SLA) job scheduling framework"* based on MapReduce is presented. The primary aim of the proposed framework is to explore task-to-slot mapping problem as a special case of energy-aware scheduling in deadline-constrained scenario.

Chapter 7: Conclusion and Future Scope: Thesis concludes with this chapter by highlighting the major contributions made by the proposed research work along with future directions.

Chapter 2

Literature Review

This chapter highlights the significant contributions made in the literature pertaining to the use of Electric Vehicles (EVs) and Data Centers (DCs) for grid frequency support. Additionally, it also discusses the aspect of minimizing the overall energy consumption of cloud DCs; which in turn plays an essential role in keeping the demand and supply gap under control. The chapter also throws light on the limitations of the existing approaches and the motivation for pursuing this research initiative. Further, the objectives of the thesis are also laid down in this chapter.

For the sake of readability, the literature review is segregated into two parts, *i.e.*, *i) EVs for grid frequency support* and *ii) DCs for grid frequency support*.

2.1 Electric Vehicles for Grid Frequency Support

Frequency regulation is a distinguished market service that tends to maintain the delicate balance between demand and supply. Even the minute deviations in grid's frequency can trigger significant disturbances in the form of blackouts, brownouts and voltage fluctuations. Hence, in order to effectively manage these deviations, the demand and supply sides need

to elastically adjust their power consumptions in accordance with their consumption and generation obligations. Traditionally, frequency support is provided using conventional generators (at the supply side) powered by non-renewable sources of energy. However, the use of these agents is accompanied with the emission of harmful gases, degraded heat rate and associated wear and tear [22]. Additionally, it also results in loss of opportunity to generate more power under normal circumstances [36]. On the contrary, commercial buildings, aggregated residential loads and energy storage devices provide more environmentally friendly support at the demand side [16, 37]. However, these agents too accompanied with certain drawbacks, *i.e.*, installation of battery storage devices involve heavy investment while the commercial buildings waste huge amount of energy to support the HVAC facility cite.

More recently, EVs have been identified as the major frequency regulation agents (at the demand side) due to their inherent ability to provide instantaneous frequency support [38, 39]. According to International Energy Agency's survey, the proportion of EVs has already exceeded 1,000,000 globally by 2015 [40]. The penetration of EVs in the global market is estimated to reach 400 million by 2020 [41] as depicted using Fig. 2.1. Further, EV's penetration in the Indian market is forecasted to be equivalent to 35%, 51%, and 62% in America by 2020, 2030, and 2050 respectively. This rapid acceptance of EVs in the market can be attributed to the hike in fuel prices and limited availability of fossil fuels. Further, the use of renewables for charging EVs brings additional benefits to global environmental status by reducing the emission of carbon footprints.

However, future integration of huge number of EVs in the power grids is bound to trigger several unseen challenges. Amongst these, the increased dependence on electricity by the EVs to accommodate transportation needs is of paramount importance. Additionally, unregulated charging of widely dispersed EVs can affect the grid's stability adversely. Hence, to cater these challenges, Kempton and Letendre introduced the novel concept of Vehicle-to-Grid

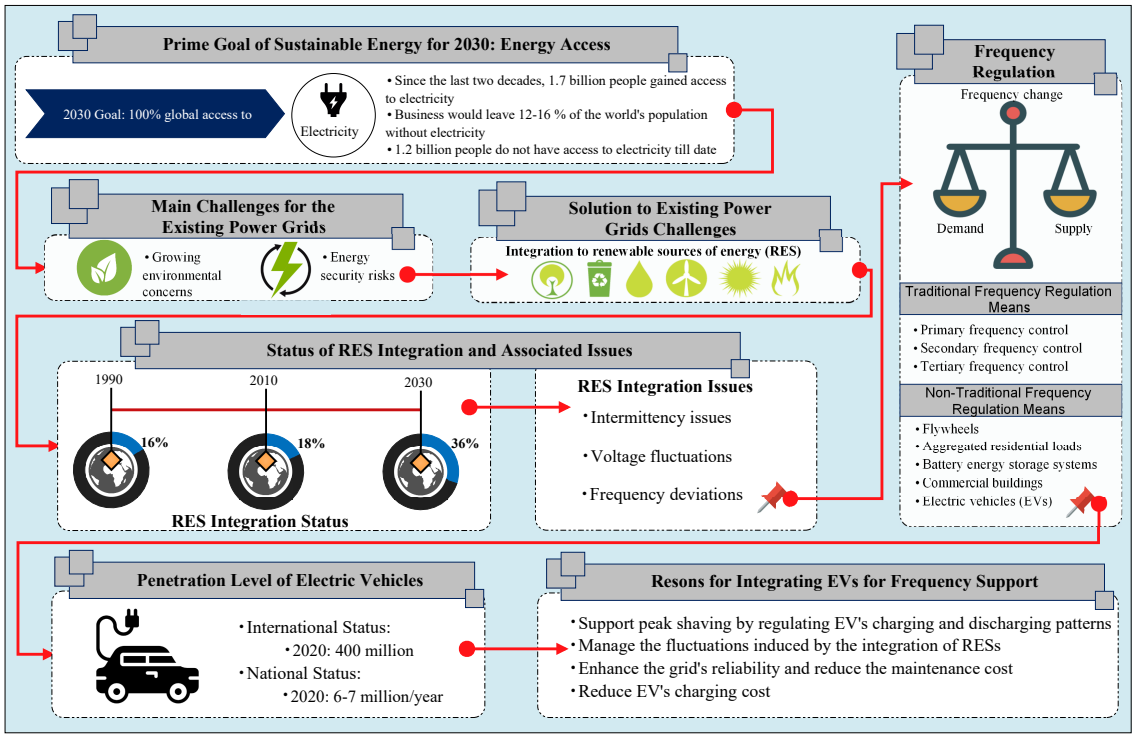

Figure 2.1: Need for regulating frequency in the present scenario.

(V2G) in the year 1997 [42]. The central ideology behind this technology is to unleash the bi-directional charging and discharging of EV's batteries. This implies that the energy available in the batteries could be delivered to the grid for peak shaving, while the excess energy from the grid could be used to feed EVs for valley filling. Thus, this capability makes them suitable candidates to be effectively utilized as energy storage and generation reservoirs, and spinning reserves; and for voltage stability, frequency regulation and various types of ancillary services.

Keeping in view the mutual development of power grids and EVs, the utilization of EVs for regulating grid frequency deviations has become irresistible. This is because modern EVs can flexibly contribute in the regulation market due to the following facts: (i) ability to provide instantaneous frequency support by flexibly adjusting the charging and discharging rates of their batteries, (ii) capability to adjust the charging and discharging cycles of the batteries, and (iii) scheduling of EV's charging and discharging periods in accordance with

the regulation signals. To add to this further, EVs remains idle for majority for their time (i.e., 22 hours) on daily basis [43]. Hence, their aggregated power capacities could not be left without utilization during these hours. Further, their fast response towards power deviations makes them the ideal candidate to provide instantaneous frequency support. Hence, it can be concluded that frequency support using fleet of EVs has emerged as the most promising ancillary service.

2.1.1 Advantages of involving EVs for Frequency Support

The key benefits of involving fleet of EVs in stabilize frequency deviations at grid level are manifold. These are elaborated as follows:

1. Support peak shaving by regulating EV's charging and discharging patterns. This in turn, would reduce the startup expenses of the generating reserves during peak hours and under frequency fluctuations.

2. Considerable reduction in investment cost by the grid utility provider and manage the fluctuations induced by the integration of RESs.

3. Enhance the grid's reliability and reduce the maintenance cost to a great extent.

4. Reduce EV's charging cost; thereby bringing economic benefits to the consumers and amplifying EV's green energy participation.

2.1.2 Related Work

With the rapid and parallel developments in the field of SG and EVs, the utilization of EVs for Secondary Frequency Regulation (SFR) would become irresistible. Kempton and Tomic [44] were the first to suggest that EVs can be utilized in V2G infrastructure for frequency support,

since they have fast battery response, thereby, stabilizing frequency instantly. The major pilot projects carried out in [45, 46] further validate the efficacy of V2G mechanism in grid frequency support. Working in this direction, numerous proposals with respect to EV's integration for SFR have been explored in the literature. For example, Peng *et al.* [47] performed a comprehensive review on the different types of the dispatch strategies with respect to SFR using fleet of EVs. According to the authors, these strategies could be broadly classified into two main streams, *i.e.*, *frequency-aware* and *economic-aware*. While, the former deals with maintaining the grid's frequency within the nominal range, the latter deals with the economic benefits linked with the association of V2G services for frequency regulation.

i) Frequency-aware Dispatch Strategies

Some of the significant *frequency-aware* dispatch strategies in V2G setup are illustrated as under. These strategies can be further classified into two types, *i.e.*, *unidirectional* and *bidirectional dispatch strategies*. The former on one hand, deals with either the charging or the discharging aspects of the participating EVs. The bidirectional dispatch strategies, on the other hand, support both the charging and discharging of EVs' batteries while they contribute to the ancillary services.

Various strategies have been proposed by the researchers under the umbrella of unidirectional frequency-aware dispatch strategies. For instance, a hierarchical control mechanism was also presented for re-balancing frequency deviations and catering EVs' growing energy demands, but it was limited to unidirectional V2G mechanism [48]. Working in the similar direction, proposals in [49–51] focused primarily on unidirectional V2G services for SFR. The authors in [52] devised a robust optimization framework for scheduling the regulation capacities of the EVs. However, the major emphasis of their work was limited

to unidirectional V2G support. Moreover, associated battery degradation issues were not explored by the authors. In the similar context, a comprehensive review of EV's battery degradation for providing effective frequency support services was discussed in [53]. In another work [54], particle swarm optimization was utilized to formulate a multi-objective optimization problem for frequency and voltage regulation using inverter-based PV systems, EVs and domestic controllable loads. Some of the other interesting findings related to EVs were reported in [55–57].

Ota *et al.* [49] proposed an autonomous V2G mechanism for regulating frequency fluctuations using droop control mechanism. However, this approach concentrated on EVs' charging only. In another work, Kamboj *et al.* [50] developed a multi-agent coalition system using EVs for supporting regulation market, but their work primarily focused on EVs' charging requirements. In [51], the authors suggested a decentralized V2G mechanism for effective utilization of fleet of EVs in providing effective frequency support at grid level. However, the major emphasis of their work was centered on EVs' charging. Li *et al.* [58] presented a 2-layer hierarchical control approach for regulating frequency fluctuations using data centers and EVs. However, this approach relied on historical data and neglected the real-time charging and discharging requirements of EVs. Moreover, it focused primarily on EVs' charging and neglected EVs' discharging benefits to a great extent. Likewise, Fuzzy Logic Controller (FLC) was used in [59] for providing frequency support using photo voltaic (PV) plants and EVs. However, this scheme required EVs' State of Charge (SOC) to be maintained within 80-90%. In other words, it neglected EVs' discharging requirements and concentrated primarily on their charging. In [60, 61], the authors focused on supporting ancillary services using EVs, but they confined their work with unidirectional V2G mechanism, i.e., EV's charging needs. On the similar lines, Izadkhast *et al.* [62] proposed a model using fleet of EVs. Like the previous proposals [51, 58–61], this scheme too was limited to EVs' charging. Likewise, Ma and

Mohammed [63] proposed a centralized aggregator based on FLC particularly for frequency support. Nevertheless, this controller primarily focused on EVs' charging and neglected their discharging. Moreover, these controllers [63, 64] could not be used up to their full potential since, their underlining fuzzy logic implementations have linguistic representation which may lead to uncertainties. In addition to this, with the increasing number of membership functions in FLCs, their overall tuning process becomes a complex task.

It is evident from the above discussion, that majority of the unidirectional dispatch strategies concentrate on the charging of EVs' batteries. Nevertheless, researchers have also explored the discharging of EVs' batteries for SFR. For instance, in [37], the authors proposed a frequency support mechanism using EVs and heat pump water heaters. However, the participating EVs were assumed to be having 85% state of charge (SoC), which in turn neglected EVs' charging activities. Janfeshan *et al.* [64] designed a distributed FLC for frequency support in V2G. This controller managed the EVs' discharging on the basis of regulation demand and EVs' SOC. However, it completely neglected EVs' charging activities for frequency support. In another work, Masuta and Yokoyama [36] utilized BESS, EVs and heat pump water heaters for stabilization of frequency imbalances at grid level using Load Frequency Control (LFC) signals. However, the authors neglected EVs' charging in their proposed approach. Furthermore, BESS have been exploited for regulating frequency deviations to a great extent [65, 66]. But, the deployment of BESS is a not a cost effective option and their associated economic benefits are still questionable. In contrast with BESS, EVs are found to be more cost effective as their maintenance cost is borne by the users. Additionally, they can be intelligently utilized to serve dual purposes, *i.e.*, provide frequency support along with transportation facilities.

Another significant area of research in V2G domain involves the coordination between the EVs and utility. Hence, an intermediate interface in the form of aggregators (AGs)

between the two parties ensures real-time coordination and synchronization. Working in this direction, various proposals have been put forth by the researchers. Han *et al.* [67] proposed an optimal charging control strategy particularly for frequency regulation using a V2G aggregator. Likewise, Wu *et al.* [68] proposed an interaction game, based on game theoretical approach to exhibit the communication between EVs and AGs. However, the proposed scheme did not consider explicitly the charging and discharging targets of individual EVs. Likewise, Pilaai and Jensen [69] developed an aggregated EV-based storage system for western Danish power system for regulating frequency fluctuations instantaneously. Unfortunately, their approach neglected control of individual EVs.

Baboli *et al.* [70] also asserted on the notion of utilizing fleet of EVs for restoring frequency deviations at the grid level. The major drawback of this scheme was the negligence related to EVs' individual energy requirements. Zarogiannis *et al.* [71] analyzed the dynamic response of EVs under different frequency deviation scenarios. The authors utilized the frequency droop controller to tweak EVs' energy exchanges in V2G mode. However, this approach was found to be more grid-oriented and neglected EVs' charging and discharging preferences to a great extent. Likewise, Mu *et al.* [72] also utilized EVs for providing frequency support in Great Britain power system. Nevertheless, the approach proposed by the authors was relatively simple, as it involved total disconnection of EVs from the grid during large frequency disturbances. Such an approach in turn is capable enough to trigger greater grid disturbances, if the disconnected V2G power exceeds the regulation signal.

The above mentioned approaches are specifically unidirectional in nature which may undermine the relative importance of EV's batteries for effective SFR. In view of this concern, various researchers have also explored the potential of bidirectional V2G for grid frequency support. For instance, Yang *et al.* [73] proposed a dynamic model for frequency support by considering the battery's charging and discharging characteristics. However, their model

depicted limited communication between neighboring EVs and distribution substations. Likewise, Ota *et al.* [49] used the distributed energy from EVs for frequency support, but could not support simultaneous charging and discharging of EVs. Shimizu *et al.* [37] also proposed a model for EVs' integration in V2G scenario for frequency support. In this model, charging and discharging of participating EVs were regulated based on LFC signals. However, the major shortcoming of this model was that, it did not cater EVs' charging and discharging needs simultaneously. Liu *et al*. [74] implemented a distributed V2G control scheme, which controlled EVs' power with respect to frequency deviations. However, this scheme did not support simultaneous charging and discharging of EVs. In other words, it was more oriented towards frequency support and neglected EVs' energy demands to a greater extent. Kamboj *et al.* [75] presented an implementation of a multi-agent system that allowed EVs to participate in the frequency support market. Although, their system supported both charging and discharging requirements of EVs but it failed to regulate EVs' charging and discharging rates. Kim *et al.* [76] proposed a feedback controller based on Dynamic Programming (DP) for frequency regulation using fleet of EVs; based on bidirectional V2G support. However, the main limitation of DP based controllers is the difficulty involved in keeping track of the intermediate and partial solutions before obtaining an optimal solution.

Apart from this, authors in [77, 78] used game theoretical models to address energy related issues of data centers using RESs and EVs. Likewise, authors in [79], designed a consolidated energy management system powered with batteries and supported by hybrid RESs using Mixed Integer Linear Programming (MILP). Similarly, MILP was also utilized in [80], wherein energy storage optimization was performed in the grid setup to address the associated economic issues. MILP is a well researched topic and has been extensively exploited by the researchers to address various issues related to SG. For instance, MILP has been used to model the energy management issues in smart railways powered by photo voltaic

generation [81]. On the similar lines, MILP based model has been designed in context of smart houses equipped with RESs, energy storage devices and home appliances [82]. Another MILP-based solution has been proposed in [83], wherein the authors have exploited the advantages of EVs for effective demand response mechanism using Vehicle-to-Home (V2H) and V2G services. MILP-based solutions has also been presented for energy management in Micro Grids (MG). For instance, authors in [84] used mobile and stationary energy storages for efficient energy management in MG setup. MILP has also been utilized in context of university building energy management using charging and discharging characteristics of a fleet of EVs [85].

ii) Incentive-aware Dispatch Strategies

In addition to the above proposals, the *economic-aware* or *incentive-aware* dispatch strategies for grid frequency support using fleet of EVs have been explored in the literature. For instance, authors in [53] used optimization to maximize the benefits of EVs' users while supporting necessary ancillary services. Han and Han [86] also suggested that prospective income is linked with EVs' involvement in V2G frequency support mechanism. Their results demonstrated that EVs' integration for frequency support is an economical solution. Similarly, Brooks also suggested that integration of EVs with SG is feasible and has the potential to create income for the EVs' users [87]. In addition to this, authors also developed an AG with communication capabilities. However, their AG supported a limited functionality and could not provide adequate controlling features. Further, Dallinger *et al.* [88] evaluated the impact of EVs' uncertain mobility patterns for providing regulation but their work was confined to the economic perspective linked with V2G.

In [42], authors explored the financial benefits of incorporating EVs in the regulation market using stochastic optimization. However, this work neglected the discharging capa-

bilities of EVs and their associated battery deterioration impacts. Working in the similar direction, Yao *et al.* [89] explored the financial benefits of incorporating EVs in the regulation market. A stochastic optimization problem was formulated by the authors, to estimate the bid of aggregators in the day-ahead market. Nevertheless, EV's discharging needs and the associated battery degradation issues were not explored in this work. Likewise, Sortomme and El-Sharkawi [90] proposed an algorithm to maximize aggregator's profit in V2G environment. In addition to this, the authors also calculated the preferred operating point based on EV's charging rate. However, their work was limited with respect to unidirectional V2G scenario, i.e., EVs' charging. Tan and Wang [91] presented an effective business model for providing frequency support using fleet of EVs. However, authors' major concentration was on modeling a hierarchical game-theoretical approach with respect to EVs' charging which neglected their discharging to a great extent. In [32], authors explored the financial benefits of incorporating EVs in the regulation market using stochastic optimization. However, this work too neglected the discharging capabilities of EVs and associated battery deterioration impacts. Similarly, an optimal bidding strategy was formulated using fleet of EVs in the regulation market [61]. However, the major focus of this work was confined to unidirectional V2G mechanism. The major drawback associated with the unidirectional V2G support is the reduced frequency regulation and limited reserve capacity of the EVs; thereby restricting EVs to discharge their available Frequency Regulation Capacity (FRC) during peak hours.

2.1.3 Motivation

It is evident from the above discussions that, noticeable amount of work has been carried out by the researchers a number of proposals exist in the literature pertaining to EVs' utilization for frequency support. However, there are a few challenges that needs to be addressed in order to realize the best potential usage of V2G technology. First and foremost, there is a need to design

an efficient control methodology for utilizing the limited energy capacity of participating EVs in a sustainable manner. This can be achieved using a hierarchical controlling approach which relies on distributed control of participating EVs. This is in accordance with Pham *et al.*'s work [92], which highlights the use of distributed controllers for efficient frequency support over the centralized controllers. Secondly, the control philosophy should not be limited to grid requirements, but strive for a perfect balance between EVs' and SG's requirements. These challenges can be addressed by coordinating EVs' charging and discharging activities and redistributing the load according to EVs' energy capacities.

Thirdly, it is also essential to support bidirectional V2G services. However, limited work has been done related to regulation of EVs' simultaneous charging and discharging activities [37, 75]. For instance, majority of the proposals as suggested in [49–51, 58–62, 93] have concentrated on EVs' charging, while the work in [36] has focused primarily on EVs' discharging requirements. On the other hand, the scheme proposed in [51] has neglected EVs' individual energy requirements and involved them in V2G operations as per the regulation signals.

Keeping all the above mentioned issues in mind, it becomes quite essential to cater EVs' growing energy demands while regulating frequency deviations. So, this thesis presents different techniques to handle these issues in V2G scenario using hierarchical control mechanisms. This has been achieved using different controllers equipped with communication facilities to achieve effective control of EVs' batteries for regulating their charging and discharging activities. Consequently, three different schemes have been put forth in this thesis in order to overcome the above mentioned challenges. Their detailed description can be found in the upcoming Chapters 3, 4 and 5 respectively.

2.2 Data Centers for Grid Frequency Support

The technological drift in the field of Information and Communication Technology has paved way to the Cloud Computing (CC) platform. It helps in processing of data on large scale using task parallelization frameworks like MapReduce and Hadoop [94–97]. This in turn helps CC to produce results with minimum latency and due to this reason it is considered to be the next most vital paradigm shift in the world of computing. It particularly comprises of massive DCs equipped with UPSes which form its structural and operational foundation. However, its rapid popularity has brought numerous challenges for the research community. The major challenge is the energy-efficiency of cloud DCs [98]. According to [24], the CC infrastructure alone consumed approximately 623 TWh of energy in 2007. Furthermore, this consumption is expected to rise as high as 1963.74 TWh by 2020 [99]. It is evident from the above statistics that DCs would be the major consumers of electricity in the near future. Moreover, it has been projected that the DCs consume nearly 2% of the electricity in US [24, 100], which is higher than the NYSIO's regulating reserve's capacity of 1% [101]. Hence, cloud DCs can be attributed as bulk consumers of electricity which are liable to cause significant electricity disturbances in the near future; if left unmanaged [102]. Keeping these issues in mind, this thesis explores the benefits of incorporating DCs for overall frequency support at the grid level; while catering their energy requirements. Some of the significant contributions in this direction are illustrated as under.

Frequency-aware control strategies at DC level have recently attracted the attention of various researchers. For instance, Li *et al.* [103] proposed a power control strategy to use DCs for grid frequency regulation. In this, Dynamic Voltage Frequency Scaling (DVFS) was adopted by the authors to adjust the aggregated power consumption of DCs. However, the main disadvantage of their work was that, it considered equal distribution of workload amongst the servers irrespective of their current workload. Likewise, Aikema *et al.* [104] also

explored the potential of DCs in the ancillary services market. However, the scheme proposed by the authors failed to meet the required Quality of Service (QoS) parameters. Towards this end, Qureshi *et al.* [105] correctly pointed out that even reduced electricity prices can trigger higher electricity consumption and hence, greater emission of green house gases (GHG).

Working in similar direction, Ghamkari and Moheseman-Rad [106] also validated the use of DCs in the ancillary market. The authors asserted that the use of load resources like DCs can have manifold advantages in terms of reduced transmission and distribution losses. Additionally, the authors also pointed out that the load reserves enhance the transmission capacity. In their work, the authors formulated profit maximization based optimization strategy particularly targeting DCs. However, their scheme did not ensure the required QoS to its end users. In another work, Chen *et al.* [107] also emphasized on DC utilization for providing necessary frequency support.

Additionally, another thread of research has also focused on dynamic provisioning of jobs based on temporal and regional variations of electricity prices; with the fundamental aim to reduce the overall electricity consumption of DCs [108, 109]. However, these works did not consider the environmental consequences.

In a nutshell, the modern DCs can dynamically adjust their power consumption by employing various strategies for fast frequency support. Amongst these, the most common techniques are DVFS [103, 110, 111], dynamic capacity provisioning [112], effective use of UPS batteries [110–112], and efficient job scheduling. DVFS deals with alerting the CPU's frequency to regulate server's overall power consumption. However, this approach can significantly affect the SLA targets in terms of average response time, and deadline violations. The capacity provisioning on the other hand, deals with turning on/off the computing servers to adjust the aggregated power consumption of the DCs. This approach however, consumes excess time and leads to extra energy consumption during server's on-and-off transitions.

Hence, job scheduling at DCs is considered as an efficient means for fast frequency support.

According to Emerson Network Power analysis [113], the overall energy utilization of a DC is due to its servers (52%) and support systems (48%); and it is increasing at the rate of 15% annually [114]. Considering this trend, there should be no surprise that the major portion of DC's operational cost would be due to energy utilization. Accordingly, various schemes have been suggested by the researchers to improve DC's energy efficiency. Some existing proposals have attempted to achieve this goal by adjusting server's CPU using efficient job-scheduling strategies [94, 115, 116], while others have tried to reduce the energy utilization of the supporting units [77, 117, 118].

Nevertheless, these computation intensive DCs are not only characterized by their energy drawing properties, but also for providing efficient data management, storage and processing services. Amongst these, the processing of big data and its applications has gained wide popularity across the academia and industry in the recent years [119]. This is achieved by using the popular "MapReduce" or its open-source implementation "Hadoop" [120, 121]. MapReduce is characterized by its distinctive features such as-automatic parallelization and distribution, fault tolerance, and high availability. Numerous real world problems and computations adhere to this framework. These problems range from wide-scale machine learning scenarios, graph computations and data processing. Thus, it becomes quite important to design a comprehensive energy-aware and SLA-driven job scheduling framework for MapReduce witnessing its significance in almost every domain. However, there are a number of key challenges in scheduling the MapReduce jobs for multi-constrained environment which are discussed as follows.

The computing infrastructure of cloud DCs is essentially heterogeneous in nature. This can be contributed to regular maintenance issues and sharing of resources by various cloud tenants. Additionally, the diversity in the performance needs of the underlying clusters induces

further variations in the computation capabilities of the underlying computing nodes. This in turn, leads to load imbalances, poor performance and low cluster utilization levels. Literature suggests that the existing schemes fall short on heterogeneous MapReduce configurations [122]. Hence, it is essential to devise an effective job scheduling technique that scales well with heterogeneous hardware and software configurations in cloud setup, while achieving an optimal balance between energy efficiency and SLA guarantee. Hence, to circumvent the challenges of heterogeneous infrastructures, an effective approach is to schedule the MapReduce jobs using task-to-slot/container mapping [94]. Moreover, the said approach is found to be favorable to MapReduce's Distributed File Sytem (DFS) because it ensures continuous data availability; unlike the traditional approach of workload consolidation on minimum number of nodes and turning off the rest of cluster during periods of inactivity.

2.2.1 Related Work

MapReduce job scheduling have been explored by researchers in the past with respect to various parameters such as-makespan [123–125], response time [124, 126], job completion time [127–129], performance [130, 131], throughput [132], budget [133], fairness [134], task prioritization [133] and energy-efficiency [94, 116, 135]. For the ease of understanding, these strategy have been classified into: *Non-energy centric* and *Energy-centric job scheduling approaches*.

Non-energy centric job scheduling approaches

Ren *et al.* [127] proposed a job scheduling strategy for optimizing the completion time of participating jobs which were relatively small. It basically banked on extending the job priorities for ensuring faster response to smaller jobs. This in turn hampered the deadlines of the other jobs. In another work, different online and offline algorithms were proposed

for MapReduce scheduling [128]. In this proposal, the major objective was to minimize the overall completion time of the participating jobs. The algorithms used in this proposal relied on linear program relaxation problem to achieve their respective objectives. A heuristic scheduling approach was formulated in [126] to maintain load balancing on the cluster. This in turn helped to reduce the overall completion time of the jobs while impeding node overloading. Similarly, Zaharia *et al.* [129] proposed Longest Approximate Time to End, a robust scheduling algorithm based on the estimation of finish times of jobs. However, this algorithm jeopardized the job's response time.

Other popular variants of job schedulers available in MapReduce tend to focus on makespan and response time minimization. For example, FIFO scheduler was initially deployed to schedule the map and reduce tasks. However, its major disadvantage was induced due to long waiting times. Subsequently, to overcome this problem, a fair scheduler was designed [136]. On the similar lines, Moseley *et al.* [123] proposed a dynamic programming based optimization strategy to minimize the makespan of the MapReduce jobs. In [125], the authors proposed a MapReduce job scheduling scheme to minimize the overall makespan of the jobs. Likewise, Wolf *et al.* [124] proposed a flexible scheduling strategy called as Flex. It targeted on optimizing different metrics like job response time and makespan. A dynamic priority and parallel task scheduling mechanism was designed for Hadoop framework in [133]. It relied on prioritizing the jobs and users to achieve optimized results with respect to job's deadline and budget.

Ibrahim *et al.* proposed an efficient scheduling mechanism exclusively for the map tasks [130]. This scheduling strategy helped to improve the overall performance of the designed solution. Similarly, authors in [131] considered the performance interferences in the virtualized environment which eventually affected the performance of the MapReduce jobs. For this, the authors devised a mechanism for predicting the interference degree between

the virtual machines, followed by task scheduling using the standard Greedy strategy. Also, the authors in [132] proposed MapReduce-based task scheduling mechanism which rapidly improved the system throughput in compute-intensive environments. However, the major drawback of the above mentioned schemes was the lack of consideration with respect to energy consumption minimization of cloud DCs based on MapReduce. The next segment explores some of the most significant contributions in this regard.

Energy centric job scheduling approaches

Authors in [135], proposed an energy driven bi-level optimization scheme with respect to job scheduling in MapReduce configuration using genetic algorithm. The major focus of this work was guaranteeing maximum data locality while improving the overall energy efficiency. On the similar lines, a scheduling approach was presented in [116]; wherein best resources assignment model was employeed. This work dodged the need to maintain idle resources, thereby reducing the overall energy consumption. The above approaches however, did not give much emphasis to other parameters such as-makespan minimization, deadline guarantee and SLA violations in conjunction with energy minimization.

In [137], GreenHadoop was proposed to maximize the green energy consumption of cloud DCs powered by solar panel and electric grid. However, the major disadvantage of the designed scheduler was its inability to minimize the overall energy utilization of the DCs. Delay of the scheduled jobs due to the unavailability of green power supply was also a significant concern in GreenHadoop. Apart from this, an energy centric strategy named Covering Subset (CS) was designed in [138]; in which fractional part of the cluster was fully powered on to support the computational load; with one replica of each data block. However, its distinctive shortcoming was induced due to lack of storage capability and write bandwidth [139].

In [139], another energy-aware strategy was suggested for MapReduce framework; wherein the incoming jobs were segregated into time-sensitive and less time-sensitive jobs. Based on this segregation, the former jobs were executed on a small subset of dedicated nodes while the latter were executed on the rest of the cluster. Working in the similar direction, All-In Strategy (AIS) was designed by Lang and Patel in [140]. AIS worked on the abstract notion of running the entire cluster at its full capacity in regular batches and powering down the cluster otherwise. However, authors in [139] suggested that jobs experience significant processing delays in AIS, particularly the small and interactive jobs; thereby inducing significant SLA violations. In order to overcome these shortcomings, authors in [94] devised an effective scheme for minimizing the overall energy utilization of the MapReduce jobs while satisfying SLA. However, the major drawback of this proposal was its inability to achieve task-to-slot mapping under varied workload scenarios.

2.2.2 Motivation

With an exponential increase in the demands from the end users for real-time data processing, the penetration of large-scale cloud DCs has become inevitable. However, with an increase in the number and size of DCs, the demand for power supply on the existing electric grids has increased manifold in the recent times. Thus, there exists a need to design efficient solutions to cater the growing demands while maintaining grid stability with respect to frequency fluctuations. Currently, frequency regulation services are provided by partially loaded power plants. However, with the growing global environmental concerns, such inefficient and environmentally hazardous means of regulation would not be suitable for the environment. Thus, an alternative mechanism is required which not only will be at par with the current regulation techniques in terms of efficiency but is environmentally friendly too. Integration of DCs into the electricity market, can act as a catalyst for provisioning fast and reliable

Table 2.1: Relative comparison of En-SLA with the current state-of-the-art schemes.

Desired Properties \ Schemes	[137]	[140]	[138]	[139]	[116]	[135]	[94]	En-SLA
Energy Minimization	✗	✓	✓	✓	✓	✓	✓	✓
SLA Adherence	✓	Partially	Partially	✓	✗	✗	✓	✓
Map/Reduce Phase Splitting	✗	✗	✗	✗	✗	✗	✗	✓
Task-to-slot Mapping	✗	✗	✗	✗	✗	Partially	✓	✓
Job Scheduling	✓	✗	✗	✗	✓	✓	✓	✓

frequency support to the electrical power system network. Moreover, with higher penetration of DCs, this approach seems to be feasible and reliable in the years to come.

An efficient approach to attain the above mentioned objective, is by leveraging the advantages of job scheduling mechanism. However, the concept of job scheduling in context of MapReduce framework in not new. Nevertheless, the major emphasis of existing schemes has been on optimization of a wide variety of parameters such as-job's makespan [123–125], response time [124, 126], job completion time [127–129], performance [130, 131], throughput [135], budget [133], fairness [134], task prioritization [133], and energy [116, 131, 138–140]. To the best for our knowledge, very limited work has been done on balancing the trade-off between energy minimization and SLA adherence with respect to MapReduce framework [94], as evident from Table 2.1. For instance, schemes proposed in [116, 135, 137, 138, 140] either concentrate on energy efficiency or SLA adherence. On the contrary, the works in [94, 139] focus on the trade-off between energy minimization and SLA guarantee. However, they have their associated shortcomings, *i.e.*, BEEMR [139] hampers the storage capacity and write bandwidth, while the work in [94] fails to schedule the Map/Reduce tasks under different workload scenarios. Additionally, the latter didn't consider the splitting the Map/Reduce phases into multiple stages for achieving higher energy savings; without compromising the performance of the submitted jobs.

Motivated from the above challenges, this thesis exploits job scheduling strategy as a special case of task-to-slot mapping in order to balance the trade-off between energy utilization

and SLA adherence. The designed energy-driven scheduling is an effective means to manage the demand and supply gap in check; thereby maintaining the frequency in its nominal range. Furthermore, the novel concept of *"Splitting the Map/Reduce phases into multiple stages"* has also been proposed; in order to achieve higher energy reductions. To the best of our knowledge, this is the first initiative of its kind, which consolidates multiple objectives for effective job scheduling in MapReduce framework. The designed scheme is referred to as *"Energy-aware and SLA-driven MapReduce Job Scheduling (En-SLA)"* and its detailed description can be found in Chapter 6.

2.3 Research Gaps

This thesis aims to provide grid frequency support by controlling the operations of DCs and fleet of EVs by devising scheduling mechanisms for jobs and EVs respectively. However, their scheduling is not a straight forward approach particularly in light of managing grid frequency deviations. Hence, the major research gaps related to the proposed work have been summarized below.

- ***Growing environmental concerns:*** Currently, frequency regulation services are supplied through partially loaded power plants. However, with the growing global environmental concerns, such an inefficient and environmentally hazardous means of regulation is bound to become problematic. Thus, an alternative mechanism is need of the present era which would not only be at par with the current regulation techniques in terms of efficiency but is environmentally friendly too.

- ***Need for fast frequency regulation agents:*** Integration of DCs and EVs into the electricity market as primary source of frequency support, can act as a catalyst for provisioning fast and reliable frequency support to the electrical power system network.

Moreover, with higher penetration of EVs and DCs, this approach seems to be more feasible and reliable in the times to come.

- ***Heavy infrastructural expenses to built future "Green Data centers":*** Recently, various researchers have put forth the concept of Green DCs, wherein the DCs would be partially or completely supported by built-in RESs for power usage. Setting up such technologically advanced DCs is likely to incur huge financial investments along with prolonged deployment time.

- ***Intermittency issues associated with RESs:*** Though the RESs are environmental friendly, but they are well known for their intermittency issues too [141]. Hence, an effective control strategy focusing primarily on scheduling of jobs and EVs would not only cater the needs of the immediate consumers, but also the related service providers [142].

- ***Peak provisioning:*** In order to provide the required services during peak hours, the DC operators often tend to deploy huge equipments. Unfortunately, many of these reserves are left unattended and powered on, even when not in use. This in turn leads to wastage of electricity and raises the operational expenses.

2.4 Objectives

The main objectives of the thesis are summarized as follows:

1. To carry out extensive literature review in accordance with different techniques used for regulating the activities of DCs and EVs under multi-constraint environment.

2. To design a hierarchical control mechanism for regulating the consolidated participation of DCs and EVs for frequency support.

3. The control mechanism would also involve effective scheduling of jobs and EVs at DC and CS level respectively. This would be achieved in accordance with jobs' response times and EVs' energy requirements respectively.

4. The thesis would also involve validation of various designed controllers on real data traces.

2.5 Concluding Remarks

The existing approaches for grid frequency support particularly using fleet of EVs and cloud DCs have been discussed in this chapter. Additionally, the need for grid frequency regulation using these modern agents is also explored, followed by the objectives of this thesis work. In the next chapter, a Colored Petri Net based frequency support scheme using fleet of EVs has been proposed.

Chapter 3

Frequency Support Scheme using Fleet of Electric Vehicles

In this chapter, an efficient scheme for grid frequency support using fleet of EVs has been proposed. In the proposed scheme, aggregators (AGs) have been modeled using Colored Petri Net (CPN) based controller which regulates the charging and discharging rates of EVs for overall frequency support. The detailed working of the proposed scheme along with its major contributions are mentioned as follows.

3.1 Contributions

The major contributions of the proposed scheme are summarized as follows.

- AGs have been modeled using CPN based controller which regulates the charging and discharging rates of EVs for overall frequency support.
- The proposed frequency support scheme handles the dynamics associated with the mobility of participating EVs, during the regulation process.

- The proposed scheme has been evaluated using the real-time data obtained from PJM and ERCOT.
- This scheme caters the energy demands of EVs while supporting frequency, unlike the previous schemes [37, 74, 90].
- The scheme is highly scalable and can provide frequency support for different time intervals such as-1 hour, 15 minutes, etc.

3.2 System Framework

The proposed system comprises of three core units namely-power generation, transmission and substation unit as depicted in Fig. 3.1. The generation unit further comprises of generation control system, turbine generation unit and regulation unit. The turbine generation unit is responsible for power generation and the output of this unit is fed to the regulation unit which provides regulatory signals to generation control system based on frequency variations. Generation control system has a vital role in controlling turbine unit's production with respect to load variations. Hence, generation unit not only provides the power but also helps in achieving *primary frequency regulation* [15]. The power generated by this unit is transmitted to substation unit via transmission unit. Control center available at substation unit monitors the frequency and load fluctuations. These fluctuations are then communicated to AGs which play a crucial role in controlling the power exchange between the charging stations (CSs) and the substation unit (SU). Hence, AGs support bi-directional mode of communication, whereas, CSs provide bi-directional flow of power as depicted in Fig. 3.2. CSs comprise of a number of charging points (CPs) for charging and discharging of EVs' batteries.

The communication link between the substation unit and AG is assumed to be a dedicated channel of fiber optics. These cables are insusceptible to electromagnetic interferences and

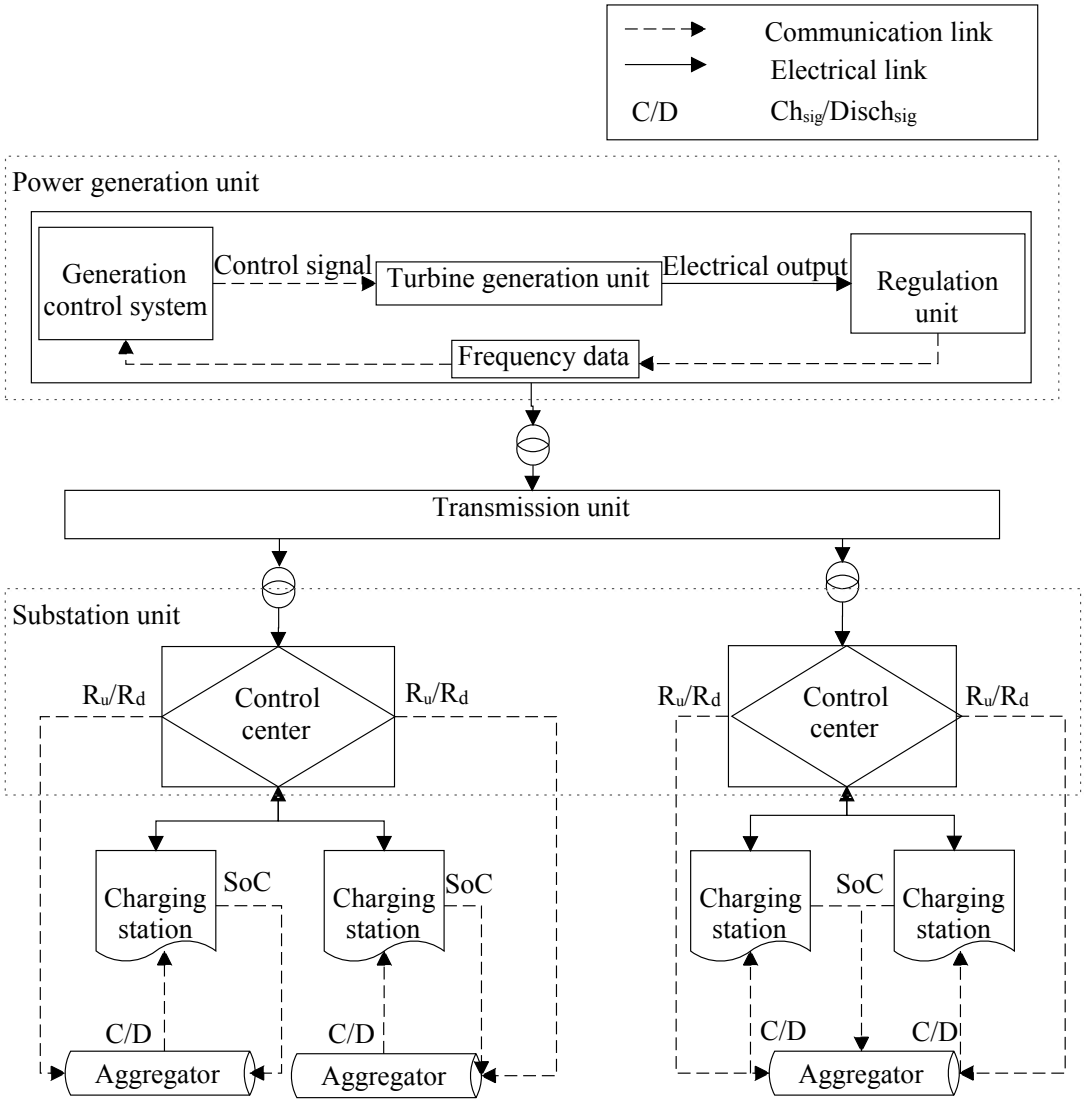

Figure 3.1: System framework of the proposed scheme.

have huge transmission capacity. Due to their robustness, these fibres are considered as one of the best communication media for medium and low voltage applications in power systems. However, in case of intermittent link failure, the proposed scheme adopts a fault tolerant mechanism. This mechanism has been elaborated in algorithm 3.1, where t_{prev} and t represent the previous and current time slots respectively. Initially, P regulation signal is generated by the substation unit which is then propagated amongst m number of AGs. In case, the link between any of the AGs (say i^{th} AG) and the substation unit fails, then the AG may not receive

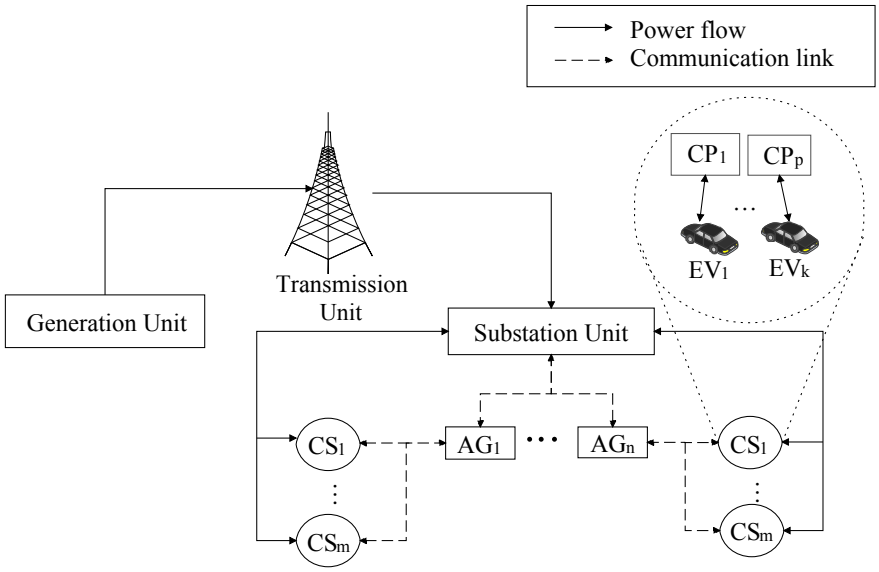

Figure 3.2: Power and communication links for the aggregators at charging stations.

the latest regulation signal (P_i). During such scenarios, the AG continues to operate but with the previously received regulation signal (P_i^{prev}). This is done in order to provide acceptable frequency support even under communication failures.

Algorithm 3.1 Frequency support during link failure.

Input: m, P_i^{prev}, P_i, P, t_{prev} and t

1: Set $P_i = P/m$ at t
2: **if** (Communication between i^{th} AG and substation unit fails) **then**
3: Set $P_i = P_i^{prev}$ from t_{prev}
4: **end if**

3.2.1 Assumptions Considered

The assumptions considered for the proposed scheme are mentioned below.

- A single substation unit is assumed to have multiple AGs.
- A single AG can coordinate with its one or more CSs.
- CSs are available at parking lots of residential, industrial and commercial buildings.

- Every EV at the CS is assumed to be participating in frequency support mechanism.
- For the sake of simplicity, realistic driving behaviors such as-drivers' driving profile and road conditions, have not been considered in this work.

3.2.2 Working Methodology

The working methodology of the proposed scheme is modeled using Fig. 3.1. The generated power is continuously monitored by the regulation unit using a frequency measuring device called frequency transducer. This transducer provides regulation signals to generation control system based on measured frequency. These signals can either be positive, or negative. Positive signals are generated whenever load exceeds supply and vice-versa. Control centers at substation unit generate regulation up (R_u) and regulation down (R_d) signals based on frequency fluctuations. These signals are then relayed to AG(s) equipped with an intelligent CPN based controller. This controller ensures that the CSs work in perfect synchronization with substation unit for overall frequency stabilization. Detailed description about this controller is illustrated in Section 3.4.

3.3 Problem Formulation

Frequency fluctuations possess significant problems for power systems and are primarily caused due to imbalances between load and generation. Standard swing equation is used to model these imbalances [15] as follows.

$$P_{mech} - P_{elec} = M\frac{\Delta\omega}{\Delta t} \tag{3.1}$$

where P_{mech} and P_{elec} represent mechanical power of the turbine and electrical power output of the generator respectively. M is an inertia constant and ω denotes the angular speed of generator's rotor as expressed in Eq. (3.2). Substituting the value of ω in Eq. (3.1) redefines it to Eq. (3.3).

$$\omega = 2\pi f \tag{3.2}$$

$$P_{mech} - P_{elec} = M2\pi\partial f/\partial t \tag{3.3}$$

Equation (3.3) relates power imbalances with frequency (f) variations. Hence, frequency can be considered as an actual measure for these imbalances. They can be managed by various frequency regulation techniques. Normally, frequency regulation is achieved with the help of generators at two levels, *i.e.*, primary and secondary. Primary frequency regulation responds to frequency deviations by altering governor's speed and controlling the valves for steam flow. The regulated steam flow further controls P_{mech} with an intent of matching P_{elec} to load fluctuations (P_{load}). The following equation represents the correlation for the same.

$$\Delta P_{elec} = \Delta P_{load} \tag{3.4}$$

These imbalances are regulated by adjusting turbine's P_{mech}, which can be expressed using the below equation.

$$\Delta P_{mech} = \Delta P_{load} + \frac{dW_k}{dt} + P_{load}^{old} \tag{3.5}$$

W_k denotes the stored kinetic energy in generator's rotor and P_{load}^{old} is the old load on this generator. The rate of increase in W_k can be determined as follows.

$$W_k = W_{k_0}\left(\frac{f_0 + \Delta f}{f_0}\right)^2 \tag{3.6}$$

where W_{k_0} denotes rotor's kinetic energy at nominal frequency (f_0) and Δf represents frequency changes. The rate of change of W_k is given by,

$$\frac{dW_k}{dt} = \frac{2W_{k_0}}{f_0}\left(\frac{d\Delta f}{dt}\right) \tag{3.7}$$

P_{load}^{old} has a dependency on frequency and is mentioned using the given equation.

$$D = \frac{\partial P_{load}^{old}}{\partial f} \tag{3.8}$$

In the above equation, D represents the change in P_{load}^{old} with respect change in f. Now, rewriting Eq. (3.5) using Eqs. (3.7) and (3.8) as follows.

$$\Delta P_{mech} - \Delta P_{load} = \frac{2W_{k_0}}{f_0}\frac{d\Delta f}{dt} + D\Delta f \tag{3.9}$$

Converting the above equation into per unit format as mentioned below.

$$\Delta P_{mech} - \Delta P_{load} = \frac{2H}{f_0}\frac{d\Delta f}{dt} + D\Delta f \tag{3.10}$$

where H is the per unit inertia constant and it is given by,

$$H = \frac{2W_{k_0}}{G_{rated}} \tag{3.11}$$

In the above equation, G_{rated} and H represents generator's rating and time during which energy is stored in rotating machines as mechanical inertia respectively. H plays a vital role in determining system's sensitivity towards frequency variations against power imbalances. In large power systems, H ranges from 6 seconds or more. However, in small power systems, this value is comparatively small. Therefore, in small systems, large frequency variations are

observed even against minor power imbalances. If extra load is added to these systems during frequency variations, then it may lead to wear and tear of control valves.

Primary and secondary frequency regulation mechanisms maintain efficient control only during normal load conditions. Unfortunately, these mechanisms fail to provide adequate frequency support during emergency conditions, especially during huge power imbalances. Therefore, need arises to provide regulation in such a manner that above mentioned problems are effectively resolved. So, V2G based approach seems to be an appropriate regulatory mechanism for regulating huge power imbalances by involving fleet of EVs.

Let us assume, P is the amount of power required for stabilizing Δf. This P can be either positive, or negative. If it is positive, then substation unit relays R_u signal to its AGs, otherwise, it relays R_d signal. These signals represent the amount of power either required or available at the substation unit in order to balance frequency deviations. Therefore, this P is distributed amongst m number of AGs using the below mentioned equation.

$$P_i = \frac{P}{m} \tag{3.12}$$

where P_i denotes the power at the i^{th} AG. Similarly, P_i is re-distributed amongst the CSs as follows.

$$P_{ij} = \frac{P_i}{n} \tag{3.13}$$

In Eq. (3.13), P_{ij} denotes the power signals at j^{th} CS of the i^{th} AG for time interval T and n denotes the total number of CSs. EVs' involvement in V2G operations is based on their battery's current state of charge (SoC_k^{cur}) and minimum SoC limit (SoC_k^{limit}). In case of charging, SoC required (SoC_k^{req}) by k^{th} EV is calculated using Eq. (3.14), whereas, in case of

discharging, excess SoC (SoC_k^{req}) is computed using Eq. (3.15).

$$SoC_k^{req} = 100 - SoC_k^{cur} \tag{3.14}$$

$$SoC_k^{req} = SoC_{cur} - SoC_k^{limit} \tag{3.15}$$

The amount energy required for charging and discharging (E_k^{req}) of the k^{th} EV, is computed as follows.

$$E_k^{req} = E^{rated} \frac{SoC_k^{req}}{100} \tag{3.16}$$

where E^{rated} is the rated energy of the EV in kWh.

The fleet of EVs available at the CS, may either participate in charging or discharging operations. Thus, the total amount of energy required for EVs' charging ($E_{ij}^{tot,char}$) and discharging ($E_{ij}^{tot,dis}$) at j^{th} CS of the i^{th} AG, are obtained using the below mentioned equations.

$$E_{ij}^{tot,char} = -\sum_{k=1}^{p} E_k^{req} \quad \forall k \in \text{EVs seeking charging} \tag{3.17}$$

$$E_{ij}^{tot,dis} = \sum_{k=1}^{q} E_k^{req} \quad \forall k \in \text{EVs seeking discharging} \tag{3.18}$$

Hence, net energy (E_{ij}^{net}) at i^{th} CS can be expressed as follows.

$$E_{ij}^{net} = E_{ij}^{tot,char} + E_{ij}^{tot,dis} \tag{3.19}$$

For providing frequency support, E_{ij}^{net} should match P_{ij} for corresponding T interval (in hours). For achieving this requirement, EVs' charging (C_{ij}^{rate}) and discharging (D_{ij}^{rate}) rates

are regulated by the controller using the below mentioned equations.

$$C_{ij}^{rate} = \frac{1}{T} \tag{3.20}$$

$$D_{ij}^{rate} = \frac{1}{T} \tag{3.21}$$

Thus, power drawn (P_{ij}^{char}) and discharged (P_{ij}^{dis}) by EVs at j^{th} CS during T is expressed as,

$$P_{ij}^{char} = E_{ij}^{tot,char} C_{ij}^{rate} \tag{3.22}$$

$$P_{ij}^{dis} = E_{ij}^{tot,dis} D_{ij}^{rate} \tag{3.23}$$

P_{ij}^{char} can also be calculated if P_{ij}^{dis} and P_{ij} are already known and vice-versa. The following equations reflect their correlation.

$$P_{ij}^{char} = P_{ij} - P_{ij}^{dis} \tag{3.24}$$

$$P_{ij}^{dis} = P_{ij} - P_{ij}^{char} \tag{3.25}$$

The time duration for which EVs participate in charging (T_{ij}^{c}) and discharging (T_{ij}^{d}) process at regulated rates are obtained using following equations.

$$T_{ij}^{c} = E_{ij}^{tot,char} / P_{ij}^{char} \tag{3.26}$$

$$T_{ij}^{d} = E_{ij}^{tot,dis} / P_{ij}^{dis} \tag{3.27}$$

Amount of energy charged (E_{ij}^{char}) and discharged (E_{ij}^{dis}) by fleet of EVs in a certain time

interval, say T_1, are deduced using the following equations.

$$E_{ij}^{char} = P_{ij}^{char} \frac{T_1}{T_2} \frac{1}{C_{ij}^{rate}} \tag{3.28}$$

$$E_{ij}^{dis} = P_{ij}^{dis} \frac{T_1}{T_2} \frac{1}{D_{ij}^{rate}} \tag{3.29}$$

where the respective P_{ij}^{char} and P_{ij}^{dis} have been obtained at regulated rates for time interval T_2. Consider the following case study to relate these equations.

Case Study: Let us assume, a fleet of EVs available at j^{th} CS can draw a total power (P_{ij}^{char}) of 200 kW at C_{rate} of 2. Now, suppose these EVs participate in the charging process for only 30 minutes (T_1=0.5) instead of 1 hour (T_2=1), then Eq. (3.28) is used to compute E_{ij}^{char} which is fetched by these EVs during T_1. In this case, E_{ij}^{char} turns out to be 50 kWh. Similarly, Eq. (3.29) is used to compute E_{ij}^{dis} in case of discharging.

During frequency support, EVs either charge or discharge themselves. As a result, their energy and SoC levels also get changed after T interval of time. The following equations summarize the new energy required or available (E_k^{new}) with the k^{th} EV and its corresponding SoC (SoC_k^{new}) level after providing frequency support.

In case of charging,

$$E_k^{new} = E_k^{req} - \frac{E_k^{req} E_{ij}^{char}}{E_{ij}^{tot,char}} \tag{3.30}$$

$$SoC_k^{new} = 100 - \frac{100 E_k^{new}}{E^{rated}} \tag{3.31}$$

In case of discharging,

$$E_k^{new} = E_k^{req} - \frac{E_k^{req} E_{ij}^{dis}}{E_{ij}^{tot,dis}} \tag{3.32}$$

$$SoC_k^{new} = \frac{100 E_k^{new}}{E^{rated}} + SoC_k^{limit} \tag{3.33}$$

The amount of power met (P_{ij}^{met}) and unmet (P_{ij}^{unmet}) during frequency support is expressed as follows.

$$P_{ij}^{met} = P_{ij}^{char} + P_{ij}^{dis} \tag{3.34}$$

$$P_{ij}^{unmet} = P_{ij} - P_{ij}^{met} \tag{3.35}$$

3.4 CPN Modeling

This section proposes a CPN based controller at AG level for regulating energy exchanges between EVs and CSs.

3.4.1 Significance of CPN based controller

CPNs are higher versions of basic Petri Nets (PNs) which aid in easy modeling, analysis and simulation of various systems. Moreover, the tokens considered in CPNs can be related to different data types such as-INT, REAL etc. In the context of this scheme, these tokens play a crucial role in simulating the real-time scenario with concrete values. Apart from this, the complex interactions between EVs and AGs can be easily modeled with the help of CPNs. These interactions may also exhibit parallelism and synchronization behaviors. Keeping the above requirements in view, the CPN based controller seems to be an ideal option for designing the controller in this work. Moreover, graphical representation of PNs aids in better visualization and understanding.

3.4.2 Working of CPN based controller

The working of the proposed CPN based controller is illustrated in Algorithm 3.2. Initially, the AG receives regulation signal (P_i) for T. The controller then, re-distributes P_i amongst

Algorithm 3.2 Frequency support algorithim to illustrate the working of CPN based controller.

Input: n, P_i and T

Output: Regulated C_{ij}^{rate} and D_{ij}^{rate} of EVs for frequency support during T time slot.

Set $P_{ij} = P_i/n$
Follow algorithm 3.1
Set $T^{new} = 0$
while $(T - T^{new} > 0)$ **do**
    Set $E_{ij}^{tot,char} = -E^{rated} \sum_{k=1}^{p} SoC_k^{rem}/100$
    Set $E_{ij}^{tot,dis} = E^{rated} \sum_{k=1}^{q} SoC_k^{rem}/100$
    if $(\mid E_{ij}^{tot,char} \mid \leq \mid E_{ij}^{tot,dis} \mid)$ **then**
        Set $C_{ij}^{rate} = 1/T$ using Eq. (3.20)
        if $(C_{ij}^{rate} > 2)$ **then**
            $C_{ij}^{rate} = 2$
        end if
        $T_{ij}^{c} = 1/C_{ij}^{rate}$
        Compute P_{ij}^{char} using Eq. (3.22)
        if $(P_{ij}^{char} \leq P_{ij})$ **then**
            Compute P_{ij}^{dis} using Eq. (3.25)
            Compute $T_{ij}^{d} = E_{ij}^{tot,dis}/P_{ij}^{dis}$
            Set $D_{ij}^{rate} = 1/T_{ij}^{d}$
            if $(D_{ij}^{rate} > 2)$ **then**
                $D_{ij}^{rate} = 2$
                $T_{ij}^{d} = 1/D_{ij}^{rate}$
                Compute P_{ij}^{dis} using Eq. (3.23)
            end if
        else
            P_{ij}^{dis}=T_{ij}^{d}=D_{ij}^{rate}=0
        end if
    else
        Set $D_{ij}^{rate} = 1/T$ using Eq. (3.21)
        if $(D_{ij}^{rate} > 2)$ **then**
            $D_{ij}^{rate} = 2$
        end if
        $T_{ij}^{d} = 1/D_{ij}^{rate}$
        Compute P_{ij}^{dis} using Eq. (3.23)
        if $(P_{ij}^{dis} \geq P_{ij})$ **then**
            Compute P_{ij}^{char} using Eq. (3.24)
            Compute $T_{ij}^{c} = E_{ij}^{tot,char}/P_{ij}^{char}$
            Set $C_{ij}^{rate} = 1/T_{ij}^{c}$

37: **if** ($C_{ij}^{rate} > 2$) **then**
38: $C_{ij}^{rate} = 2$
39: $T_{ij}^{c} = 1/C_{ij}^{rate}$
40: Compute P_{ij}^{char} using Eq. (3.22)
41: **end if**
42: **else**
43: $P_{ij}^{char} = C_{ij}^{rate} = T_{ij}^{c} = 0$
44: **end if**
45: **end if**
46: **if** ($T_{ij}^{d} = 0$) **then**
47: $E_{ij}^{char} = P_{ij}^{char}/C_{ij}^{rate}$
48: $E_{ij}^{dis} = 0$
49: **else if** ($T_{ij}^{c} = 0$) **then**
50: $E_{ij}^{char} = 0$
51: $E_{ij}^{dis} = P_{ij}^{dis}/D_{ij}^{rate}$
52: **else if** (($T_{ij}^{c} \leq T_{ij}^{d}$) && ($T_{ij}^{c} \neq 0$)) **then**
53: $E_{ij}^{char} = P_{ij}^{char}/C_{ij}^{rate}$
54: $E_{ij}^{dis} = P_{ij}^{dis}T_{ij}^{c}/(T_{ij}^{d}D_{ij}^{rate})$
55: **else**
56: $E_{ij}^{char} = P_{ij}^{char}T_{ij}^{d}/(T_{ij}^{c}C_{ij}^{rate})$
57: $E_{ij}^{dis} = P_{ij}^{dis}/D_{ij}^{rate}$
58: **end if**
59: Compute $E_{k}^{new}, SoC_{k}^{new}\ \forall$ EVs, using Eq. (3.30, 3.32) and Eq. (3.31, 3.33)
60: Compute $P_{ij}^{met}, P_{ij}^{unmet}$ using Eqs. (3.34) and (3.35)
61: Update $P_{ij} = P_{ij} - P_{ij}^{met}$
62: **if** ($T_{ij}^{c} \leq T_{ij}^{d}$) **then**
63: $T_{new} = T_{ij}^{c}$
64: **else**
65: $T_{new} = T_{ij}^{d}$
66: **end if**
67: **end while**

n number of CSs using Eq. (3.13). After this, $E_{ij}^{tot,char}$ and $E_{ij}^{tot,dis}$ are computed for all EVs available at the j^{th} CS using Eqs. (3.14)-(3.18). Once these computations are done, a comparison operation is performed on them. If $E_{ij}^{tot,char}$ is less than $E_{ij}^{tot,dis}$, then AG computes all charging parameters (C_{ij}^{rate}, T_{ij}^{c} and P_{ij}^{char}) followed by discharging parameters (P_{ij}^{dis}, D_{ij}^{rate} and T_{ij}^{d}). Otherwise, discharging parameters (D_{ij}^{rate}, T_{ij}^{d} and P_{ij}^{dis}) are computed before charging (P_{ij}^{char}, C_{ij}^{rate} and T_{ij}^{c}) parameters. Computation of these parameters are based

on different equations as mentioned in Algorithm 3.2. Moreover, the algorithm also ensures that C_{ij}^{rate} and D_{ij}^{rate} are always maintained within the maximum permissible limit.

The controller then computes E_{ij}^{char} and E_{ij}^{dis} based on T_{ij}^{c} and T_{ij}^{d} values. These values are computed using Eqs. (3.28) and (3.29) respectively as per the four cases mentioned below.

- **First Case**: This case is chosen when T_{ij}^{d} is zero, i.e, either EVs are not available for discharging at the CS or regulation signal does not permit discharging of EVs. The latter scenario arises whenever P_{ij}^{char} is less than P_{ij} (Lines 23-24). In such cases, E_{ij}^{dis} is set to zero, since T_{ij}^{d} is zero. On the other hand, E_{ij}^{char} is computed at $T_1 = T_2 = T_{ij}^{c}$ (Lines 46-48).

- **Second Case**: This case is similar to first case and is chosen when T_{ij}^{c} is zero. This happens either when EVs are not available for charging at the CS or regulation signal does not permit charging of EVs. The latter scenario arises whenever P_{ij}^{dis} is greater than P_{ij} (Lines 42-43). Here, E_{ij}^{char} is set to zero, while E_{ij}^{dis} is computed using Eq. (3.28) with $T_1 = T_2 = T_{ij}^{d}$ (Lines 49-51).

- **Third Case**: This case is chosen when T_{ij}^{c} is less than or equal to T_{ij}^{d}, i.e, EVs available at the CS support charging and discharging. Here, E_{ij}^{char} is computed at $T_1 = T_2 = T_{ij}^{c}$, while E_{ij}^{dis} is computed at $T_1 = T_{ij}^{c}$ and $T_2 = T_{ij}^{d}$ (Lines 52-54).

- **Fourth Case**: This case is similar to the above case and is chosen when T_{ij}^{d} is less than T_{ij}^{c}. Here, E_{ij}^{dis} is computed at $T_1 = T_2 = T_{ij}^{d}$, while E_{ij}^{char} is computed at $T_1 = T_{ij}^{d}$ and $T_2 = T_{ij}^{c}$ (Lines 55-57).

Based on above computations, E_{k}^{new} and SoC_{k}^{new} are computed for all EV's participating in frequency support using Eqs. (3.30, 3.32) and Eqs. (3.31, 3.33) respectively. Finally, P_{ij}^{met} and P_{ij}^{unmet} are estimated using Eqs. (3.34) and (3.35) respectively. This process is repeated till T or P_{ij} are not exhausted and is illustrated using Fig. 3.3.

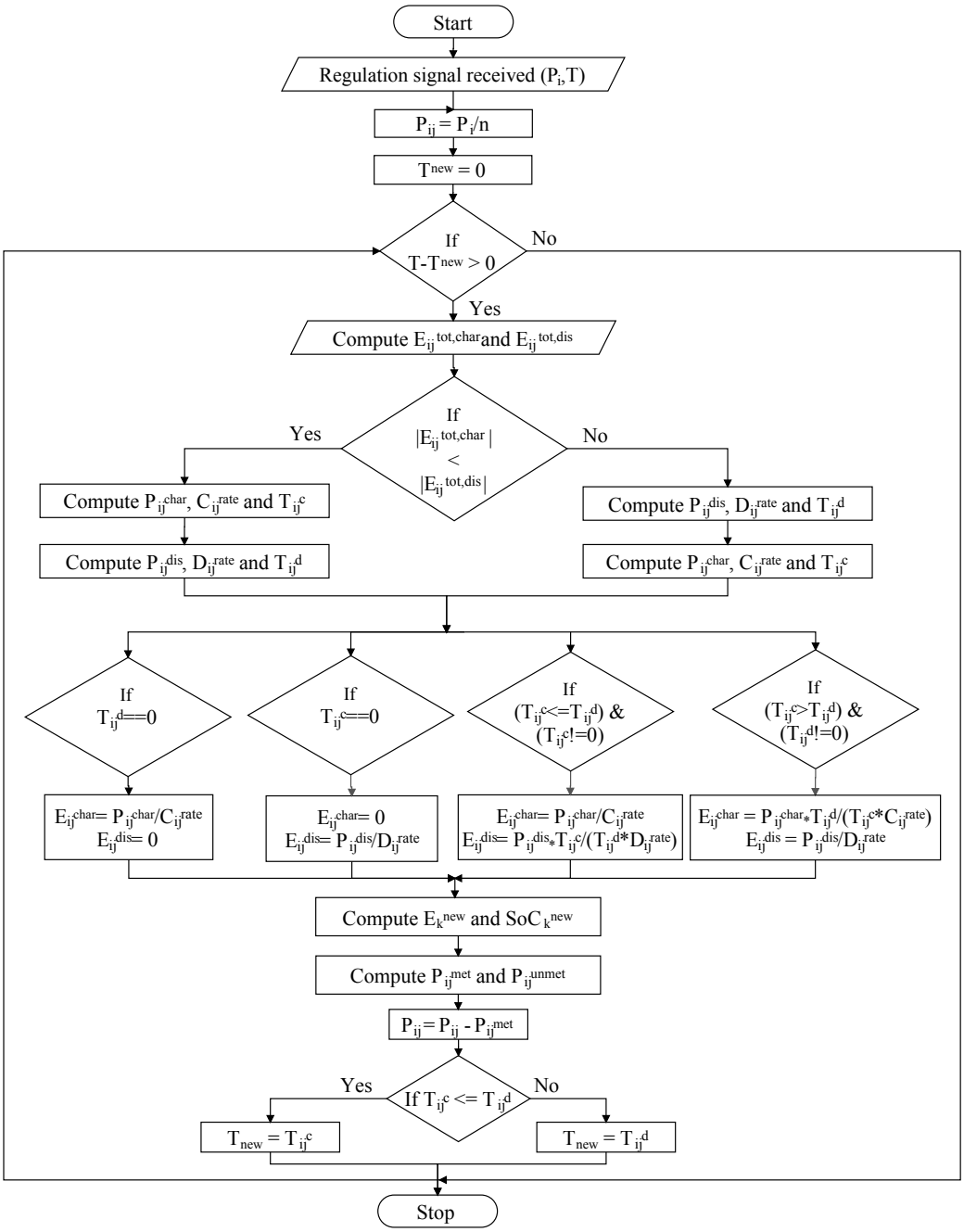

Figure 3.3: Flowchart for the proposed scheme.

3.5 Simulation and Results

This section highlights the simulation and results pertaining to the proposed scheme. For the purpose of implementation of the proposed CPN based controller, a single CS with maximum of 60 EVs at a time, have been assumed for supporting frequency fluctuations. These EVs are considered to be Chevrolet volt EVs having battery capacity of 16 kWh. The minimum and maximum SoC limit of EV's battery is assumed to be 20% and 100% respectively. This assumption has been considered in view of EVs' mobility requirements. Table 3.1 presents the simulation parameters considered in this work. Extensive simulations have been performed in different scenarios on actual power data acquired from Pennsylvania-New Jersey-Maryland (PJM) [143] and Electric Reliability Council of Texas (ERCOT) [144].

Table 3.1: Simulation Parameters.

Parameters	Values
EV's battery capacity	16 kWh
EV's battery voltage	200 V
EV's battery Ah rating	80 Ah
EV's default C_{ij}^{rate}	1
EV's default D_{ij}^{rate}	1
EV's maximum C_{ij}^{rate}	2
EV's maximum D_{ij}^{rate}	2
EV's minimum SoC limit	20%
EV's maximum SoC limit	100%

3.5.1 Case Studies

For the sake of simplicity, the proposed scheme has been evaluated with respect to a single CS on the real-time data obtained from PJM and ERCOT. However, the scheme is extensible to n number of CSs. Moreover, the entire scheme has been simulated for different time intervals (i.e, 1 hour and 15 minutes) in order to justify its effectiveness and relevance in providing frequency support. Thus, two different case studies have been considered in this work and

their related results are summarized as follows.

Case Study I: Frequency support over 1 hour time interval

For the purpose of implementation of this case study, PJM RegA regulation data have been obtained for 1^{st} June, 2014 as depicted in Fig. 3.4a [143]. This figure clearly depicts that grid undergoes several frequency imbalances through out the day. These imbalances either result in excess or deficient power availability at grid level, which are represented in the form of negative and positive regulation signals respectively.

The proposed scheme also manages the dynamics of the number of EVs as depicted in Fig. 3.4b. These EVs have been segregated into 3 broad types, *i.e.*, newly arrived, departing and operative. The EVs which participate in frequency support mechanism since the previous time slot(s), are considered as operative EVs. On the basis of this categorization of EVs, their availability in a particular time slot is computed and are considered by the controller for rendering frequency support. For instance, at 0500 hours, 2 EVs arrived at the CS for charging and exactly 2 EVs departed from the CS after charging their respective batteries. On the other hand, no EVs arrived or departed from the CS for discharging purposes. Furthermore, 28 and 30 operative EVs continued to participate in charging and discharging activities respectively, from the previous time slot(s). Hence, the controller considered total of 28 (28 -2 + 2) and 30 (30 + 0 - 0) EVs for charging and discharging purposes respectively, at the considered CS for the regulation process.

The power imbalances as depicted in Fig. 3.4a, are catered by the available EVs at the CS while catering their energy demands. The number of EVs participating in charging and discharging activities at CS are shown in Fig. 3.4c. The CPN based controller reconfigures EVs' respective C_{ij}^{rate} and D_{ij}^{rate} to manage frequency imbalances using Eqs. (3.20) and (3.21) respectively. These rates are balanced in such a manner that EVs' charging and discharging

needs are also catered while re-balancing the frequency imbalances. Fig. 3.4d reflects EVs' regulated C_{ij}^{rate} and D_{ij}^{rate}. For example, at 0500 hours, C_{ij}^{rate} of EVs seeking charging was doubled, while D_{ij}^{rate} of rest of the EVs was left unchanged, so as to manage the frequency imbalances.

As a result of these modifications in rates, P_{ij}^{char} and P_{ij}^{dis} is also affected to a larger extent as per Eqs. (3.22)-(3.25). These changes are depicted in Fig. 3.4e along with unregulated cumulative powers for charging and discharging. For instance, at 0500 hours, the unregulated cumulative charging and discharging power of available EVs were -314.72 and 233.76 kW respectively. Thus, the cumulative power drawn by EVs was merely -80.96 kW (-314.72 + 233.76 = -80.96 kW). This in turn, would not have been sufficient to manage the frequency deviations and support the current regulation signal of -486.26 kW. Therefore, the proposed controller alters the C_{rate} and D_{rate} of participating EVs. Due to these changes, P_{ij}^{char} that was drawn by EVs was almost doubled, while their P_{ij}^{dis} remained the same. The overall variations in these powers at different intervals of time due to variations in C_{ij}^{rate} and D_{ij}^{rate} are depicted in Fig. 3.4e.

Apart from managing the frequency deviations at CS level, the proposed scheme also caters the charging and discharging requirements of participating EVs in accordance with Eqs. (3.31) and (3.33) respectively. This is clearly highlighted in Fig. 3.4f, where average SoC of EVs across different slots have been depicted. For instance, at 0500 hours, average SoC of EVs which approached for charging and discharging were 31.1% and 75.3% respectively. After providing frequency support, the average SoC of EVs seeking charging increased up to 100%, whereas, those which approached for discharging were left with 44.9%.

Thus, the overall power requirements which were managed by involving fleets of EVs at the CS, are shown in Fig. 3.4g. Moreover, this figure also reflects the amount of power which was not met during regulation process. For instance, at 0500 hours P_{ij}^{met} and P_{ij}^{unmet}

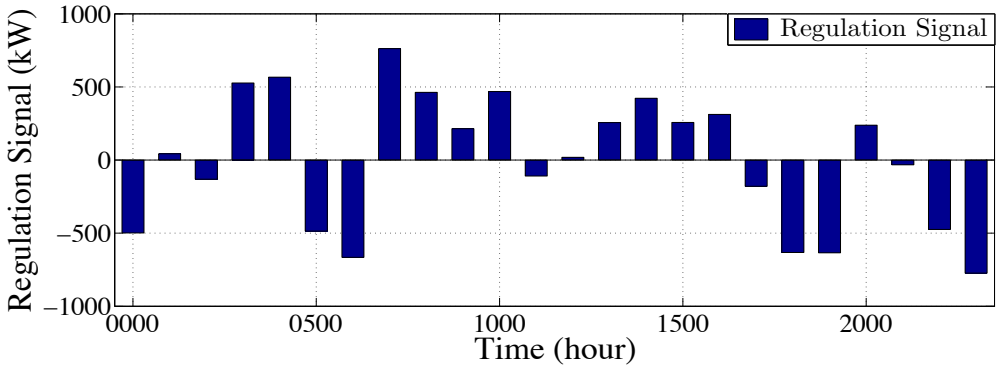

3.4(a) RegA power regulation signal data on 1st June 2014 acquired from PJM.

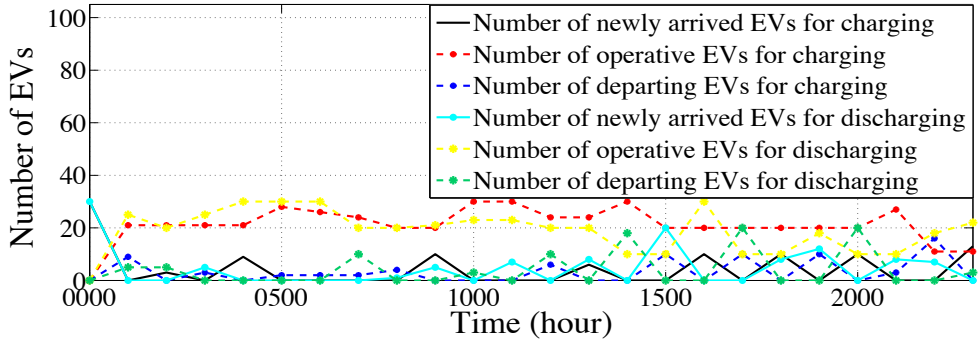

3.4(b) Dynamics involved with mobility of EVs participating for frequency support.

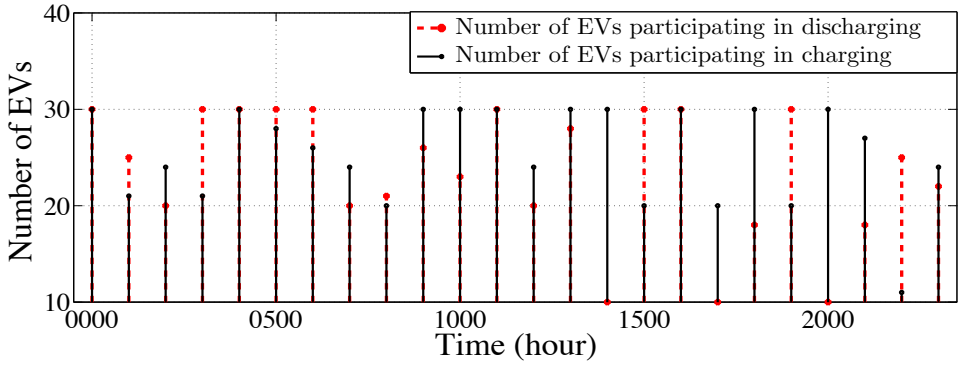

3.4(c) Number of EVs participating for frequency support.

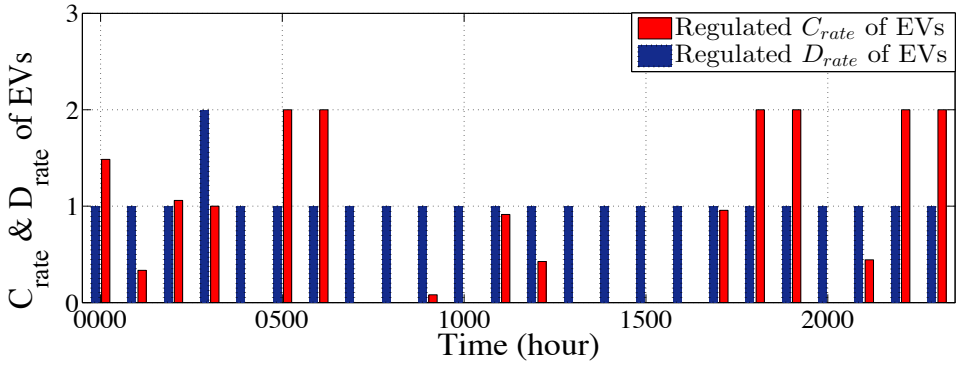

3.4(d) Regulated charging and discharging rates of EVs for frequency support.

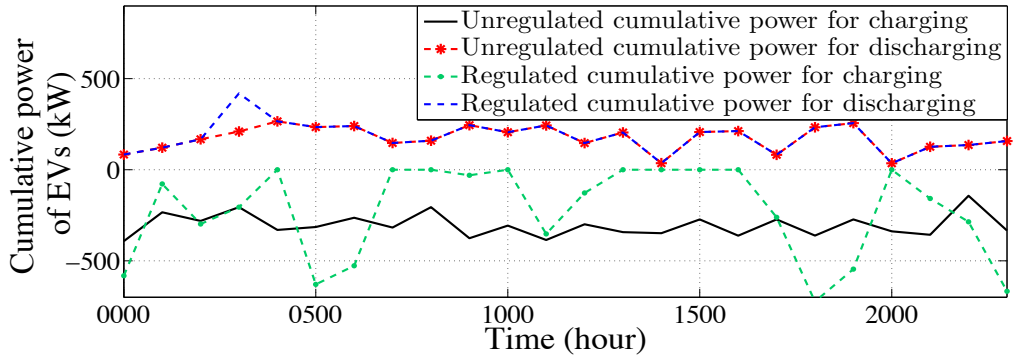

3.4(e) Regulated and unregulated charging and discharging power of EVs for frequency support.

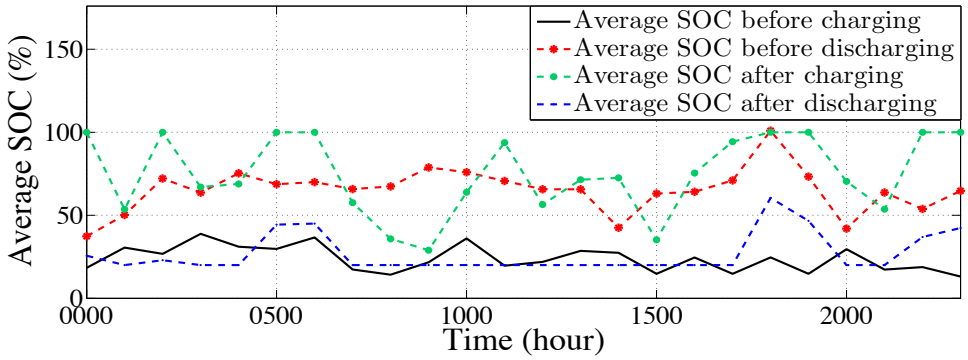

3.4(f) Average SoC comparison of EVs before and after charging and discharging.

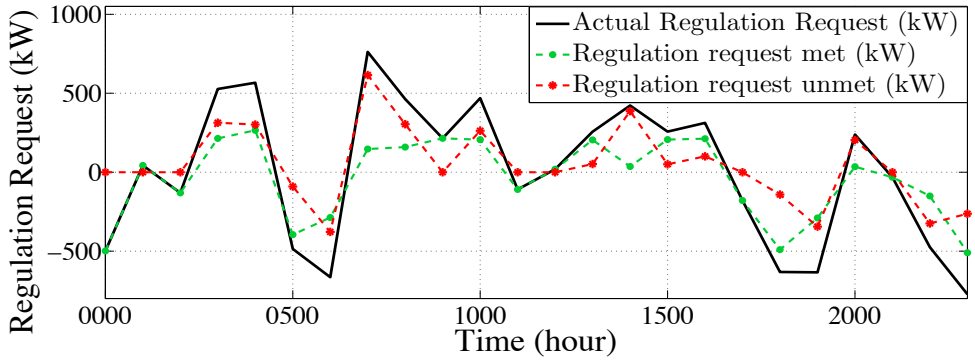

3.4(g) Regulation power met and unmet by the proposed scheme.

Figure 3.4: Case Study I: Frequency support over 1 hour time interval.

were -395.68 kW and -90.581 kW respectively. Increased values of P_{ij}^{unmet} are caused due to EVs' scarcity at the CS. This has been justified in the next case study where regulation signals are received for comparatively shorter duration of time than in this case. In order to avoid discrepancy in the results, same number of EVs have been considered in both the scenarios,

with exactly same SoC level.

Case Study II: Frequency support over 15 minutes time interval

In this case, power regulation data from ERCOT for a particular day has been considered. For the purpose of simulating the scheme at a single CS, this data has been scaled down as shown in Fig. 3.5a. The regulation signals are received after every 15 minutes and four random hours have been considered as highlighted in the figure.

Fig. 3.5b depicts the controller regulated C_{ij}^{rate} and D_{ij}^{rate} based on P_i signals received across different time intervals. These regulated rates affect P_{ij}^{char} and P_{ij}^{dis} as depicted in Fig. 3.5c. For instance, at 1500 hours, D_{ij}^{rate} of EVs seeking charging was 1, while C_{ij}^{rate} of rest of the EVs was nearly zero. Due to these changes, P_{ij}^{dis} that was discharged by EVs was almost same as their unregulated power, while P_{ij}^{char} was reduced to zero.

Participation of EVs at the CS for frequency support not only re-balances the frequency deviations, but also helps in meeting EVs' energy requirements. These results are evident from the Fig. 3.5d and have been obtained using Eqs. (3.31) and (3.33). For example, at 1500 hours, the average SoC of EVs seeking charging before and after frequency support remained same as their C_{ij}^{rate} was zero. On the other hand, average SoC of EVs seeking discharging was reduced to 20, *i.e.*, EVs were fully discharged after providing frequency support.

Fig. 3.5e depicts the relation between P_{ij}, P_{ij}^{met} and P_{ij}^{unmet}. These results have been obtained using Eqs. (3.34)-(3.35). For instance, at 1500 hours, P_{ij} was 113.3 kW which was fully met using the proposed scheme.

3.5.2 Comparison and Discussions

This segment presents an elaborated comparison of the proposed scheme with an existing V2G control strategy which is proposed by Liu *et al.* [74]. For the purpose of this analysis,

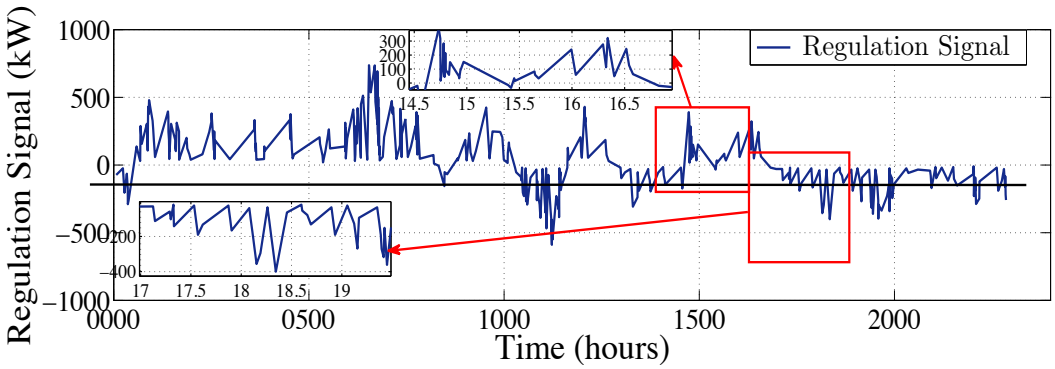

3.5(a) Regulation power signal data acquired from ERCOT.

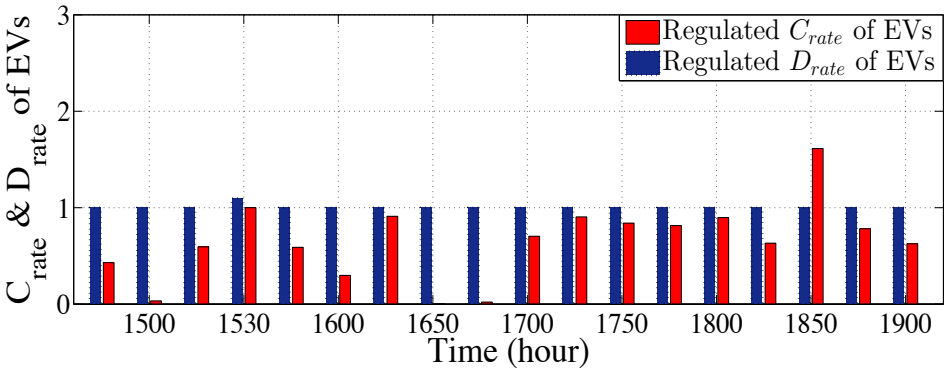

3.5(b) Regulated charging and discharging rates of EVs for frequency support.

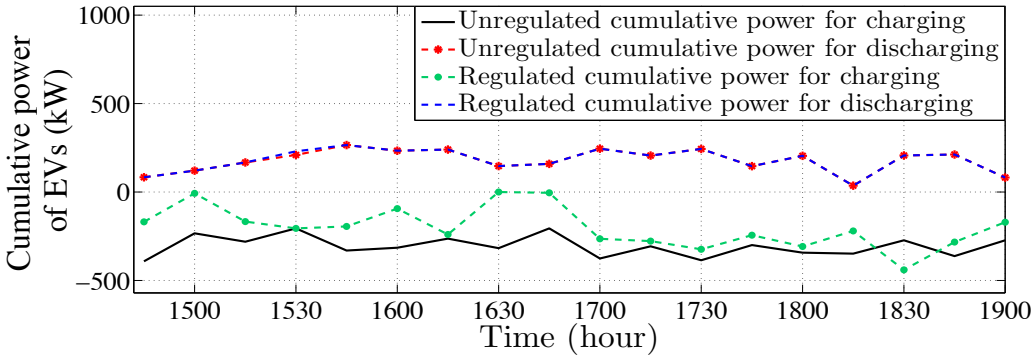

3.5(c) Regulated/unregulated charging and discharging power of EVs for frequency support.

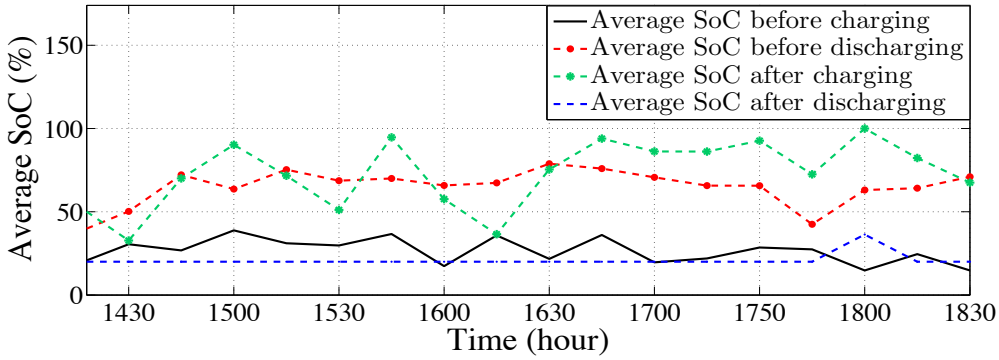

3.5(d) Average SoC comparison of EVs before and after charging and discharging.

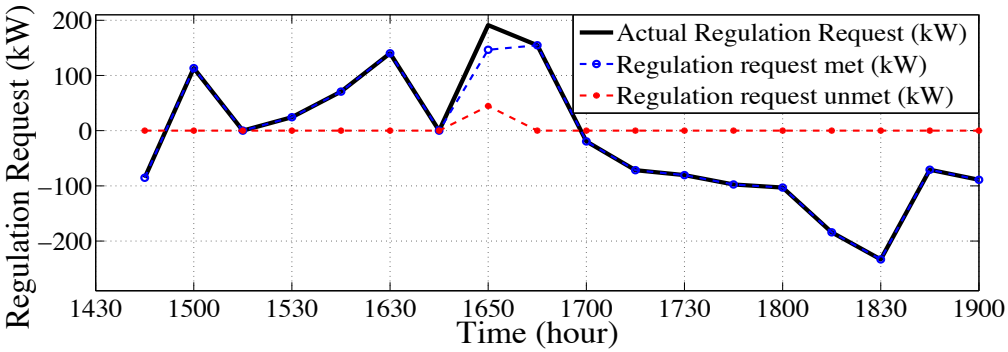

3.5(e) Regulation power met and unmet by the proposed scheme.

Figure 3.5: Case Study II: Frequency support over 15 minutes time interval.

real time PJM RegA regulation data as depicted in Fig. 3.4a have been considered. In addition to this, random number of EVs with battery capacity of 32 kW, have been considered for effective validation of both the schemes. The C_{rate} and D_{rate} of these EVs are assumed to be confined within the range of 0 to 1 for both the schemes. Extensive simulations have been performed for 24 hours with respect to varying regulation signals received at the CS level.

The amount of regulation power met during frequency support by both the schemes differs widely, due to their respective underlying methodologies. In the existing scheme [74], the regulation capacity of the participating EVs is comparatively less than the proposed scheme. This is because of the limitation imposed on the participating EVs' maximum V2G power (upto 7 kW), that can be supported by the individual EVs. Hence, the cumulative power that can be drawn or delivered by the EVs at the CS is relatively less. Apart from this, the proposed scheme is based on top-down approach which manages the received regulation signals by regulating the C_{rate} and D_{rate} of participating EVs. On the other hand, the existing scheme is based on bottom-up approach which accepts the regulation signal only if it's in accordance with the available EVs' capacity. For instance, at 1500 hours, regulation signal of 256.97 kW was generated, as shown in Fig. 3.6a. Accordingly, total power of 7.97 kW only was delivered by the participating EVs using the existing scheme, while the proposed scheme

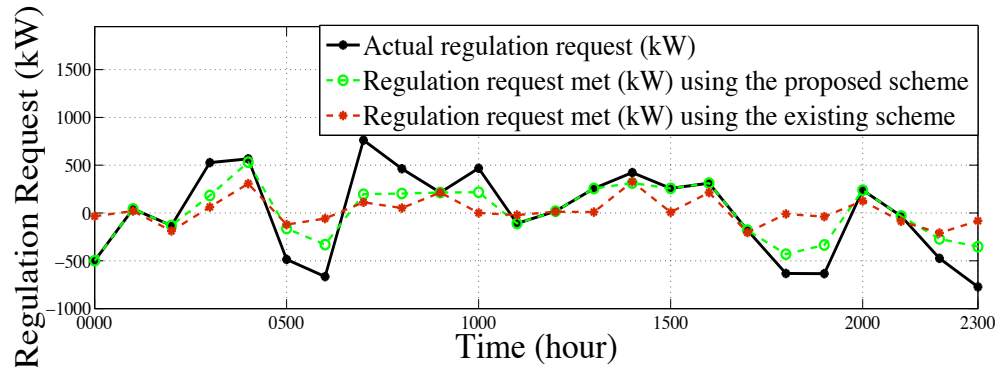

3.6(a) Regulation power met using the two schemes.

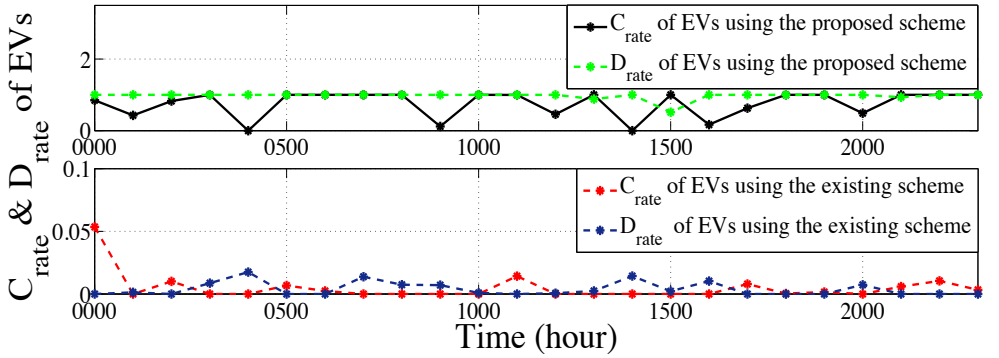

3.6(b) C_{rate} and D_{rate} comparison between the proposed and existing scheme.

Figure 3.6: Comparison of the proposed frequency support scheme with Liu *et al.*'s scheme.

exactly met the regulation signal.

In addition to this, the extent up to which EVs are charged or discharged also varies amongst the two schemes, as evident from Fig. 3.6b. For instance, at 1500 hours, the average C_{rate} and D_{rate} of participating EVs were 1 and 0.51 respectively, using the proposed scheme. On the other hand, Liu *et al.*'s scheme supported only discharging of participating EVs at 0.0022 D_{rate}. These results directly indicate that the existing scheme does not provide simultaneous charging and discharging of EVs unlike the proposed scheme. Moreover, it provides relatively reduced C_{rate} and D_{rate}. Hence, it can be inferred from the above discussions that the proposed scheme is both grid centric and user centric, as it provides adequate frequency support while catering EVs' energy requirements.

3.6 Concluding Remarks

In this chapter, a Colored Petri Net based frequency support scheme has been proposed based on hierarchical control mechanism. It pays special attention to EV's bidirectional V2G support while keeping a check on grid frequency fluctuations. In the next chapter, another hierarchical control scheme is proposed which provides adequate frequency support using fleet of EVs.

Chapter 4

Frequency Support using Electric Vehicles with an Aggregator-based Hierarchical Control Mechanism

In this chapter, an *"Aggregator-based Hierarchical Control Mechanism"* comprising of different controllers for reliable grid frequency support has been proposed. The mechanism exploits fleet of EVs to cater frequency deviations at grid level; while providing bi-directional V2G support and minimizing EV's battery degradation. For this purpose, a Multiobjective Primal Problem (Mo-PP) with multiple constraints has been designed. Additionally, an approximate solution has been formulated by decomposing the complex Mo-PP into sub-problem (SPs). The detailed working of the proposed mechanism along with its system framework is mentioned as follows.

4.1 System Framework

This section describes the details of the proposed *"Aggregator-based Hierarchical Control Mechanism"* for efficient frequency support using fleet of EVs.

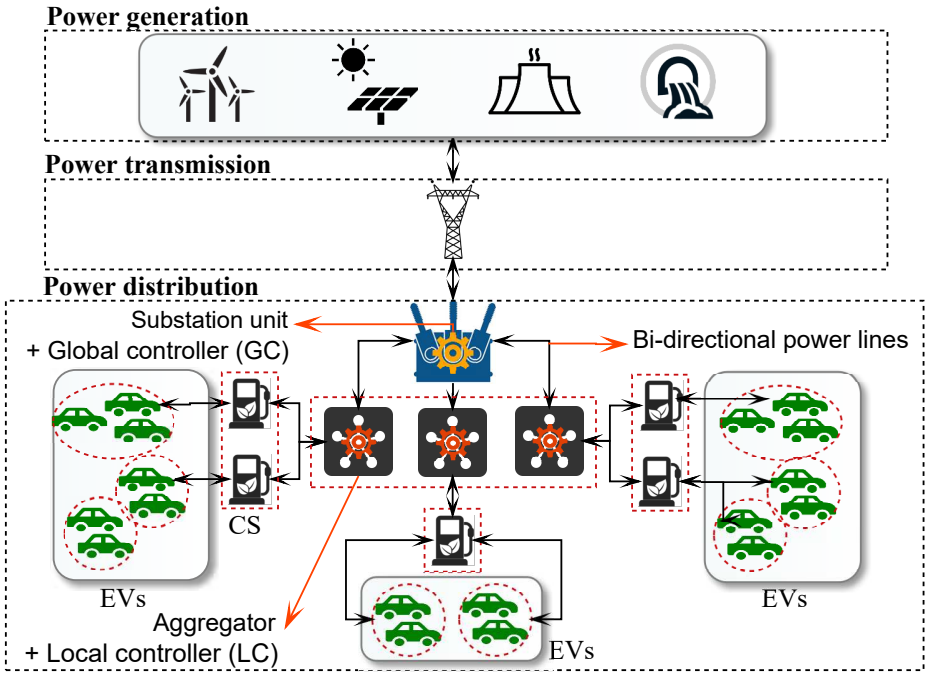

Figure 4.1: System framework of the considered V2G setup.

Consider the system setup as depicted in Fig. 4.1 which comprises of different physical entities such as-substation unit (SU), AGs, CSs and EVs; to support bidirectional V2G operations. In this setup, $\mathscr{M}$ number of aggregators $AG_i = \{AG_1, AG_2, ...AG_m\}$ and $\mathscr{N}$ number of charging stations $CS_{ij} = \{CS_{11}, CS_{12}, ...CS_{mn}\}$ have been considered. Here, AG_i represents the i^{th} AG under reference, while CS_{ij} denotes the j^{th} CS under the control of i^{th} AG. Moreover, k_j number of EVs are assumed to be available at different *CS*s for fulfilling their energy needs. Among these entities, the most important role is played by the AG and SU. Here, AG acts as an interface between the EVs and SG. On the other hand, the SU acts as the central unit that regulates various operations at the grid level. In order to effectively

involve EVs in the overall frequency regulation process, CSs are assumed to be equipped with certain hardware equipments namely plug-in spot, energy meter and communication module [145]. The bi-directional V2G support to and fro the EV and AC bus (of the SG) is provided by the plug-in spot. It's further associated with an energy meter which keeps track of the amount of power dispatched or consumed by an EV in a particular time interval. This information is communicated by the communication module at the CS level to the AG for further processing. The considered CSs equipped with sophisticated hardware equipments are assumed to be available at different commercial locations such as-offices, shopping malls, parking lots, onside roads, etc [46].

Being hierarchical, the proposed scheme comprises primarily of two types of controllers, namely Global Controller (GC) and Local Controller (LC). The deployment of these controllers is in accordance with the different physical entities as depicted in the Fig. 4.2. For instance, GC is deployed at the SU which continuously monitors the frequency imbalances and the related regulation signals at the grid level. These regulation signals can either be of positive or negative types; wherein the positive signals encourage EV's discharging (Regulation up), while the negative signals demand EV's charging (Regulation down) for re-balancing the demand-supply imbalances. Furthermore, GC also maintains the real-time information of EVs, CSs and AGs. The information comprising of EV's initial SoC levels, EV's charging or discharging needs and FRCs of CSs is estimated using LCs placed at the AGs. Using this information, the GC and LCs dispatch the regulation signals among the AGs and CSs respectively. Following this, LCs generate the charging and discharging schedule for EVs by regulating their rates. This process helps to caters EV's energy demands, while simultaneously providing effective frequency support. This entire process involves the flow of information between the controllers, and is supported by wired and wireless communication standards. These standards are Power Line Communication (PLC), Ethernet, optical fibres to IEEE

802.11, IEEE 802.15 and IEEE 802.16 [146–148].

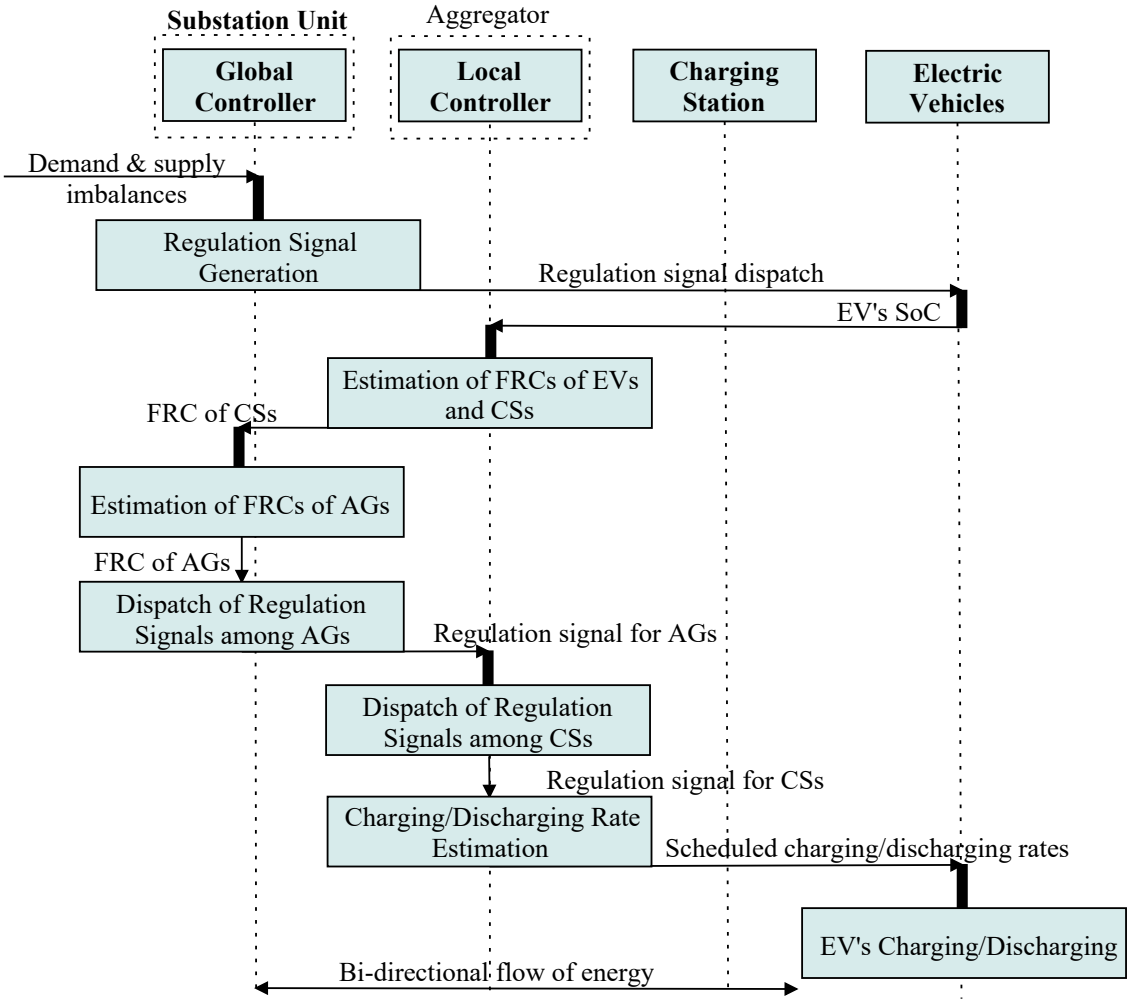

Figure 4.2: Schematic overview of the proposed scheme.

4.2 Problem Formulation

This section provides the mathematical background of the problem under consideration followed by the detailed discussion of the related objectives and constraints.

4.2.1 Problem Definition

In the considered V2G setup, it's important to manage frequency deviations ($\mathbb{F}_1(x)$) while proportionally dispatching the regulation signal ($\mathbb{F}_2(x)$ and $\mathbb{F}_3(x)$) in accordance with the FRCs of the AGs and CSs. On the other hand, it is necessary to guarantee customer's energy requirements while minimizing the impact on EVs' batteries ($\mathbb{F}_4(x)$). These objectives can be expressed using the following Mo-PP:

$$\min \mathbb{F}(x) = f(\mathbb{F}_1(x), \mathbb{F}_2(x), \mathbb{F}_3(x), -\mathbb{F}_4(x)) \tag{4.1}$$

$$s.t. \begin{cases} x \in S \end{cases}$$

The above mentioned Mo-PP can be viewed as a complex problem having multiple objectives ($\mathbb{F}_1(x), \mathbb{F}_2(x), \mathbb{F}_3(x)$, and $\mathbb{F}_4(x)$) under different constraints; wherein $\mathbb{F}(x)$ is the overall multi-objective function under consideration. Variable x denotes the optimal solution which belongs to the available set of solutions (S).

The next segment illustrates some preliminary details which are useful in understanding the considered constraints and objective functions.

4.2.2 Preliminary Details

Power Consumption of EVs' batteries

LCs compute the SoC required for charging ($SoC^c_{ijk}(t)$) and discharging ($SoC^d_{ijk}(t)$) EVs' batteries, across all CSs. These computations are done using the following equations at time

instant t as follows:

$$SoC^{c}_{ijk}(t) = SoC^{max} - SoC^{c,ini}_{ijk}(t); \forall i,j,k \tag{4.2}$$

$$SoC^{d}_{ijk}(t) = SoC^{d,ini}_{ijk}(t) - SoC^{min}; \forall i,j,k \tag{4.3}$$

Eq. (4.2) is used to compute the SoC required for charging an EV at t. Here, $SoC^{c}_{ijk}(t)$ denotes the SoC required for charging the k^{th} EV available at the j^{th} CS of the i^{th} AG, at time t. It is based on the maximum SoC limit of the EV's battery (SoC^{max}) and initial SoC level of the EV seeking charging ($SoC^{c,ini}_{ijk}(t)$). Similarly, Eq. (4.3) estimates the SoC that the k^{th} EV can discharge at t while maintaining its minimum SoC requirement (SoC^{min}). Here, $SoC^{d,ini}_{ijk}(t)$ represents the initial SoC of the k^{th} EV seeking discharging and available at the j^{th} CS of the i^{th} AG.

LCs then compute the cumulative power required for charging ($P^{c}_{ijk}(t)$) and discharging ($P^{d}_{ijk}(t)$) with respect to EVs available at the j^{th} CS. It is computed in accordance with following equations:

$$\begin{cases} P^{c}_{ijk}(t) & = \dfrac{-SoC^{c}_{ijk}(t) \times E^{rated}_{ijk}}{100 \times T} \\ P^{d}_{ijk}(t) & = \dfrac{SoC^{d}_{ijk}(t) \times E^{rated}_{ijk}}{100 \times T} \\ P^{est}_{ijk}(t) & \in \{P^{c}_{ij}(t), P^{d}_{ij}(t)\}; \forall i,j,k \end{cases} \tag{4.4}$$

In the above equations, the estimated power values, *i.e.*, $P^{c}_{ijk}(t)$ and $P^{d}_{ijk}(t)$ are cumulatively represented using the variable $P^{est}_{ijk}(t)$. Also, E^{rated}_{ijk} denotes the user defined energy rated capacity of k^{th} EV while T represents the time period (in hours) for which frequency support needs to be provided by the participating EVs.

These power capacities of the EVs can be maximized ($P^{c,max}_{ijk}(t)$ and $P^{d,max}_{ijk}(t)$) by alter-

ing the charging ($C_{ijk}(t)$) and discharging rates ($D_{ijk}(t)$) of the EVs' batteries to provide instantaneous frequency support. This is achieved as per the following equations.

$$\begin{cases} P_{ijk}^{c,max}(t) & = \dfrac{-SoC_{ijk}^{c}(t) \times E_{ijk}^{rated} \times C_{ijk}^{max}}{100} \\ P_{ijk}^{d,max}(t) & = \dfrac{SoC_{ijk}^{d}(t) \times E_{ijk}^{rated} \times D_{ijk}^{max}}{100} \\ P_{ijk}^{est,max}(t) & \in \{P_{ijk}^{c,max}(t), P_{ijk}^{d,max}(t)\}; \forall i,j,k \end{cases} \tag{4.5}$$

where, the parameters C_{ijk}^{max} and D_{ijk}^{max} are the maximum allowed charging and discharging rates respectively. The estimated values of $P_{ijk}^{c,max}(t)$ and $P_{ijk}^{d,max}(t)$ are referred using the variable $P_{ijk}^{est,max}(t)$.

Frequency Regulation Capacities of AGs and CSs

The aggregated power capacities for charging ($P_{ij}^{c}(t)$) and discharging ($P_{ij}^{d}(t)$) are estimated across all the CSs as follows.

$$\begin{cases} P_{ij}^{c}(t) & = \sum\limits_{k \in k_j} P_{ijk}^{c}(t) \\ P_{ij}^{d}(t) & = \sum\limits_{k \in k_j} P_{ijk}^{d}(t) \\ P_{ij}^{est}(t) & \in \{P_{ij}^{c}(t), P_{ij}^{d}(t)\}; \forall i,j \end{cases} \tag{4.6}$$

For the sake of simplicity, these terms are referred to as FRCs of the CSs throughout the text and cumulatively expressed using the variable $P_{ij}^{est}(t)$; wherein $P_{ij}^{est}(t)$ represents the estimated FRC of the j^{th} CS under i^{th} AG at t. Additionally, their corresponding maximum

limits ($P_{ij}^{est,max}(t)$) are estimated in accordance with the following equations.

$$\begin{cases} P_{ij}^{c,max}(t) & = \sum\limits_{k \in k_j} P_{ijk}^{c,max}(t) \\ P_{ij}^{d,max}(t) & = \sum\limits_{k \in k_j} P_{ijk}^{d,max}(t) \\ P_{ij}^{est,max}(t) & \in \{P_{ij}^{c,max}(t), P_{ij}^{d,max}(t)\}; \forall i, j \end{cases} \tag{4.7}$$

On the similar lines, the GC keeps track of the FRCs of the AGs ($P_i^{est}(t)$) as per the following set of equations.

$$\begin{cases} P_i^{c}(t) & = \sum\limits_{j \in \mathcal{N}} P_{ij}^{c}(t) \\ P_i^{d}(t) & = \sum\limits_{j \in \mathcal{N}} P_{ij}^{d}(t) \\ P_i^{est}(t) & \in \{P_i^{c}(t), P_i^{d}(t)\}; \forall i \end{cases} \tag{4.8}$$

Further, the maximum counterparts of $P_i^{est}(t)$, *i.e.*, $P_i^{est,max}(t)$ are estimated as below.

$$\begin{cases} P_i^{c,max}(t) & = \sum\limits_{j \in \mathcal{N}} P_{ij}^{c,max}(t) \\ P_i^{d,max}(t) & = \sum\limits_{j \in \mathcal{N}} P_{ij}^{d,max}(t) \\ P_i^{est,max}(t) & \in \{P_i^{c,max}(t), P_i^{d,max}(t)\}; \forall i \end{cases} \tag{4.9}$$

4.2.3 List of Constraints

Reference Signal Constraints

Let $\mathfrak{R}_i^{ref,sch}(t)$ denote the reference signal scheduled by the proposed scheme for the i^{th} AG at t time instant. The below mentioned constraint represents the upper and lower bounds on

$\mathfrak{R}_i^{ref,sch}(t)$.

$$0 \leq \mathfrak{R}_i^{ref,sch}(t) \leq \max\{P_i^{est}(t) + \frac{(f - f_0)}{R}, P_i^{est,max}(t)\}; \forall i \tag{4.10}$$

The above mentioned constraint ensures that the AGs are never assigned regulation signals beyond their respective FRCs (*i.e.*, over-utilized). Moreover, it also guarantees that AGs are neither left without utilization by dispatching them too little or no regulation signal (*i.e.*, under-utilized). In other words, power capacity-based proportionate dispatch of regulation signals helps to build a stable and reliable system. Hence, $\mathfrak{R}_i^{ref,sch}(t)$ is maintained within the reasonable limits wherein, the right hand side of equation selects the optimal choice between $P_i^{est}(t) + \frac{(f - f_0)}{R}$ and $P_i^{est,max}(t)$. Here, the later denotes the maximum available FRC of AG under consideration (estimated using Eq. (4.9)). On the other hand, the former term represents the reference signal computation using droop control mechanism as highlighted using the below mentioned equation.

$$R = \left(\frac{\Delta f}{\Delta P}\right) = \left(\frac{f - f_0}{P - P_0}\right) \tag{4.11}$$

where, frequency droop constant (R) is defined as the change in frequency with respect to change in power. In the above equation, Δf and ΔP denote the change in system frequency and power respectively. The symbols f_0 and P_0 represent system's nominal frequency and nominal power capacity. Further, f and P refer to the new operating frequency and power of the system under consideration.

On the similar lines, the estimation of the scheduled reference signals for the CSs ($\mathfrak{R}_{ij}^{ref,sch}(t)$) is also done. The below mentioned equation highlights the related constraint. It helps in maintaining and dispatching the reference signals among the CSs according to their

respective FRCs and utilizing them in the most efficient manner.

$$0 \leq \Re_{ij}^{ref,sch}(t) \leq \max\{P_{ij}^{est}(t) + \frac{(f - f_0)}{R}, P_{ij}^{est,max}(t)\}; \forall i, j \tag{4.12}$$

EVs' Charging and Discharging Constraints

The proposed scheme also ensures that the scheduled charging and discharging powers of individual EVs ($P_{ijk}^{c,sch}(t)$ and $P_{ijk}^{d,sch}(t)$) always fall in the permissible range. The following constraints depict the same.

$$P_{ijk}^{c,sch}(t) \leq P_{ijk}^{c,max}(t); \forall i, j, k \tag{4.13}$$

$$P_{ijk}^{d,sch}(t) \leq P_{ijk}^{d,max}(t); \forall i, j, k \tag{4.14}$$

where, $P_{ijk}^{c,max}(t)$ and $P_{ijk}^{d,max}(t)$ are the maximum FRCs of the k^{th} EV available at the j^{th} CS of the i^{th} AG. The commutation of these parameters is done in accordance with C_{ijk}^{max} and D_{ijk}^{max} respectively using Eq. (4.5).

EV's Battery Degradation Constraints

In addition to the above constraints, the proposed scheme also ensures that it minimizes the impact of charging and discharging cycles on EVs' batteries. For achieving the same, it takes into account the following three key-points (KPs).

•*KP 1-Charging and discharging rate regulation:* Alerting the charging and discharging rates of the participating EVs is an important technique for providing instantaneous frequency support. However, the same can lead to battery depletion if left unmanaged [149]. Hence, the proposed scheme ensures the same by imposing an upper limit on $C_{ijk}(t)$ and $D_{ijk}(t)$.

The same is reflected using the following two equations wherein, C_{ijk}^{max} and D_{ijk}^{max} denote the maximum rate limits up-to which EVs can be charged or discharged.

$$C_{ijk}(t) \leq C_{ijk}^{max}; \forall i, j, k \tag{4.15}$$

$$D_{ijk}(t) \leq D_{ijk}^{max}; \forall i, j, k \tag{4.16}$$

•*KP 2-State of charge regulation:* According to [52], EVs' batteries should be neither be fully charged nor completely depleted to follow the random regulation signal. Preventing the same can help to prolong the battery's overall life time. Hence, the same has been taken care of, using the following constraint.

$$SoC_{ijk}^{cur}(t) \leq SoC^{max}; \forall i, j, k \tag{4.17}$$

$$SoC_{ijk}^{cur}(t) \geq SoC^{min}; \forall i, j, k \tag{4.18}$$

In the above equations, the current SoC levels of EVs' batteries ($SoC_{ijk}^{cur}(t)$) is always maintained within the permissible range of SoC^{min} and SoC^{max}.

•*KP 3-Segregation of EVs into interactive and non-interactive modes:* In addition to the above constraints, the proposed scheme also helps to segregate the EVs into interactive and non-interactive types. This segregation of EVs helps to prevent battery degradation by always maintaining $SoC_{ijk}^{cur}(t)$ within the reasonable limits. In other words, it decides whether to involve a particular EV in V2G operations or not based on its battery condition. This is achieved by always keeping $SoC_{ijk}^{cur}(t)$ in accordance with the following boundaries [150].

$$SoC_{ijk}^{cur}(t) \leq SoC^{th} + \left(SoC^{max} - SoC^{th}\right) \times \mathfrak{S}_{ijk}(t) \tag{4.19}$$

$$SoC_{ijk}^{cur}(t) \geq SoC^{min} + \left(SoC^{th} - SoC^{min}\right) \times \mathfrak{S}_{ijk}(t) \tag{4.20}$$

here, SoC^{th} represents the threshold SoC value for EVs' batteries. Observance of these boundaries sets the value of the status variable ($\mathfrak{S}_{ijk}(t)$) to 1, *i.e.*, considered EV is in interactive mode and can participate in V2G operations. On the other hand, any violations of these constraints sets $\mathfrak{S}_{ijk}(t)$ to 0. Thereby, preventing the EV from participating in frequency support, *i.e.*, non-interactive mode; as depicted below.

$$\mathfrak{S}_{ijk}(t) = \begin{cases} 1, \text{ If } k^{th} \text{ EV is set to interactive mode} \\ 0, \text{ otherwise.} \end{cases}$$

4.2.4 List of Objective Functions

Minimization of grid frequency deviations

This objective function deals with maintaining the trade-off between fulfilling EVs' energy demands and providing maximum grid support (in terms of minimizing frequency deviations) using the available FRCs of the EVs. This is achieved in accordance with the following objective function ($\mathbb{F}_1$) and constraints.

$$\min \mathbb{F}_1 = \left(\mathfrak{R}^{ref}(t) - \sum_{i \in \mathscr{M}} \sum_{j \in \mathscr{N}} \sum_{k \in k_j} P^{sch}_{ijk}(t) \times \mathfrak{T}_{ijk}(t) \times \mathfrak{S}_{ijk}(t) \right)$$

$$s.t. \begin{cases} P^{sch}_{ijk}(t) = (P^{c,sch}_{ijk}(t) + P^{d,sch}_{ijk}(t)) \\ P^{c,sch}_{ijk}(t) = -SoC^{c}_{ijk}(t) \times E^{rated}_{ijk} \times C^{sch}_{ijk}(t)/100 \\ P^{d,sch}_{ijk}(t) = SoC^{d}_{ijk}(t) \times E^{rated}_{ijk} \times D^{sch}_{ijk}(t)/100 \\ \sum_{i \in \mathscr{M}} \sum_{j \in \mathscr{N}} \sum_{k \in k_j} (P^{c,sch}_{ijk}(t) + P^{d,sch}_{ijk}(t)) \times \mathfrak{T}_{ijk}(t) \times \mathfrak{S}_{ijk}(t) \leq \mathfrak{R}^{ref}(t) \\ \mathfrak{T}_{ijk}(t) \in 0,1; \forall i,j,k \\ \mathfrak{S}_{ijk}(t) \in 0,1; \forall i,j,k \end{cases}$$

$$s.t. \begin{cases} \text{Eqs. } (4.13) - (4.14) \end{cases}$$

The first constraint estimates the value of $P_{ijk}^{sch}(t)$ as the sum of $P_{ijk}^{c,sch}(t)$ and $P_{ijk}^{d,sch}(t)$. The next two constraints estimate the values $P_{ijk}^{c,sch}(t)$ and $P_{ijk}^{d,sch}(t)$ by adjusting the scheduled charging ($C_{ijk}^{sch}(t)$) and discharging ($D_{ijk}^{sch}(t)$) rates of the participating EVs. The fourth constraint ensures that the accumulated V2G power provided/drawn by the participating EVs does not exceed the reference signal ($\mathfrak{R}^{ref}(t)$). Additionally, fifth constraint provides the integrality restriction on $\mathfrak{T}_{ijk}(t)$, wherein, it marks the binary decision variable and is defined as follows:

$$\mathfrak{T}_{ijk}(t) = \begin{cases} 1, \text{ If } k^{th} \text{ EV is scheduled for V2G support} \\ 0, \text{ otherwise.} \end{cases}$$

Similarly, sixth constraint imposes the integrality restriction on $\mathfrak{S}_{ijk}(t)$ as defined earlier. The other constraints as depicted using Eqs. (4.13)-(4.14) impose the upper limit on the scheduled power used for charging and discharging EVs' batteries.

Optimal regulation signal dispatch among AGs

This problem deals with optimal segregation of the $\mathfrak{R}^{ref}(t)$ among the AGs in accordance with their respective FRCs (Eqs. (4.8) and (4.9)) and conventional droop mechanism as illustrated below.

$$\min \mathbb{F}_2 = \left(\mathfrak{R}^{ref}(t) - \{\mathfrak{R}_1^{ref,sch}(t) + ... + \mathfrak{R}_m^{ref,sch}(t)\}\right)$$
$$\implies \mathbb{F}_2 = \left(\mathfrak{R}^{ref}(t) - \sum_{i \in \mathscr{M}} \mathfrak{R}_i^{ref,sch}(t)\right)$$

$$s.t. \begin{cases} \sum_{i \in \mathscr{M}} \mathfrak{R}_i^{ref,sch}(t) \leq \mathfrak{R}^{ref}(t) \\ \text{Eq. (4.10)} \end{cases}$$

In the above objective function ($\mathbb{F}_2$), parameter $\mathfrak{R}_i^{ref,sch}(t)$ is the real-valued decision variable under consideration, wherein the overall objective of $\mathbb{F}_2$ is to minimize the difference between actual reference signal that needs to be compensated ($\mathfrak{R}^{ref}(t)$) and sum of the scheduled reference signals for the AGs ($\sum_{i \in \mathscr{M}} \mathfrak{R}_i^{ref,sch}(t)$). Apart from this, the first constraint imposes the upper bound restriction on $\sum_{i \in \mathscr{M}} \mathfrak{R}_i^{ref,sch}(t)$. While the second constraint restricts the value of $\mathfrak{R}_i^{ref,sch}(t)$ within a permissible range.

Optimal regulation signal dispatch among CSs

The nature of considered problem is similar with the problem discussed in Section 4.2.4. Hence, the details about objective function ($\mathbb{F}_3$) can be best understood in lines of $\mathbb{F}_2$.

$$\min \mathbb{F}_3 = \left(\mathfrak{R}_i^{ref,sch}(t) - \{ \mathfrak{R}_{i1}^{ref,sch}(t) + ... + \mathfrak{R}_{in}^{ref,sch}(t) \} \right)$$
$$\implies \mathbb{F}_3 = \left(\mathfrak{R}_i^{ref,sch}(t) - \sum_{j \in \mathscr{N}} \mathfrak{R}_{ij}^{ref,sch}(t) \right)$$

$$s.t. \begin{cases} \sum_{j \in \mathscr{N}} \mathfrak{R}_i^{ref,sch}(t) \leq \mathfrak{R}_i^{ref,sch}(t) \\ \text{Eq. (4.12)} \end{cases}$$

Maximize V2G support to EV users while minimizing EV's battery degradation

The objective of this problem is to maximize the scheduling of the participating EVs while considering the trade-off with battery degradation issues. The same is justified using following

objective function $\mathbb{F}_4$, with $C_{ijk}^{sch}(t)$ and $D_{ijk}^{sch}(t)$ being the decision variables.

$$\max \mathbb{F}_4 = \left(\sum_{i \in \mathscr{M}} \sum_{j \in \mathscr{N}} \sum_{k \in k_j} \mathfrak{S}_{ijk}(t) \times (C_{ijk}^{sch}(t) - D_{ijk}^{sch}(t)) \right)$$

$$s.t. \begin{cases} \mathfrak{T}_{ijk}(t) \in 0,1; \forall i,j,k \\ \mathfrak{S}_{ijk}(t) \in 0,1; \forall i,j,k \\ \text{Eqs. (4.15)-(4.20)} \end{cases}$$

First and second constraints ensure the integrality restriction on $\mathfrak{T}_{ijk}(t)$ and $\mathfrak{S}_{ijk}(t)$. Remaining constraints ensure that the impact of charging/discharging on EVs' batteries is minimized as explained in Section 4.2.3.

4.3 Decomposition and Solution

It is evident from the problem formulation that the decision variables ($\mathfrak{T}_{ijk}(t)$, $\mathfrak{R}_i^{ref,sch}(t)$, $C_{ijk}^{sch}(t)$ and $D_{ijk}^{sch}(t)$) in the suggested Mo-PP belong to different layers of computation. Additionally, the overall relationship between these variables is tightly coupled. Hence, minimizing frequency fluctuations while simultaneously providing bi-directional V2G support and minimizing the impact on battery degradation is a complex task. Thus, this section presents an approximate solution for the considered Mo-PP to achieve an optimal trade-off between V2G-powered frequency support and EV's individual energy requirement with different battery characteristics. For this, the considered Mo-PP has been segregated into three SPs which are then solved using the standard optimization techniques. The illustrative information about these SPs has been presented as follows.

4.3.1 Detailed working of the scheme

The overall working philosophy of the proposed scheme and sequence of solving the SPs iteratively could be best understood using Fig. 4.3. As depicted in the figure, the first step after regulation signal generation is estimation of FRCs of EVs ($P_{ijk}^{est,max}(t)$ and $P_{ijk}^{est}(t)$), CSs ($P_{ij}^{est,max}(t)$ and $P_{ij}^{est}(t)$) and AGs ($P_{i}^{est,max}(t)$ and $P_{i}^{est}(t)$). The detailed technical description about the same has already been discussed in Section 4.2.2 and 4.2.2. Using the values of $P_{i}^{est,max}(t), P_{i}^{est}(t), P_{ij}^{est,max}(t)$ and $P_{ij}^{est}(t)$, the GC solves SP-II (*i.e.*$\mathbb{F}_2$) to generate the list of optimal reference signals for the AGs $\{\mathfrak{R}_{1}^{ref,sch}(t), \mathfrak{R}_{2}^{ref,sch}(t) \ldots \mathfrak{R}_{m}^{ref,sch}(t)\}$. Similarly, LCs compute the optimal reference signals for the CSs $\{\mathfrak{R}_{11}^{ref,sch}(t), \mathfrak{R}_{12}^{ref,sch}(t), \ldots, \mathfrak{R}_{mn}^{ref,sch}(t)\}$ by solving SP-III (*i.e.*$\mathbb{F}_3$). Moreover, LCs check the current SoC of participating EVs as per Eqs. (4.19) and (4.20). Any violations to these boundaries, sets the parameter $\mathfrak{S}_{ijk}(t)$ to 0, *i.e.*, EVs are set to non-interactive mode. On the contrary, $\mathfrak{S}_{ijk}(t)$ remains 1, thereby allowing EVs to participate in V2G operations (*i.e.*, interactive mode). This operation is performed iteratively till EVs are either set to non-interactive mode or finally depart from the CS. Following this, SP-IV is executed by the LCs to cater EVs' charging and discharging needs while minimizing the impact on their batteries. This is done in accordance with the objective function $\mathbb{F}_4$ (*i.e.*SP-IV), wherein the binary decision variable $\mathfrak{S}_{ijk}(t)$ is the output of this step. Using this value, the GC finally generates the charging and discharging schedule for the participating EVs in order to minimize the grid frequency deviations. This is achieved by solving $\mathbb{F}_1$ (*i.e.*SP-I) as already explained in Section 4.2.4.

It is important to mention here that the nature of all objective functions namely-$\mathbb{F}_1$, $\mathbb{F}_2$, $\mathbb{F}_3$ and $\mathbb{F}_4$ throughout the considered SPs is linear in nature. Additionally, their associated constraints are also linearly defined. These SPs are typically linear programming problems which are solved iteratively using interior-point method [151]. This in turn helps to solve the considered Mo-PP approximately.

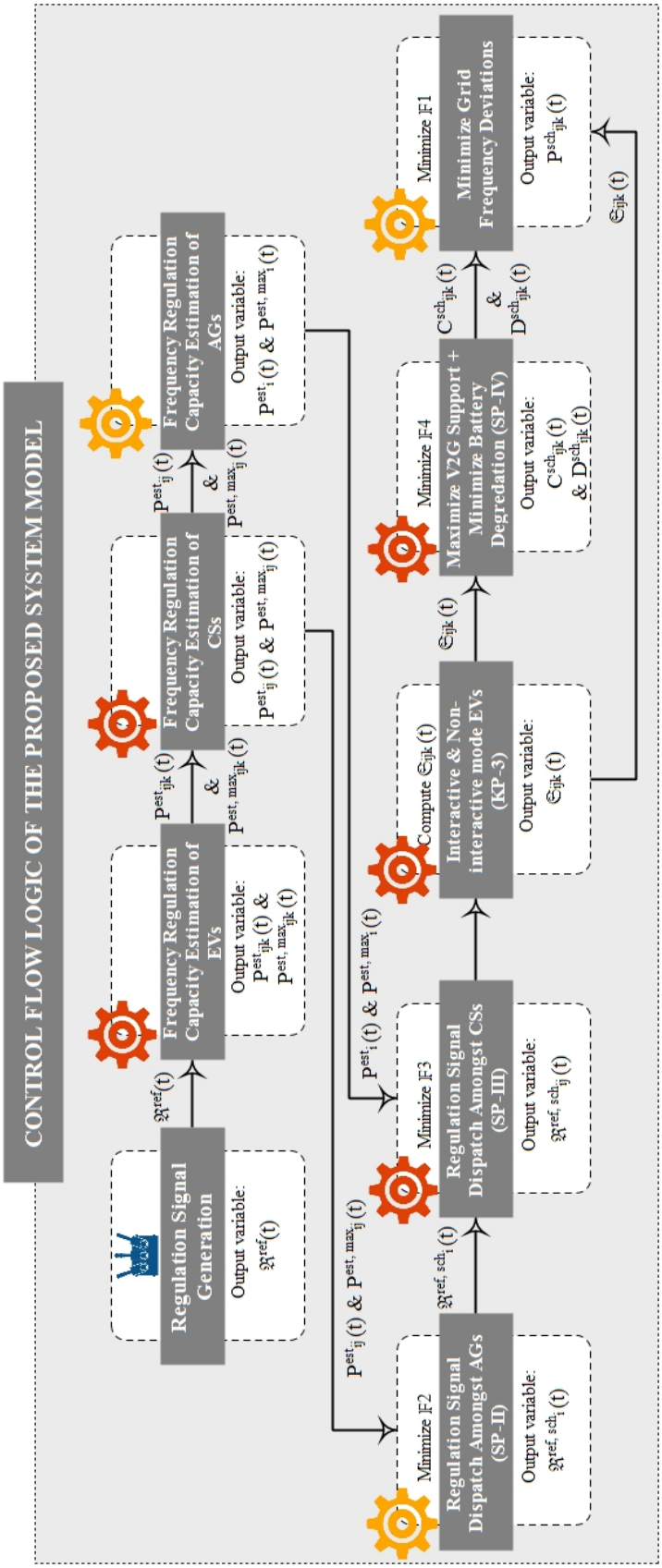

Figure 4.3: Overall control logic of the proposed scheme.

Algorithm 4.1 Control algorithm of the proposed 2-layer hierarchical control scheme for grid frequency support.

Input: Regulation signal ($\mathfrak{R}^{ref}(t)$).
Output: $P^{sch}_{ijk}(t)$, $\mathfrak{T}_{ijk}(t)$, $\mathfrak{S}_{ijk}(t)$, $C^{sch}_{ijk}(t)$, $D^{sch}_{ijk}(t)$, $\mathfrak{R}^{ref,sch}_{i}(t)$ and $\mathfrak{R}^{ref,sch}_{ij}(t)$.

procedure FUNCTION(FREQUENCY-SUPPORT-EVs)
    Regulation signal generation, *i.e.*, $\mathfrak{R}^{ref}(t)$ by the SU
    Step 1: V2G power capacity estimation of EVs ▷ Performed by LC
    Compute $SoC^{c}_{ijk}(t)$ & $SoC^{d}_{ijk}(t)$ using Eqs. (4.2) & (4.3)
    Compute $P^{est}_{ijk}(t)$ & $P^{est,max}_{ijk}(t)$ using Eqs. (4.4) & (4.5)
    Step 2: V2G power capacity estimation of CSs ▷ Performed by LC
    Compute $P^{est}_{ij}(t)$ & $P^{est,max}_{ij}(t)$ using Eqs. (4.6) & (4.7)
    Step 3: V2G power capacity estimation of AGs ▷ Performed by GC
    Compute $P^{est}_{i}(t)$ & $P^{est,max}_{i}(t)$ using Eqs. (4.8) & (4.9)
    Step 4: Regulation signal dispatch among AGs ▷ Performed by GC
    $\{\mathfrak{R}^{ref,sch}_{1}(t), \mathfrak{R}^{ref,sch}_{2}(t), ..., \mathfrak{R}^{ref,sch}_{m}(t)\} \leftarrow$ Minimize $\mathbb{F}_2$
    Step 5: Regulation signal dispatch among CSs ▷ Performed by LC
    $\{\mathfrak{R}^{ref,sch}_{11}(t), \mathfrak{R}^{ref,sch}_{12}(t), ..., \mathfrak{R}^{ref,sch}_{mn}(t)\} \leftarrow$ Minimize $\mathbb{F}_3$
    Step 6: Determination of interactive and non-interactive mode EVs ▷ Performed by LC
    Compute $\mathfrak{S}_{ijk}(t)$ using Eqs. (4.19) & (4.20)
    Step 7: V2G support maximization + minimizing battery degradation ▷ Performed by LC
    $\{C^{sch}_{ijk}(t), D^{sch}_{ijk}(t)\} \leftarrow$ Maximize $\mathbb{F}_4$
    Step 8: Grid frequency fluctuation minimization ▷ Performed by GC
    $\mathfrak{T}_{ijk}(t) \leftarrow$ Minimize $\mathbb{F}_1$
end procedure
Return $P^{sch}_{ijk}(t)$, $\mathfrak{T}_{ijk}(t)$, $\mathfrak{S}_{ijk}(t)$, $C^{sch}_{ijk}(t)$, $D^{sch}_{ijk}(t)$, $\mathfrak{R}^{ref,sch}_{i}(t)$ and $\mathfrak{R}^{ref,sch}_{ij}(t)$

4.4 Simulation and Results

This section illustrates the results of the extensive simulations performed to validate the efficacy of the proposed frequency support scheme in V2G setup.

4.4.1 Simulation Setup

For the purpose of evaluation of the proposed scheme, widely accepted PJM and ERCOT regulation data traces have been considered [143, 144].

Additionally, following assumptions have been considered during the performance evaluation of the proposed scheme. It has been assumed that all CSs can accommodate at maximum 60 EVs with variable energy requirements. The arrival of EVs at CSs is assumed to be normally distributed $N(\mu, \sigma^2)$; wherein μ and σ represent the mean and standard deviation respectively. For experimental evaluation, the values of μ and σ are assumed to be 60 and 2.2 [152, 153]. However, the participating EVs are supposed to be having variable initial SoC levels, but with fixed values of 100% and 20% for SoC^{max} and SoC^{min} respectively. Furthermore, six different types of EVs having energy rating capacities of 16, 20, 24, 30, 40 and 50 kWh respectively, are assumed to be participating in the V2G frequency support mechanism.

4.4.2 Case Studies Considered

For the extensive evaluation of the proposed scheme for SFR using fleet of EVs, a set of two distinctive case studies have been considered. Their detailed information is given below:

Case Study-I (SFR across 1 hour time interval)

The setup of the considered case study comprises of 3 AGs (AG_1, AG_2, AG_3) and 6 CSs (CS_{11}, CS_{12}, CS_{21}, CS_{31}, CS_{32}, CS_{33}). The scaled down PJM regulation data that needs to be regulated using the proposed scheme is shown in Fig. 4.4a [143]. These regulation signals are triggered periodically after an interval of 1 hour. In order to manage these $\mathfrak{R}^{ref}(t)$, GC dispatches them among the AGs as depicted in Fig. 4.4b. For instance, at 0800 hours, $\mathfrak{R}^{ref}(t)$ of 1424.2 kW was triggered which was then dispatched among the AG_1, AG_2

and AG_3 respectively as 493.43, 255.42 and 675.31 kW. These computations are done by solving the objective function $\mathbb{F}_2$. After this, LCs segregate $\mathfrak{R}_i^{ref,sch}(t)$ among the CSs using objective function $\mathbb{F}_3$ as shown in Fig. 4.4c. At 0800 hours, *AG* level regulation signal was dispatched among the respective CSs into 198.48, 294.95, 255.42, 215.25, 246.66 and 213.4 kW respectively. The optimal dispatch of signals is done according to individual FRCs of AGs and CSs.

LCs deployed at the AG level, also regulate $C_{ijk}^{sch}(t)$ and $D_{ijk}^{sch}(t)$ of EVs available at different CSs. This is done in order to suppress frequency deviations while catering customers' transportation needs. This task is performed as per the objective function $\mathbb{F}_4$. The related outcomes are clearly highlighted using Fig. 4.4d. At 0800 hours, $C_{ijk}^{sch}(t)$ and $D_{ijk}^{sch}(t)$ of participating EVs at CS_{11} were settled at 0.22285 and 1 respectively, in order to cater $\mathfrak{R}^{ref}(t)$ of 198.48 kW. It is noteworthy to mention here that the proposed frequency support scheme successfully caters EVs' charging and discharging requirements while managing frequency deviations. This is verified from the results as summarized in Figs. 4.4e and 4.4f. For illustration, at 0800 hours the average SoC level of EVs seeking charging and discharging respectively, at CS_{11} were merely 59.667% and 52.667% respectively. After participating in the V2G frequency support, their SoC levels were settled at 68.655% and 20% respectively. Further, the proposed scheme also reduced the battery degradation impact induced due to the participation of EVs in the regulation market. This is evident from Fig. 4.4g in which segregation of EVs into interactive and non-interactive modes is clearly highlighted.

The proposed scheme also helps in managing the frequency fluctuations at grid level. This is evident from the results summarized in Fig. 4.4h. In this figure, the cumulative FRC provided by the fleet of EVs has been compared with the $\mathfrak{R}^{ref}(t)$. The results clearly indicate that the proposed scheme is capable of re-balancing the power and supply imbalances in real-time. For instance, $\mathfrak{R}^{ref}(t)$ of 1260.73 kW was generated in the time interval of

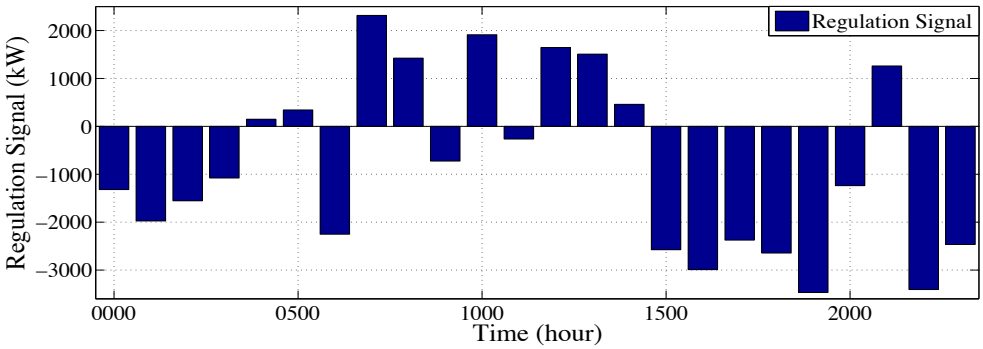

4.4(a) PJM regulation signals with respect to 6^{th} June 2014.

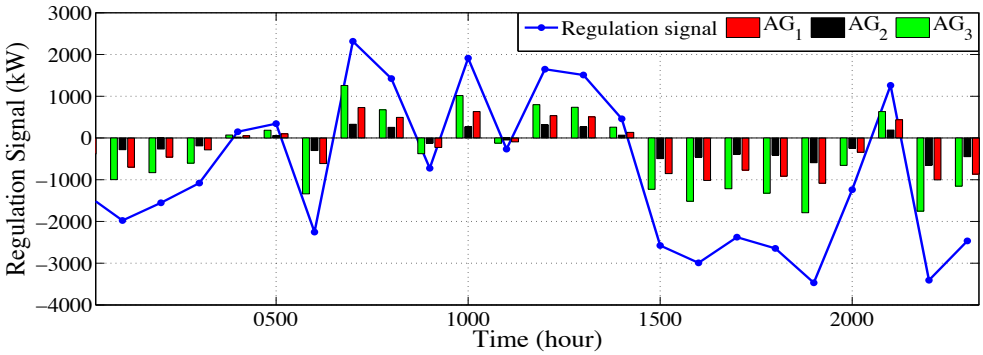

4.4(b) Dispatch of regulation signals across aggregators.

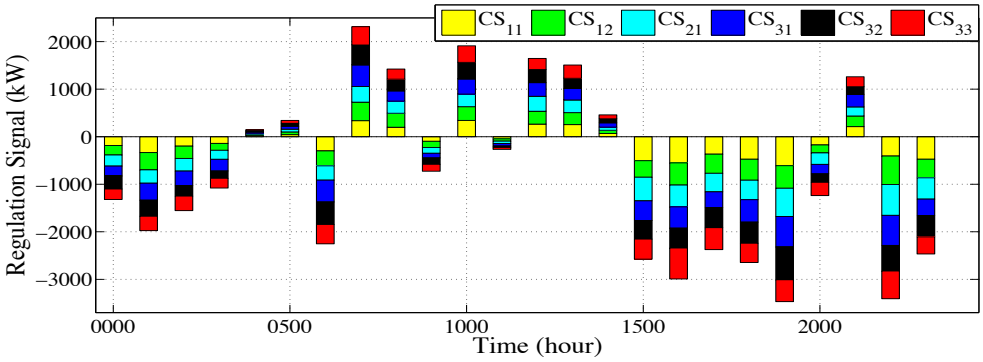

4.4(c) Dispatch of regulation signals across charging stations.

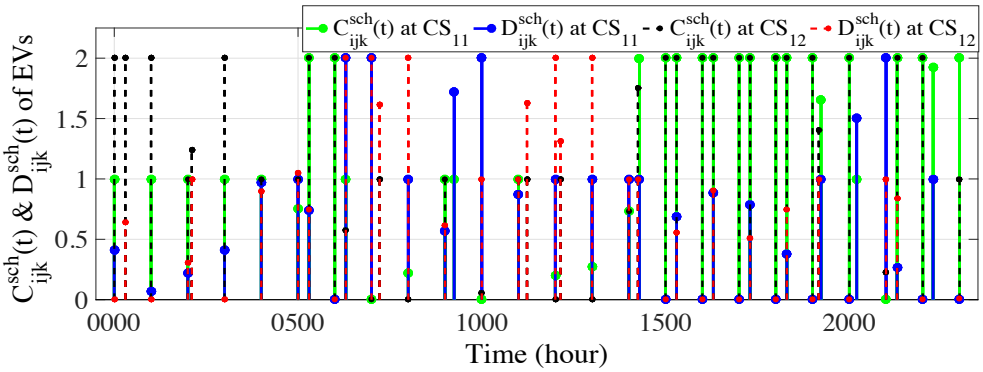

4.4(d) $C^{sch}_{ijk}(t)$ and $D^{sch}_{ijk}(t)$ of participating EVs at CS_{11} and CS_{12}.

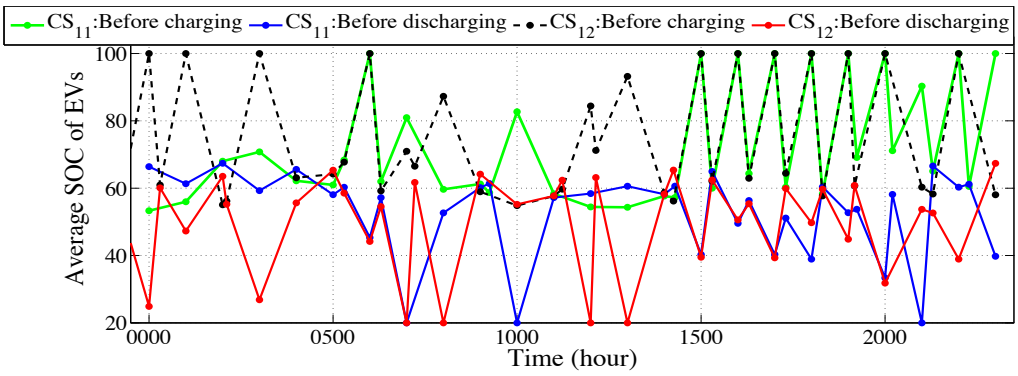

4.4(e) Average SoC of EVs before participating in frequency support at CS_{11} and CS_{12}.

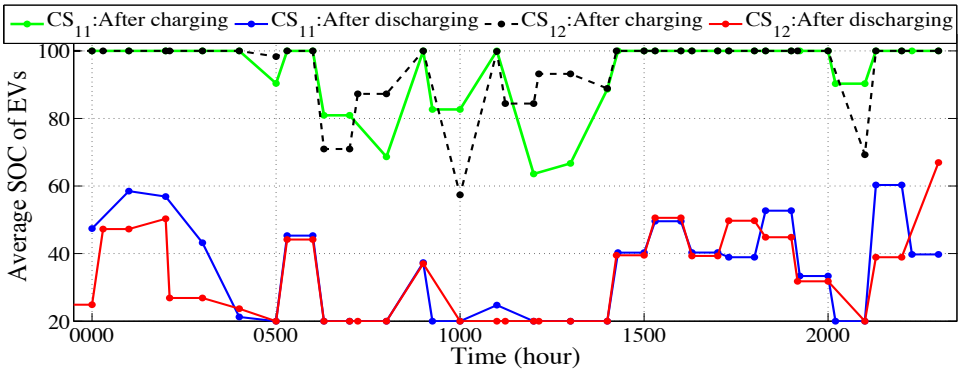

4.4(f) Average SoC of EVs after participating in frequency support at CS_{11} and CS_{12}.

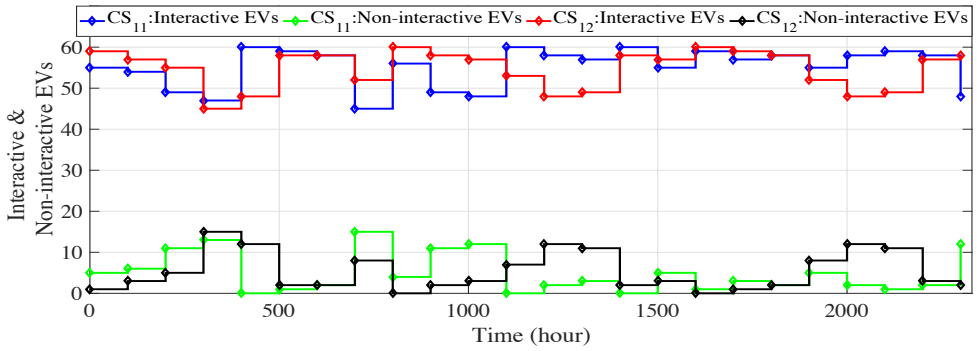

4.4(g) Segregation of participating EVs into interactive and non-interactive types at CS_{11} and CS_{12}.

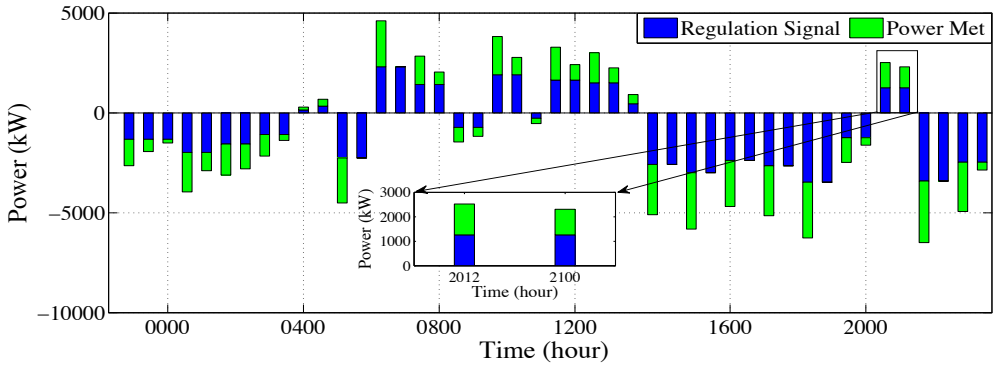

4.4(h) Power met using the proposed scheme.

Figure 4.4: Case Study-I: Results obtained using the proposed aggregator-based hierarchical control mechanism on PJM regulation data across 1 hour time interval.

2000-2100 hours. It was managed using the proposed scheme across two different time slots by exploiting EVs' FRCs. As evident from Fig. 4.4h, $\mathfrak{R}^{ref}(t)$ was completely satisfied during the first slot, *i.e.*, 2000-2012 hours. On the other hand, 1048.24 kW of $\mathfrak{R}^{ref}(t)$ was met during the next slot, *i.e.*, 2012-2100 hours. It is worth observing that the results obtained in the second slot could not satisfy the entire range of $\mathfrak{R}^{ref}(t)$. This is primarily due to the non-availability of EVs in the considered time slot.

Case Study-II (SFR across 15 minutes time interval)

In comparison with the previously discussed case study, this case study considers the dispatch of $\mathfrak{R}^{ref}(t)$ across 15 min time interval. The considered $\mathfrak{R}^{ref}(t)$ traces are depicted in Fig. 4.5a. These traces have been acquired from ERCOT [144] and have been scaled downed with respect to the availability of fleet of EVs at a single CSs. The obtained results have been summarized in Fig. 4.4. For instance, at 1600 hours, $\mathfrak{R}^{ref}(t)$ of 140.23 kW was triggered. It was balanced by leveraging the FRCs of the available EVs at the CS, while providing the necessary V2G support. This is evident from Fig. 4.5b wherein $C^{sch}_{ijk}(t)$ and $D^{sch}_{ijk}(t)$ values were found to be 1 and 1.0161 respectively in the considered time interval. Subsequently, the variations in SoC levels of EV's batteries were also witnessed and the associated findings have been drawn in Figs. 4.5c and 4.5d. As a result of this participation, EVs were successful in tracking the $\mathfrak{R}^{ref}(t)$ as evident from Fig. 4.5e.

4.4.3 Comparison and Discussions

The performance of the proposed scheme has been validated against the two state-of-art schemes, based on different controllers to provide frequency support using fleet of EVs. The former employees the CPN-based controller [149] while the latter exploits the proportional integral derivative (PID) controller [153]. The detailed evaluation results are mentioned as

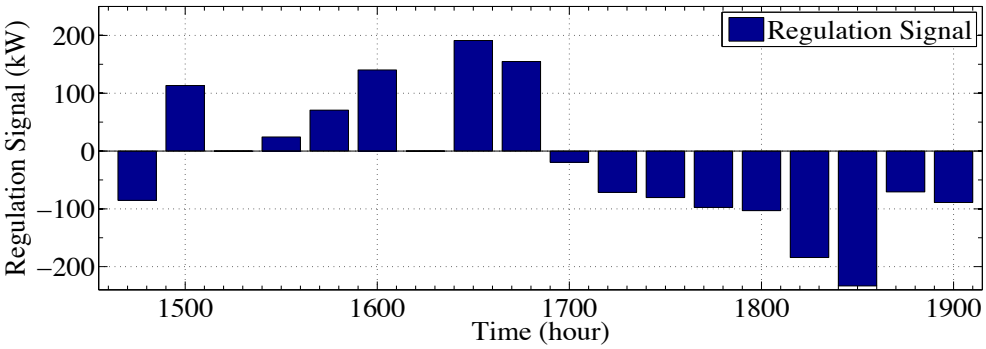

4.5(a) Regulation signal data acquired from ERCOT.

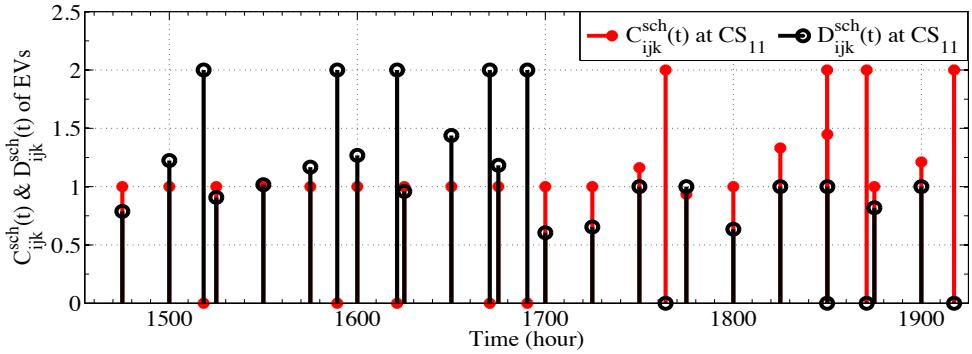

4.5(b) $C^{sch}_{ijk}(t)$ and $D^{sch}_{ijk}(t)$ of participating EVs at CS_{11}.

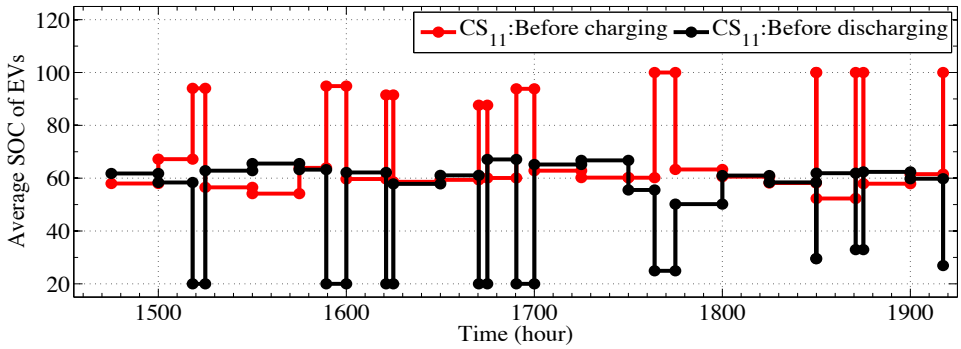

4.5(c) Average SoC of EVs before participating in frequency support at CS_{11}.

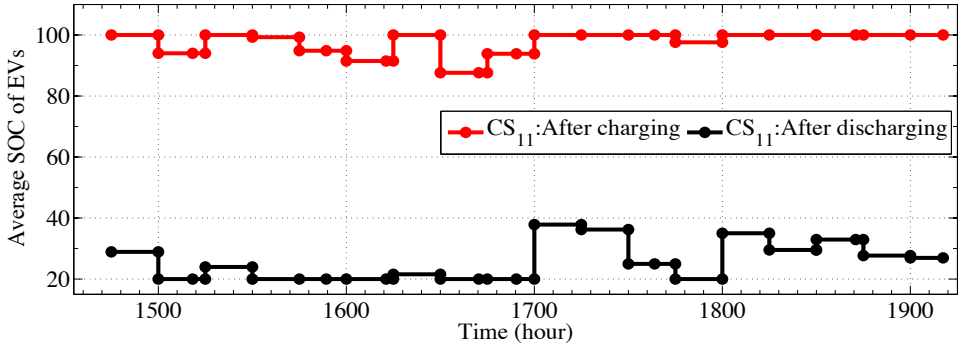

4.5(d) Average SoC of EVs after participating in frequency support at CS_{11}.

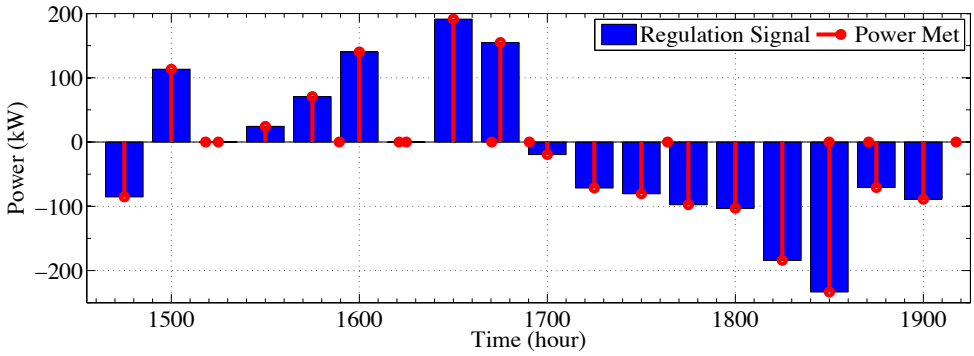

4.5(e) Power met using the proposed scheme.

Figure 4.5: Case Study-II: Results obtained using the proposed aggregator-based hierarchical control mechanism on ERCOT regulation data across 15 minutes time interval.

follows:

With an existing scheme based on CPN controller

This section elaborates the relative comparison of the proposed scheme with an existing scheme as proposed in [149]. This comparison is in-line with Case Study-I and PJM regulation data as depicted in Fig. 4.4a.

Significant deviations in the performance of both the schemes are due to their respective underlying methodologies, particularly with respect to dispatch of regulation signal among AGs and CSs. The relative results are evident from Figs. 4.4b and 4.6a. The proposed scheme adopts an *"Aggregator-based Hierarchical Control Mechanism"* to dispatch the regulation signals among the AGs and CSs. This is in accordance with the FRC of the participating EVs. On the other hand, the existing scheme completely neglects this aspect and emphasizes on equal dispatch of regulation signals among the AGs and CSs.

Due to the above mentioned reasons, the proposed scheme is more effective in managing frequency deviations at grid level relative to the existing scheme. This is evident from the results summarized in Fig. 4.6b, wherein the power met using both the schemes have been depicted. Between 2000-2100 hours, $\mathfrak{R}^{ref}(t)$ of 1260.73 kW was triggered which was

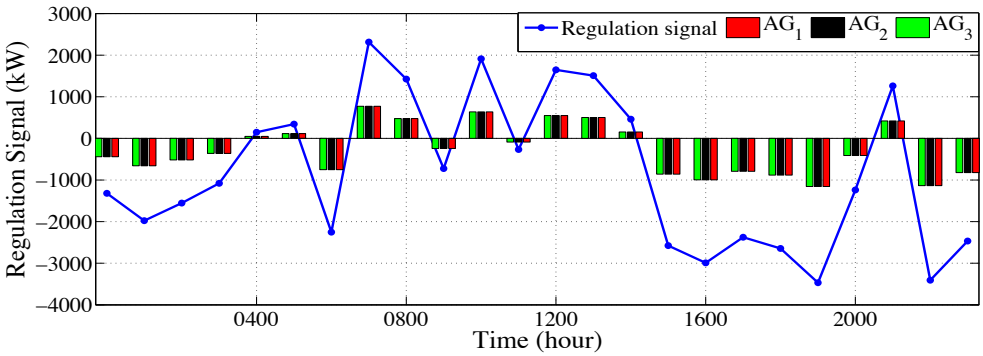

4.6(a) Dispatch of regulation signals across aggregators using the existing scheme.

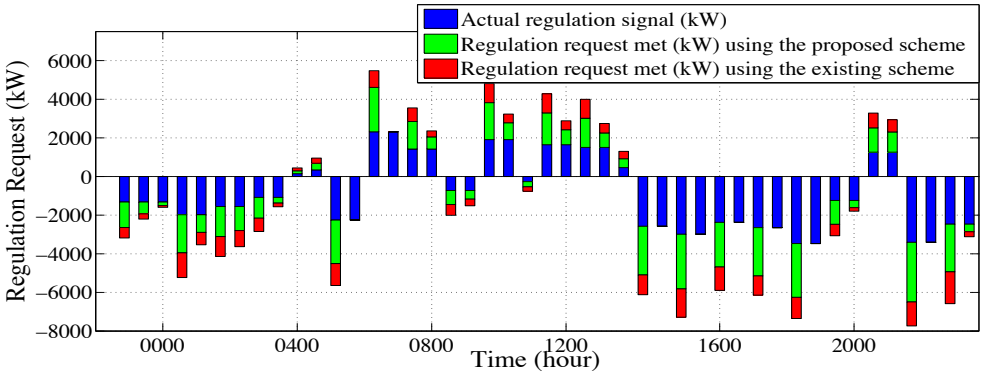

4.6(b) Comparison of the proposed scheme with an existing scheme in terms of regulation signal met.

Figure 4.6: Comparison of the proposed scheme with an existing scheme based on CPN controller.

managed in two time slots using both the schemes. During the first slot, *i.e.*, between 2000 to 2012 hours, $\mathfrak{R}^{ref}(t)$ was completely managed by the proposed scheme. On the other hand, the existing scheme was able to fulfill only 761.98 kW of regulation request. Similar behavior was observed in the next time slot, *i.e.*, 2012-2100 hours, where 1048.2 and 633.54 kW of regulation request was met by the proposed and existing scheme respectively. Thus, the above mentioned results clearly depict that the proposed scheme achieves 22.6% better results in tracking the regulation signal in comparison with the existing scheme.

With an Existing Scheme based on PID Controller

The authors in [153] suggested PID controller based frequency support scheme by exploiting the capabilities of the V2G mechanism. The designed scheme considered the uncertainties imposed due to the driving profile of EVs and communication delays. This section presents the performance comparison of this scheme with the proposed scheme.

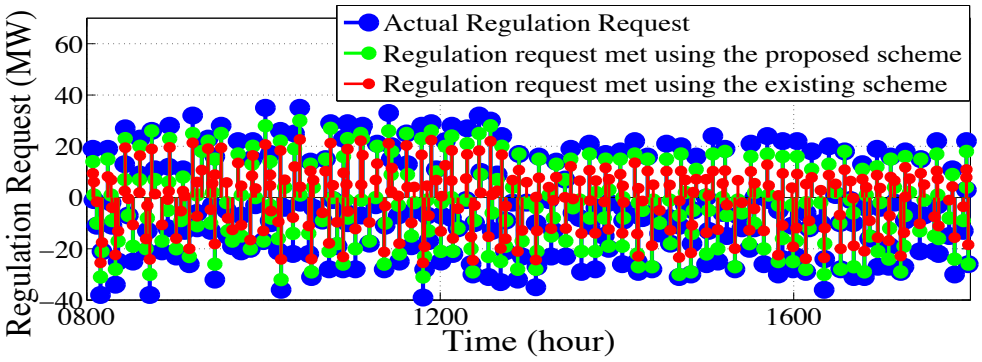

Figure 4.7: Comparison of the proposed scheme with an existing scheme based on PID controller.

The regulation signal traces and the simulation setup has been adopted from [153] and the two schemes have been compared with long term load changes. The achieved results are highlighted using Fig. 4.7, wherein the regulation signal met using the two schemes has been illustrated. It's quite clear from the results, that the proposed scheme performed significantly better in majority of the cases. This variation in the performance of two schemes can be attributed to the difference in estimation of $C_{ijk}^{sch}(t)$ and $D_{ijk}^{sch}(t)$. For instance, at 0900 hours, $\mathfrak{R}^{ref}(t)$ of -25 MW was triggered; out of which only -20 MW support was provided by the proposed scheme, while -17 MW request was handled by the existing scheme.

4.5 Concluding Remarks

EV's battery degradation is an important issue in V2G setup which can easily exaggerate with the unregulated charging and discharging of EVs' batteries. In view of this issue, this chapter presented a hierarchical control scheme using fleet of EVs while maintaining grid's operating frequency within the nominal range. In the next chapter, another frequency support scheme has been proposed based on *"Mixed Integer Linear Programming (MILP)"*.

Chapter 5

Coordinated Power Control of Electric Vehicles for Grid Frequency Support

In this chapter, an integrated solution for effective SFR using fleet of EVs using a 2-level hierarchical control scheme has been presented. Further, an optimal scheduling policy for charging and discharging of EVs using *"Mixed Integer Linear Programming (MILP)"* is designed to minimize the frequency deviations at the grid level while supporting bidirectional V2G capabilities. Using the designed MILP based strategy, optimal regulation signal dispatch amongst AGs and CSs is achieved; while reducing EV's battery degradation and increasing their overall revenue for providing ancillary services. The detailed working of the proposed scheme with its system model is as under.

5.1 System Model

The proposed scheme is a 2-layer hierarchical control scheme having MILP-based optimization. The detailed architectural diagram is depicted in Fig. 5.1. As evident from the figure, the scheme works at the distribution level wherein fleet of EVs, group of CSs and AGs play a significant role in providing SFR. In the proposed V2G setup, $\mathscr{M}$ number of AGs and

$\mathcal{N}$ number of CSs are assumed to be available. These entities along with SU comprise of the physical layer and are assumed to be equipped with the bi-directional and reliable communication links. On the other hand, MILP-based optimizer and FRC estimator deployed at the SU unit, AG and CS levels comprise of the control layer. Due to the presence of these two layers, the proposed scheme is referred as the *2-layer hierarchical control scheme*. At the first level, the proposed framework estimates the regulation signals to be compensated using the joint participation of EVs. Additionally, it also segregates the regulation signal between the AGs and CSs. At the second level, optimal charging and discharging schedules for EVs are determined, while simultaneously minimizing the grid frequency imbalances and maximally satisfying the EVs' power requirements. The proposed scheme also minimizes the effect

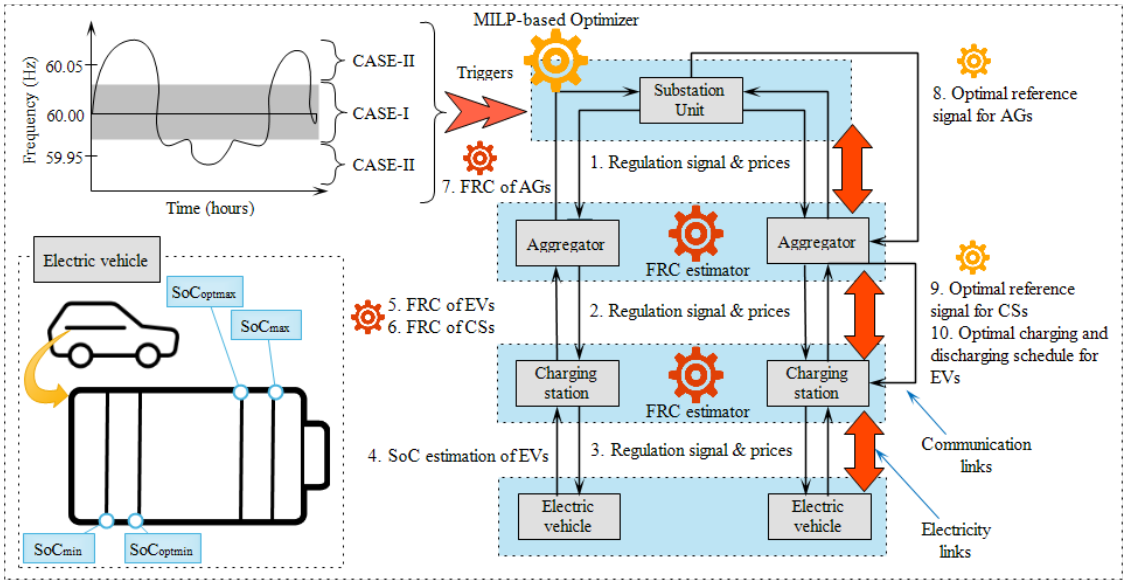

Figure 5.1: System model of the proposed MILP-based hierarchical control scheme.

of frequent charging and discharging on EV's batteries induced due to their participation in the regulation market. This is achieved as follows. SG's frequency index is chosen as an indicator to determine the charging/discharging of EV's batteries; wherein the range of the frequency decides the optimal $[SoC_{optmin}, SoC_{optmax}]$ and suboptimal $[SoC_{min}, SoC_{max}]$ SoC range for EVs' charging and discharging. As depicted in the figure, frequency dead-band

used in primary frequency regulation has been taken into account to identify normal (Case-I) and emergency (Case-II) for effective frequency support [154]. In the former case, the SoC range of the EV's battery is kept within the optimal range, while the suboptimal range is used in the latter case. In either case, it is assumed that the decision about charging and discharging of EV's batteries is completely user specific. Additionally, EVs' users participate in the secondary regulation process in order to earn higher rewards. Hence, SoC of the EVs when they are to be used by their respective owners is either maintained between the optimal SoC range or the suboptimal range.

The working philosophy of the scheme is diagrammatically shown using Fig. 5.1. Here, SU is used for monitoring frequency fluctuations and relaying the real-time regulation signals ($\mathfrak{R}^{ref}(t)$). Also, the SU relays regulation up and down prices at time t ($\mathfrak{Pr}^{up}(t)$ & $\mathfrak{Pr}^{down}(t)$). In response to these signals, FRC estimators (deployed at AG and CS levels) compute the FRCs of the participating EVs, CSs and AGs. Using this information, MILP-based optimizer at SU level generates an optimal schedule for charging and discharging EVs across the time horizon (T), to track the regulation signal. This is done while simultaneously minimizing battery degradation and maximizing EV's revenue in the entire process. Additionally, MILP-based optimizer also dispatches the regulation signal amongst the AGs and CSs in an optimal manner.

In order to support real time SG operations, the underlying communication channel in SG should be capable of low latency along with improved capacity, coverage and high data rate. This is in accordance with the latest guidelines released by NIST [155]. With this, the communication technologies in SG domain has witnessed a major blow in the last couple of years; ranging from PLC, IEEE 802.15.4 (ZigBee), IEEE 802.11 (Wireless LAN), IEEE 802.16 (WiMAX), GSM, and GPRS to Optical Fiber and LTE/ LTE-A. However, the most sought after wireless technology is this regard is 3GPP Long Term Evolution (LTE) Release

8 [156]. One of the distinctive advantages of LTE is its ability to schedule resources in both Time Domain Duplex (TDD) and Frequency Domain Duplex (FDD) modes. Hence, the communication links from the higher levels to lower ones in the considered hierarchical setup are assumed to be supported by the robust LTE, in view of minimal communication delay. However, in case of possible disturbances (like link failures), the proposed scheme adopts a fault tolerant mechanism as detailed in Algorithm 5.1. Nevertheless, the proposed mechanism does not provided exact frequency support but is capable of providing acceptable frequency support during communication breakdowns.

Algorithm 5.1 Coordinated grid frequency support during communication disturbances.

Input: $\mathfrak{R}_{ij}^{ref}(t)$, $\mathfrak{R}_{ij}^{ref}(t-1)$, t, and $t-1$

1: **if** (Communication between i^{th} AG and j^{th} CS collapses) **then**
2: Set $\mathfrak{R}_{ij}^{ref}(t) = \mathfrak{R}_{ij}^{ref}(t-1)$ from time stamp $(t-1)$
3: **end if**

The working of the algorithm can be understood as follows. Say the communication channel between the i^{th} AG and j^{th} CS collapses at time stamp t; due to which the latest regulation signal ($\mathfrak{R}_{ij}^{ref}(t)$) could not be communicated. Under such scenarios, the affected CS, *i.e.*, j^{th} CS continues to operates with the previously relayed regulation signal ($\mathfrak{R}_{ij}^{ref}(t-1)$) at time stamp $t-1$.

5.2 Problem Formulation

The problem is formulated as follows:

1. min $\mathbb{F}(C_{ij}^{sch}(t), D_{ij}^{sch}(t)) = \mathbb{F}_1 - \mathbb{F}_2 - \mathbb{F}_3 + \mathbb{F}_4 - \mathbb{F}_5$ *subject to:*
2. total FRC constraint Eqs. (5.10)-(5.18)
3. battery constraints Eqs. (5.19)-(5.21)

4. reference signal dispatch constraint Eq. (5.5)

5. $C_{ij}^{sch}(t) \geq 0; \forall i, j$

6. $D_{ij}^{sch}(t) \geq 0; \forall i, j$

7. $C_{ijk}^{sch}(t) \geq 0; \forall i, j, k$

8. $D_{ijk}^{sch}(t) \geq 0; \forall i, j, k$

The above defined problem takes into account multiple objectives such as-minimization of frequency deviations ($\mathbb{F}_1$), maximal V2G support ($\mathbb{F}_2$ and $\mathbb{F}_3$), optimal dispatch of reference signals ($\mathbb{F}_4$) and EV's revenue maximization ($\mathbb{F}_5$). The constraints taken into consideration impose restrictions on EV's battery charging and discharging processes to prevent battery degradation. Along with this, FRCs of EVs, CSs and AGs are also kept in check so as to provide reliable frequency support and ensure optimal dispatch of reference signals accordingly. It is worth mentioning here, that the proposed work considers equal weights for all the objective functions, since these weights depict the relative importance of an objective function over another in the given context. The concept has been adopted in order to compute the optimal solution without prioritizing any function over the other [157–160].

The problem formulated above is '*Mixed Integer Linear Programming Problem*', wherein $C_{ij}^{sch}(t)$ and $D_{ij}^{sch}(t)$ are the decision variables. These variables denote the scheduled charging and discharging rates of the EV under consideration. The defined problem is solved using the Mosek solver [161].

5.2.1 List of Objective Functions

Minimization of Frequency Deviations

Objective function ($\mathbb{F}_1(C_{ij}^{sch}(t), D_{ij}^{sch}(t))$) deals with the minimization of frequency deviations wherein the cumulative FRCs of EVs is used to track the $\mathfrak{R}^{ref}(t)$ across all time stamps t. This is mathematically expressed as follows.

$$\begin{aligned}\min\ \mathbb{F}_1(C_{ij}^{sch}(t), D_{ij}^{sch}(t)) = \\ \mathfrak{R}^{ref}(t) - \Big(\sum_{i\in\mathscr{M}} \sum_{j\in\mathscr{N}} \Big(\sum_{k\in k_j} \frac{-SoC_{ijk}^{c}(t) \times E_{ijk}^{rated}}{100} \Big) \times C_{ij}^{sch}(t) \\ + \sum_{i\in\mathscr{M}} \sum_{j\in\mathscr{N}} \Big(\sum_{k\in k_j} \frac{SoC_{ijk}^{d}(t) \times E_{ijk}^{rated}}{100} \Big) \times D_{ij}^{sch}(t) \Big)\end{aligned} \tag{5.1}$$

In the above equations, $SoC_{ijk}^{c}(t)$ is equivalent to either $(SoC_{optmax} - SoC_{ijk}^{c,ini}(t))$ or $(SoC_{max} - SoC_{ijk}^{c,ini}(t))$ as per C-I or C-II respectively. Similarly, $SoC_{ijk}^{d}(t)$ is defined such that $C_{ij}^{sch}(t)$ and $D_{ij}^{sch}(t)$ depict the scheduled charging and discharging rates for EVs available at the j^{th} CS of i^{th} AG.

Maximal V2G Support

Another important contribution of the present manuscript is to provide maximal V2G support for simultaneous charging and discharging of EVs. This is achieved using the below mentioned functions namely-$\mathbb{F}_2(C_{ij}^{sch}(t), 0)$ and $\mathbb{F}_3(0, D_{ij}^{sch}(t))$ respectively.

$$\begin{aligned}\max\ \mathbb{F}_2(C_{ij}^{sch}(t), 0) = \\ \Big(\sum_{i\in\mathscr{M}} \sum_{j\in\mathscr{N}} \Big(\sum_{k\in k_j} \frac{-SoC_{ijk}^{c}(t) \times E_{ijk}^{rated}}{100} \Big) \times C_{ij}^{sch}(t) \Big)\end{aligned} \tag{5.2}$$

$$\begin{aligned}\max\ \mathbb{F}_3(0, D_{ij}^{sch}(t)) = \\ \Big(\sum_{i\in\mathscr{M}} \sum_{j\in\mathscr{N}} \Big(\sum_{k\in k_j} \frac{SoC_{ijk}^{d}(t) \times E_{ijk}^{rated}}{100} \Big) \times D_{ij}^{sch}(t) \Big)\end{aligned} \tag{5.3}$$

Optimal Reference Signal Dispatch amongst CSs and AGs

As mentioned in the previous section, optimal reference signal dispatch amongst the CSs ($\mathfrak{R}_{ij}^{ref,sch}(t)$) and AGs ($\mathfrak{R}_{i}^{ref,sch}(t)$) is also an important consideration for achieving reliable frequency support using fleet of EVs. This is particularly important so that maximum available FRCs of the CSs and AGs could be exploited in the best possible manner. Additionally, it also ensures that none of the AGs and CSs are left under-utilized or over-utilized by randomly dispatching them reference signals. Here, negative reference signals depict regulation down signals, while positive reference signals represent regulation up signals. The computation of $\mathfrak{R}_{ij}^{ref,sch}(t)$ is done as per the below mentioned function, *i.e.*, $\mathbb{F}_4(C_{ij}^{sch}(t), D_{ij}^{sch}(t))$.

$$\begin{aligned}&\min\ \mathbb{F}_4(C_{ijk}^{sch}(t), D_{ijk}^{sch}(t)) = \\ &\left(\mathfrak{R}^{ref}(t) - \sum_{i\in\mathscr{M}}\sum_{j\in\mathscr{N}}\{\mathfrak{R}_{11}^{ref,sch}(t) + ... + \mathfrak{R}_{mn}^{ref,sch}(t)\}\right)\end{aligned} \tag{5.4}$$

where,

$$\mathfrak{R}_{ij}^{ref,sch}(t) = \begin{cases}\mathfrak{R}^{ref}(t) \times \dfrac{\mathfrak{F}_{ij}^{up}(t)}{\sum_{i\in\mathscr{M}}\sum_{j\in\mathscr{N}}\mathfrak{F}_{ij}^{up}(t)}; \text{if } \mathfrak{R}^{ref}(t) \geq 0 \\ \mathfrak{R}^{ref}(t) \times \dfrac{\mathfrak{F}_{ij}^{down}(t)}{\sum_{i\in\mathscr{M}}\sum_{j\in\mathscr{N}}\mathfrak{F}_{ij}^{down}(t)}; \text{if } \mathfrak{R}^{ref}(t) < 0\end{cases} \tag{5.5}$$

Moreover, the computation of reference signals for the individual AGs ($\mathfrak{R}_{i}^{ref,sch}(t)$) is done as follows.

$$\mathfrak{R}_{i}^{ref,sch}(t) = \sum_{j=1}^{\mathscr{N}}\mathfrak{R}_{ij}^{ref,sch}(t);\ \forall i \tag{5.6}$$

Revenue Maximization of EVs for SFR

EV's which participate in ancillary market are also provided incentives from ISO. Generally, this payment is made $\$/MW$ and it varies for both the regulation up ($\mathfrak{Pr}^{up}(t)$) and down ($\mathfrak{Pr}^{down}(t)$) services. Hence, the cumulative revenue earned by the fleet of EVs in a particular time interval (t) is formulated using the below mentioned function ($\mathbb{F}_5(C_{ij}^{sch}(t), D_{ij}^{sch}(t))$.

$$\max\ \mathbb{F}_5(C_{ij}^{sch}(t), D_{ij}^{sch}(t)) = \sum_{i\in\mathscr{M}}\sum_{j\in\mathscr{N}}\sum_{k\in k_j}\Big((\mathfrak{F}_{ijk}^{up}(t)\times\mathfrak{Pr}^{up}(t)) + (\mathfrak{F}_{ijk}^{down}(t)\times\mathfrak{Pr}^{down}(t)\Big) \tag{5.7}$$

In detail, the above equation can be represented as follows:

For Case-I:

$$\begin{aligned}\max\ \mathbb{F}_5(C_{ij}^{sch}(t), D_{ij}^{sch}(t)) = \sum_{i\in\mathscr{M}}\sum_{j\in\mathscr{N}}\sum_{k\in k_j}\Bigg(\Bigg(\Big(SoC_{ijk}^{d,ini}(t) - SoC_{optmin}\Big)\times\frac{E_{ijk}^{rated}\times D_{ijk}^{sch}(t)}{100}\\ \times\mathfrak{Pr}^{up}(t)\Big) + \Big(-\Big(SoC_{optmax} - SoC_{ijk}^{c,ini}(t)\Big)\times\frac{E_{ijk}^{rated}\times C_{ijk}^{sch}(t)}{100}\times\mathfrak{Pr}^{down}(t)\Big)\Bigg)\end{aligned} \tag{5.8}$$

For Case-II:

$$\begin{aligned}\max\ \mathbb{F}_5(C_{ij}^{sch}(t), D_{ij}^{sch}(t)) = \sum_{i\in\mathscr{M}}\sum_{j\in\mathscr{N}}\sum_{k\in k_j}\Bigg(\Bigg(\Big(SoC_{ijk}^{d,ini}(t) - SoC_{min}\Big)\times\frac{E_{ijk}^{rated}\times D_{ijk}^{sch}(t)}{100}\\ \times\mathfrak{Pr}^{up}(t)\Big) + \Big(-\Big(SoC_{max} - SoC_{ijk}^{c,ini}(t)\Big)\times\frac{E_{ijk}^{rated}\times C_{ijk}^{sch}(t)}{100}\times\mathfrak{Pr}^{down}(t)\Big)\Bigg)\end{aligned} \tag{5.9}$$

The detailed explanation with respect to $\mathfrak{F}_{ijk}^{up}(t)$ and $\mathfrak{F}_{ijk}^{down}(t)$ is provided in the upcoming segment.

5.2.2 List of Constraints

Estimation of FRCs of EVs, CSs and AGs

The available FRC of EVs is calculated in response of the regulation up and down signals. Hence, EV's FRCs is symbolically represented using two symbols, *i.e.*, $\mathfrak{F}^{up}_{ijk}(t)$ and $\mathfrak{F}^{down}_{ijk}(t)$. Here, $\mathfrak{F}^{up}_{ijk}(t)$ denotes the FRC of the i^{th} EV for providing regulation up services, whereas the parameter $\mathfrak{F}^{down}_{ijk}(t)$ represents the FRC of the EV for sustaining regulation down services at t instant. The mathematically representation for the same is illustrated as follows:

$$\mathfrak{F}^{up}_{ijk}(t) = \begin{cases} \left(SoC^{d,ini}_{ijk}(t) - SoC_{optmin}\right) \times \dfrac{E^{rated}_{ijk} \times D^{sch}_{ijk}(t)}{100}; C\text{-}I \\ \left(SoC^{d,ini}_{ijk}(t) - SoC_{min}\right) \times \dfrac{E^{rated}_{ijk} \times D^{sch}_{ijk}(t)}{100}; C\text{-}II \end{cases} \tag{5.10}$$

$$\mathfrak{F}^{down}_{ijk}(t) = \begin{cases} -\left(SoC_{optmax} - SoC^{c,ini}_{ijk}(t)\right) \times \dfrac{E^{rated}_{ijk} \times C^{sch}_{ijk}(t)}{100}; C\text{-}I \\ -\left(SoC_{max} - SoC^{c,ini}_{ijk}(t)\right) \times \dfrac{E^{rated}_{ijk} \times C^{sch}_{ijk}(t)}{100}; C\text{-}II \end{cases} \tag{5.11}$$

In the above equations, the indices i and j denote the respective AG and CS under consideration. The initial SoC of k^{th} EV seeking charging/discharging at time t is represented using $SoC^{c,ini}_{ijk}(t)$/$SoC^{d,ini}_{ijk}(t)$. EV's scheduled charging and discharging rates are denoted using $C^{sch}_{ijk}(t)$ and $D^{sch}_{ijk}(t)$ respectively. Moreover, values of $\mathfrak{F}^{up}_{ijk}(t)$ and $\mathfrak{F}^{down}_{ijk}(t)$ are computed in accordance with the categorization of frequency deviations into Case-I (*C-I*) and II (*C-II*) respectively. These computed FRC values ($\mathfrak{F}^{up}_{ijk}(t)$ and $\mathfrak{F}^{down}_{ijk}(t)$) are nothing but the amounts of the power that are either dispatched from the vehicles to grid (*i.e.*, V2G) or withdrawn by the vehicle from the grid (*i.e.*, Grid-to-Vehicle). Additionally, EV's charging/discharging time would be proportional to its corresponding FRC. In other words, it is considered as a function of EV's initial SoC level ($SoC^{d,ini}_{ijk}(t)$ and $SoC^{c,ini}_{ijk}(t)$), E^{rated}_{ijk}, $C^{sch}_{ijk}(t)$ and $D^{sch}_{ijk}(t)$.

It is worth mentioning here that the above mentioned approach helps to keep the final SoC level of EV's battery either in the optimal or the suboptimal SoC range. Nevertheless, the proposed scheme can also be extended to the case; wherein user's specify the EV's final SoC range. This can be achieved by remodeling Eqs. (5.10) and (5.11) with the following equations respectively.

$$\mathfrak{F}_{ijk}^{up}(t) = \left(SoC_{ijk}^{d,ini}(t) - SoC_{min}^{usr}\right) \times \frac{E_{ijk}^{rated} \times D_{ijk}^{sch}(t)}{100} \tag{5.12}$$

$$\mathfrak{F}_{ijk}^{down}(t) = -\left(SoC_{max}^{usr} - SoC_{ijk}^{c,ini}(t)\right) \times \frac{E_{ijk}^{rated} \times C_{ijk}^{sch}(t)}{100} \tag{5.13}$$

In the above equations, the FRCs of the participating EVs is computed in accordance with the user specified SoC ranges for charging (SoC_{max}^{usr}) and discharging (SoC_{min}^{usr}) respectively. However, such an approach may undermine the relative importance of the proposed scheme for minimizing battery degradation.

Using the above equations, the FRCs of CSs ($\mathfrak{F}_{ij}^{up}(t)$ and $\mathfrak{F}_{ij}^{down}(t)$) and AGs ($\mathfrak{F}_{i}^{up}(t)$ and $\mathfrak{F}_{i}^{down}(t)$) for regulation up and down services is computed using the following set of equations.

$$\mathfrak{F}_{ij}^{up}(t) = \sum_{j \in \mathcal{N}} \sum_{k \in k_j} \mathfrak{F}_{ijk}^{up}(t) \tag{5.14}$$

$$\mathfrak{F}_{ij}^{down}(t) = \sum_{j \in \mathcal{N}} \sum_{k \in k_j} \mathfrak{F}_{ijk}^{down}(t) \tag{5.15}$$

$$\mathfrak{F}_{i}^{up}(t) = \sum_{i \in \mathcal{M}} \sum_{j \in \mathcal{N}} \sum_{k \in k_j} \mathfrak{F}_{ijk}^{up}(t) \tag{5.16}$$

$$\mathfrak{F}_{i}^{down}(t) = \sum_{i \in \mathcal{M}} \sum_{j \in \mathcal{N}} \sum_{k \in k_j} \mathfrak{F}_{ijk}^{down}(t) \tag{5.17}$$

Total FRC Constraint

The total FRC ($\mathfrak{F}^{tot}(t)$) of the considered V2G setup is computed using the following equation, wherein $\mathfrak{F}^{tot}(t)$ is defined as the sum of the total FRCs of the participating EVs supporting both regulation up and down services.

$$\mathfrak{F}^{tot}(t) = \sum_{i \in \mathcal{N}} \mathfrak{F}^{up}(t) + \sum_{i \in \mathcal{N}} \mathfrak{F}^{down}(t) \tag{5.18}$$

EV's Battery Charging & Discharging Constraint

Studies suggest that maintaining the SoC level of the EV's batteries in a reasonable range plays a significant role in maximizing the battery's lifetime. Existing research studies suggest to maintain SoC levels with the permissible range of [SoC_{max}, SoC_{min}]. Here, parameters SoC_{max} and SoC_{min} denote the minimum and maximum SoC levels up to which the EV's batteries should be charged and discharged respectively [149, 162]. However, recent experimental validation done by National Renewable Energy Laboratory on Li-ion batteries has lead to contrasting results [154]. The obtained results indicate that the batteries which maintain their SoC levels in the range of 30-50% (throughout their life time) have comparatively slower battery degradation rates than the batteries which maintain their SoC in the ranges of 70-90% and 20%-40%. Hence, motivated by this fact, authors in [154] have used the battery characteristics as depicted in Fig. 5.1. As indicated in the figure, EV's batteries can have different SoC level namely-SoC_{max}, SoC_{optmax}, SoC_{optmin} and SoC_{min}. EV's batteries in the proposed frequency support setup are categorized to provide SFR support under varied circumstances. For instance, during normal circumstances (C-I); EV's maintain their current SoC levels ($SoC^{cur}_{ijk}(t)$) in an optimal range of $SoC_{optmin} \leq SoC^{cur}_{ijk}(t) \leq SoC_{optmax}$. On the other hand, EVs tend to provide enhanced FRCs by pushing their SoC levels in the suboptimal

range $SoC_{min} \leq SoC_{ijk}^{cur}(t) \leq SoC_{max}$ under C-II. This is represented as follows.

$$SoC_{ijk}^{cur}(t) = \begin{cases} SoC_{optmin} \leq SoC_{ijk}^{cur}(t) \leq SoC_{optmax}; C\text{-}I \\ SoC_{min} \leq SoC_{ijk}^{cur}(t) \leq SoC_{max}; C\text{-}II \end{cases} \tag{5.19}$$

Apart from maintaining the SoC levels of the EV's batteries within the optimal range, the present work also extends the concept of maintaining $C_{ijk}^{sch}(t)$ and $D_{ijk}^{sch}(t)$ in the optimal and sub-optimal ranges. It is mathematically represented as follows:

$$C_{ijk}^{sch}(t) = \begin{cases} C_{optmin} \leq C_{ijk}^{sch}(t) \leq C_{optmax}; C\text{-}I \\ C_{min} \leq C_{ijk}^{sch}(t) \leq C_{max}; C\text{-}II \end{cases} \tag{5.20}$$

$$D_{ijk}^{sch}(t) = \begin{cases} D_{optmin} \leq D_{ijk}^{sch}(t) \leq D_{optmax}; C\text{-}I \\ D_{min} \leq D_{ijk}^{sch}(t) \leq D_{max}; C\text{-}II \end{cases} \tag{5.21}$$

5.3 Results and Discussions

This section presents in detail the simulation strategy considered for the evaluation of the proposed scheme on real-time traces acquired from PJM [143] and CAISO [163]. The results have been evaluated using Mosek solver [161]. Additionally, it also highlights the comparison of the proposed scheme against the existing technique [162].

The considered simulation setup takes into account the parameters illustrated in Table-5.1 for evaluating the proposed scheme on 24 hours timescale. As evident from the table, the case-study comprises of 3 AGs (AG_1, AG_2, AG_3) and 6 CSs ($CS_{11}, CS_{12}, CS_{21}, CS_{22}, CS_{23}, CS_{31}$) in total for providing effective grid ancillary services using fleet of EVs. However, the proposed scheme is extensible for $\mathscr{M}$ number of AGs and $\mathscr{N}$ of CSs.

Table 5.1: Simulation parameters considered

Parameters	**Values**	**Parameters**	**Values**
No. of AGs	3	Case-I:$\lvert\Delta f\rvert$	≤ 0.2
No. of CSs	6	Case-II:$\lvert\Delta f\rvert$	≥ 0.2
No. of EVs/CS	0-60	E_{ijk}^{rated}	16
SoC_{optmax}	70	C_{optmax}/D_{optmax}	1.5
SoC_{max}	90	C_{max}/D_{max}	2
SoC_{optmin}	40	C_{optmin}/D_{optmin}	0.5
SoC_{min}	20	C_{min}/D_{min}	0

The real-time traces have been acquired from PJM and CAISO for performing extensive simulations. Data from the two sources corresponds to the real-time regulation signals and prices for providing reliable regulation up and down services respectively. These data sets have depicted using Figs. 5.2a and 5.2b. For instance, at 2000 hours $\mathfrak{R}^{ref}(t)$ of -176.88 kW was triggered due to demand and supply imbalances. The corresponding regulation prices offered by the ISO to manage the frequency deviations were 5.5 \$/kW and 3.5 \$/kW respectively for regulation up and down services. These deviations in grid's frequency is depicted using Fig. 5.2c. At 2000 hours, frequency deviations of -0.01 Hz (C-I) was observed due to demand and supply imbalances. The total number of the EVs considered in the simulation setup is shown using Fig. 5.2d, wherein 179 and 180 EVs at the CSs were participated in charging and discharging activities respectively. The rebalancing of these fluctuations is catered as follows.

The FRC estimator computed the cumulative FRCs of the AGs, *i.e.*, $\mathfrak{F}_i^{up}(t)$ and $\mathfrak{F}_i^{down}(t)$. The estimated values across 24 hours are shown using Fig. 5.2e. For instance, at 2000 hours $\mathfrak{F}_i^{up}(t)$ and $\mathfrak{F}_i^{down}(t)$ values were found to be 412.6 and -830.4 kW respectively. Based on these values, the regulation signal of -176.88 kW was dispatched amongst the AGs and CSs using the designed MILP-based problem. The reference signals segregated amongst the AGs and CSs are highlighted in Figs. 5.2f and 5.2g. At 2000 hours, the scheduled reference signals for the CSs were found to be -40.61, -22.70, -25.94, -47.75, -15.71, and -24.14 kW respectively. This segregation of $\mathfrak{R}^{ref}(t)$ is in accordance with the respective FRCs of the CSs.

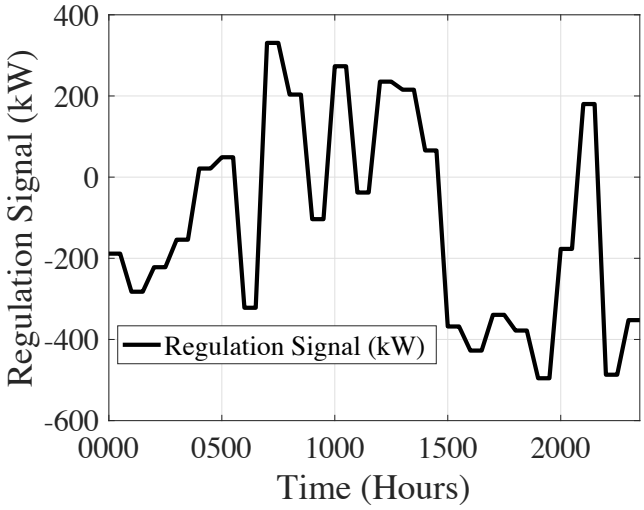

5.2(a) PJM regulation signals with respect to 6^{th} June 2014.

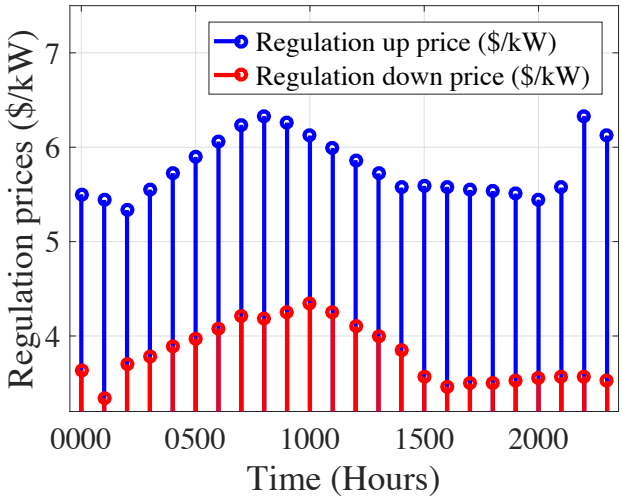

5.2(b) Regulation up and down prices acquired from CAISO for the year 2014.

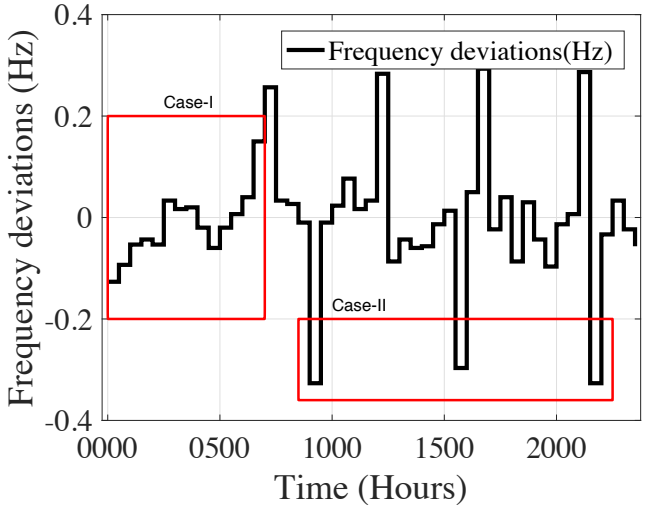

5.2(c) Grid frequency fluctuations.

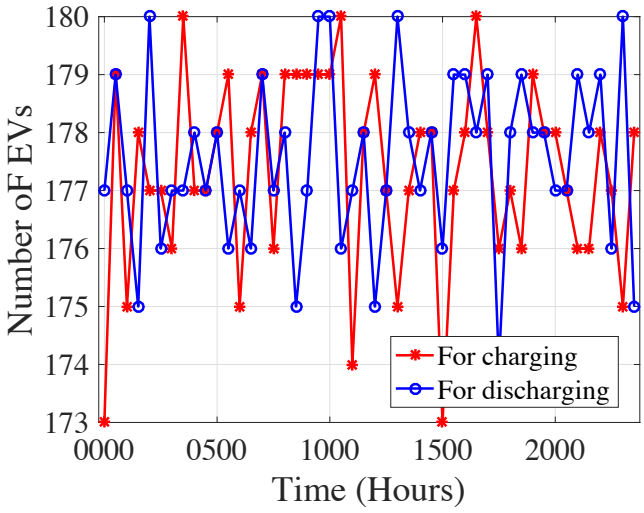

5.2(d) Total number of EVs for charging and discharging

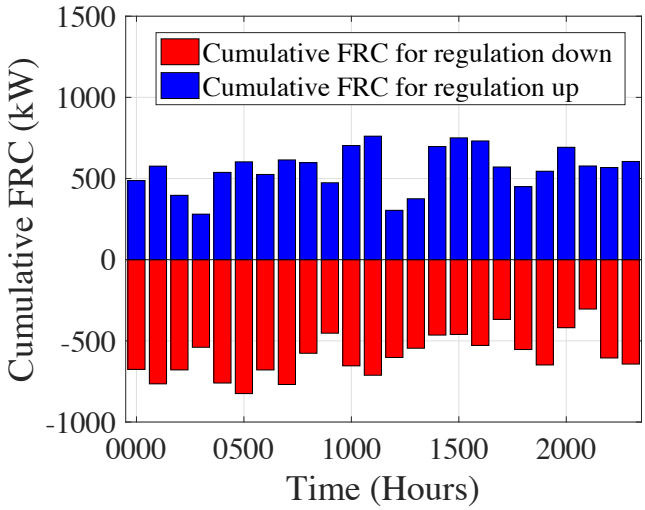

5.2(e) Cumulative FRCs for regulation up and down services.

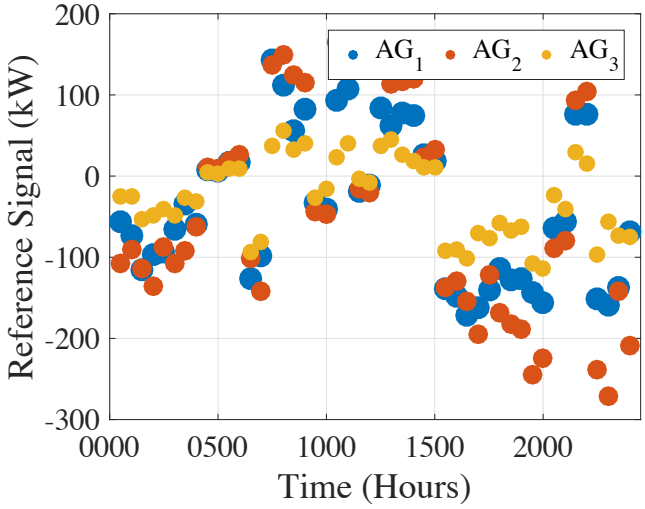

5.2(f) Dispatch of regulation signals across aggregators.

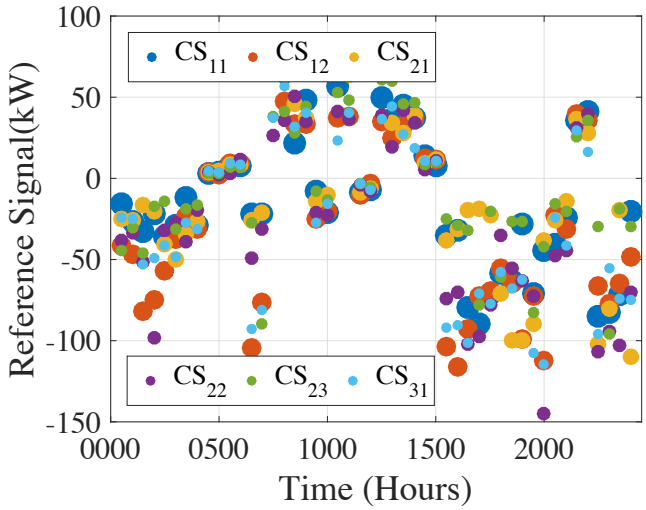

5.2(g) Dispatch of regulation signals across charging stations.

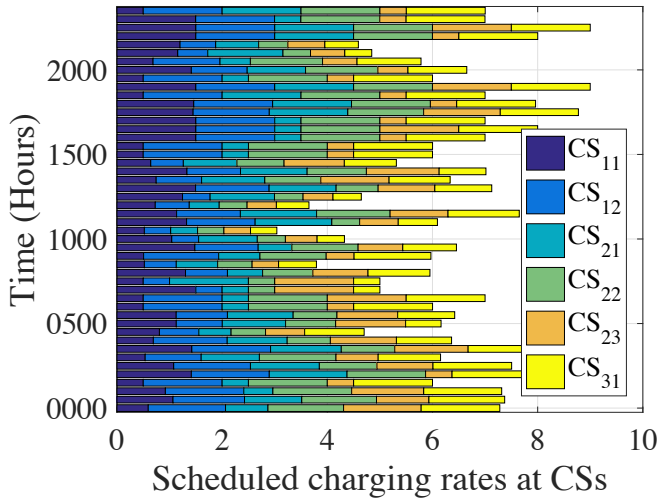

5.2(h) Scheduled $C_{ij}^{sch}(t)$ of participating EVs at different CSs.

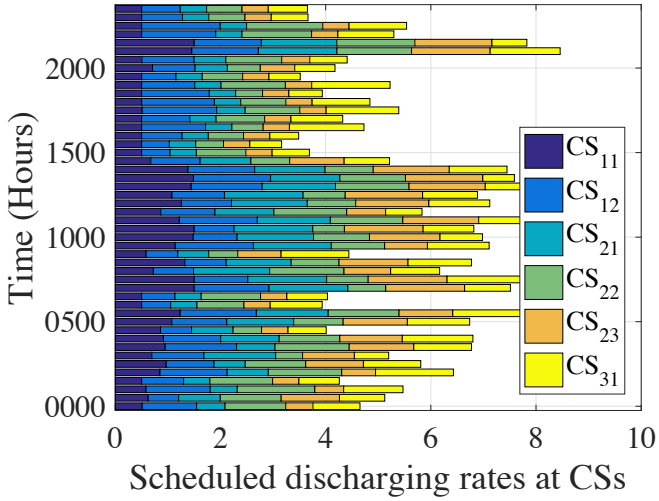

5.2(i) Scheduled $D_{ij}^{sch}(t)$ of participating EVs at different CSs.

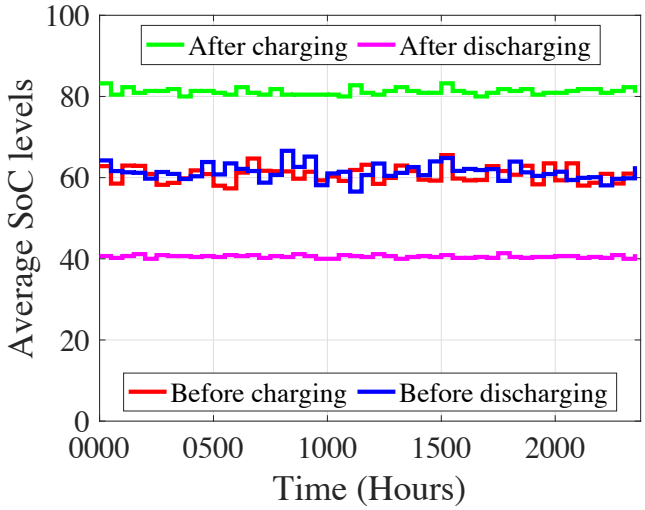

5.2(j) Average SoC variations before and after charging and discharging activities.

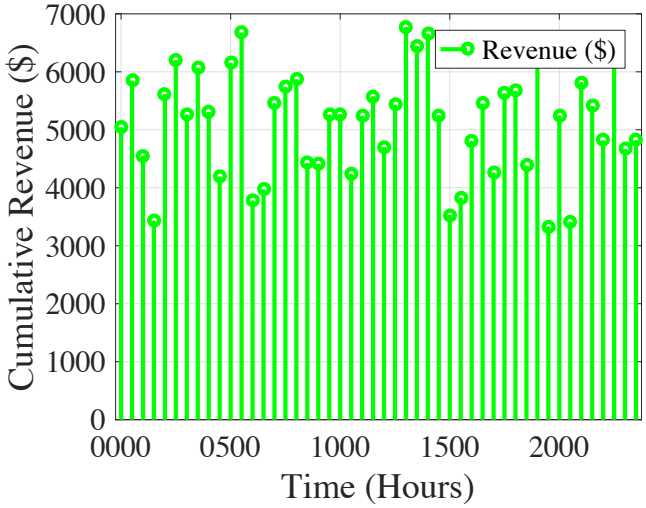

5.2(k) Cumulative revenue earned by the EVs available at different CSs.

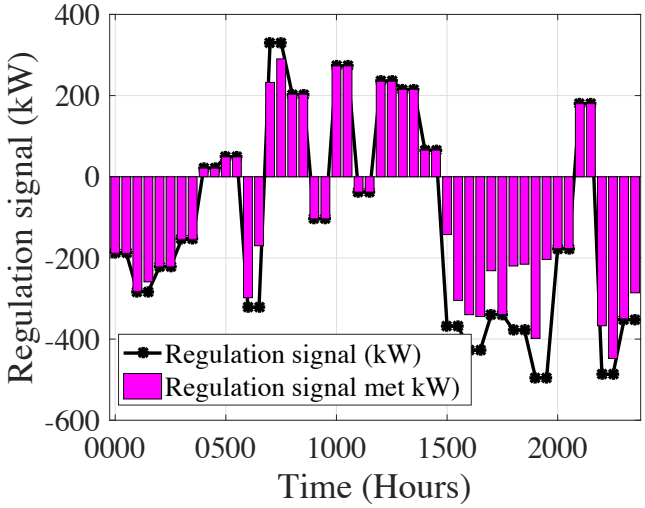

5.2(l) Regulation support using the proposed scheme.

Figure 5.2: Performance results obtained using the proposed scheme.

This is done so as to achieve the full capacity of the underlying CSs for providing effective and reliable frequency support. In order to reflect the same, the concept of optimal and maximum/minimum charging/discharging has been introduced in Section 5.2.2. The related results have been pictorially represented using Figs. 5.2h and 5.2i respectively. For instance, at 2000 hours, the $C_{ij}^{sch}(t)$ and $D_{ij}^{sch}(t)$ varied between the optimal range as the frequency deviations were classified as C-I. Thereby, reducing the battery degradation impacts on the EVs' batteries.

Due to the alteration in $C_{ij}^{sch}(t)$ and $D_{ij}^{sch}(t)$ values, significant change in the SoC levels of the participating EVs was observed. The corresponding results have been represented using Fig. 5.2j. The figure clearly depicts the average SoC variations of the EVs' batteries over the regulation process; wherein, the SoC levels of the batteries were always maintained within the optimal range; hence, minimizing the impact of battery degradation. In addition to this, the results also indicate the proposed scheme caters the charging and discharging requirements of the EVs across all the CSs.

In addition to the above mentioned contributions, the proposed scheme also aims to maximize EVs' profit margins by involving them in different time slots as per $\mathfrak{Pr}^{up}(t)$ and $\mathfrak{Pr}^{down}(t)$ values. Hence, the corresponding findings to maximize EV's revenue are summarized in Fig. 5.2k. As depicted in the figure, the cumulative revenue earned by EVs across all the CSs at 2000 hours was found to be approximately \$5245.7.

Finally, the primary agenda of the proposed scheme was to minimize the frequency fluctuations using integrated fleet of EVs. Hence, the regulation power met using the proposed scheme is highlighted using Fig. 5.2l. The results clearly depict the proposed scheme tracks the regulation signal in majority of the cases *e.g.* at 2000 hours.

5.3.1 Comparison with an existing scheme

To evaluate the efficacy of the proposed scheme, an existing scheme presented in [162] has been taken into account. It has the maximum resemblance to the proposed technique except the consideration of EV's revenue and their battery degradation. Hence, it has been chosen for evaluating the efficacy of the proposed scheme.

For the sake of clarity, the datasets as shown in Figs. 5.2a and 5.2b along with the parameters highlighted in Table-5.1 have been considered for performing the comparative evaluation of the two schemes. The results obtained are highlighted using Fig. 5.2. The considered existing scheme is ideally a 2-layer hierarchical control scheme (HCM) based on droop mechanism using which it segregates the reference signals amongst the CSs and AGs. On the other hand, the proposed scheme is based on the robust MILP-based optimization technique which dispatches the reference signals according the FRCs of the participating AGs and CSs. Additionally, the computation of $C_{ijk}^{sch}(t)$ and $D_{ijk}^{sch}(t)$ is also widely apart. Due to these reasons, the two schemes defer in achieving reliable frequency support as shown in Fig. 5.3c. It is evident from the results that the proposed scheme achieves superior results than the existing scheme in terms of tracking the regulation signal.

Moreover, the relative comparison of the two schemes in terms of regulating the $C_{ijk}^{sch}(t)$ and $D_{ijk}^{sch}(t)$ is shown using Figs. 5.2h and 5.3a, and Figs. 5.2i and 5.3b respectively. The results clearly depict the existing scheme fails to maintain the $C_{ijk}^{sch}(t)$ and $D_{ijk}^{sch}(t)$ within the optimal limits even during normal scenario (C-I), leading to higher battery degradation issues. On the other hand, the proposed scheme tracks the regulation signal much more efficiently while keeping the $C_{ijk}^{sch}(t)$ and $D_{ijk}^{sch}(t)$ within the optimal range. Thus, the results clearly validate the efficacy of the proposed scheme in terms of its implementation in real-time scenario.

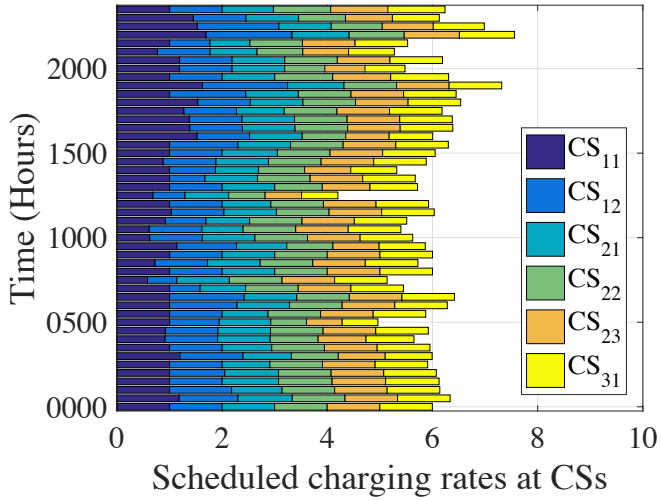

5.3(a) Scheduled $C_{ij}^{sch}(t)$ using the existing scheme.

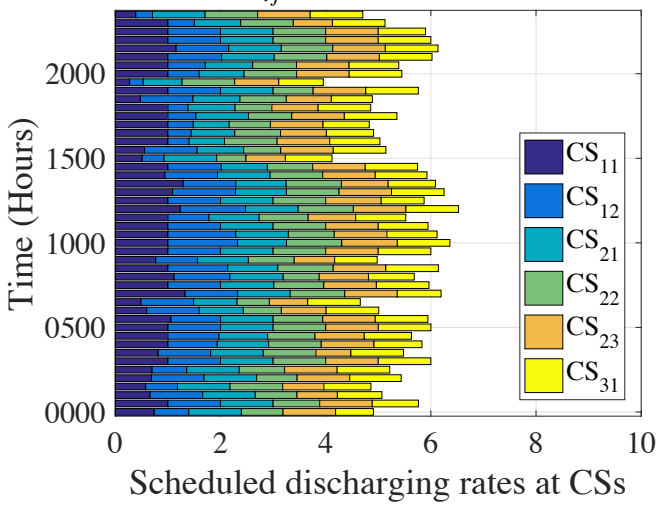

5.3(b) Scheduled $D_{ij}^{sch}(t)$ using the existing scheme.

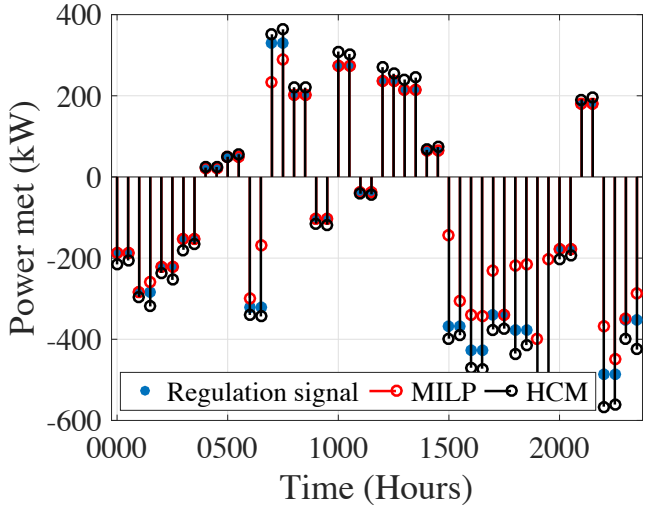

5.3(c) Regulation support using the proposed scheme and the existing scheme.

Figure 5.3: Comparison of the proposed scheme and the existing scheme.

5.4 Concluding Remarks

In this chapter, a hierarchical controlling approach for grid frequency support has been proposed. The designed approach regulates frequency fluctuations using fleet of EVs in multi-constraint V2G setup and has been modelled using MILP. Different competing objective functions considered in this approach incorporate: optimal regulation signal dispatch, minimal battery degradation, and optimal V2G support with enhanced revenue. In the next chapter, potential role of DCs in grid frequency stabilization is explored; wherein the major concentration is on energy minimization using effective job scheduling mechanism.

Chapter 6

Energy-aware and SLA-driven MapReduce Job Scheduling Framework for Cloud Data Centers

In this chapter, a MapReduce based job scheduling strategy has been proposed. It is as a special case of task-to-slot mapping which balances the trade-off between energy utilization and SLA adherence. Moreover, it introduces the novel concept of splitting the Map/Reduce phases into multiple stages in order to achieve higher energy reductions. The detailed working of the proposed scheme is as under.

6.1 Problem Formulation

MapReduce and its open-source implementation Hadoop have been widely adopted by various IT giants such as-Google, Yahoo, Facebook, HP, *etc.* for faster job processing and task parallelization. MapReduce framework is typically characterized by the two main phases, *i.e.*, map phase and reduce phase. Fig. 6.1 depicts the working of these two phases and

their respective relationships with each other. As evident from the figure, a submitted job is segregated into two main phases; wherein the map phase precedes the reduce phase. In the former phase, data blocks are read from the distributed file system (DFS) to process and produce the intermediate key-value pairs. These intermediate results are then submitted to the reduce phase, which initially shuffles and sorts them. Finally, the result in the form of key-value pairs is generated by the reduce phase.

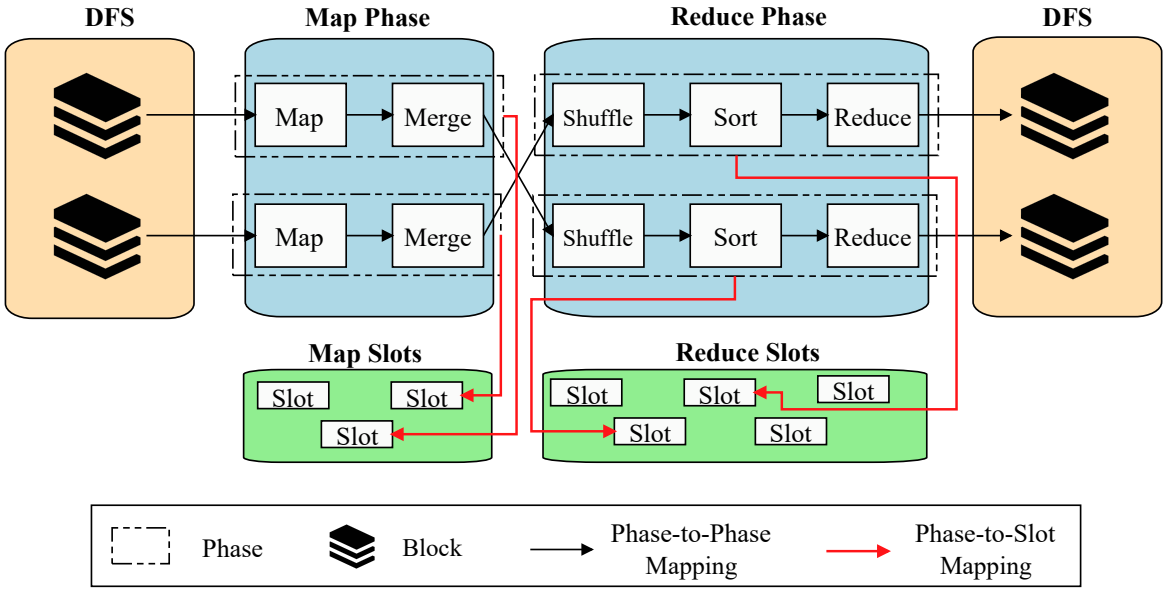

Figure 6.1: Phases of MapReduce.

This entire process of executing the map and reduce tasks is achieved by mapping these tasks to their respective containers (referred as slots in rest of the thesis) as depicted in the Fig. 6.1. This task-to-slot mapping can be done with the optimization of different parameters such as-energy, makespan, SLA, deadline guarantee, throughput, availability, etc. However, the primary aim of the present work is to explore this task-to-slot mapping problem as a special case of energy-aware scheduling in deadline-constrained scenario. Hence, this problem can be viewed as a complex multi-objective problem comprising of different constraints. In detail, the problem is closely coupled with the SLA targets (deadline guarantee) and non-shareable property of map and reduce slots; in addition to overall energy consumption minimization.

Due to the involved complexity of the overall problem, it is further divided into three smaller and manageable SPs. These SPs are described as follows and pictorially represented using Fig. 6.2.

1. **SP 1:** Segregation of job deadline between the two independent phases, *i.e.*, Map and Reduce phase. This is done in order to maintain the required SLA bounds across both the phases; as the former precedes the latter and both require dedicated deadlines.

2. **SP 2:** Energy-aware scheduling of map tasks within the computed job deadline for map phase.

3. **SP 3:** Energy-aware scheduling of reduce tasks within the computed job deadline for reduce phase.

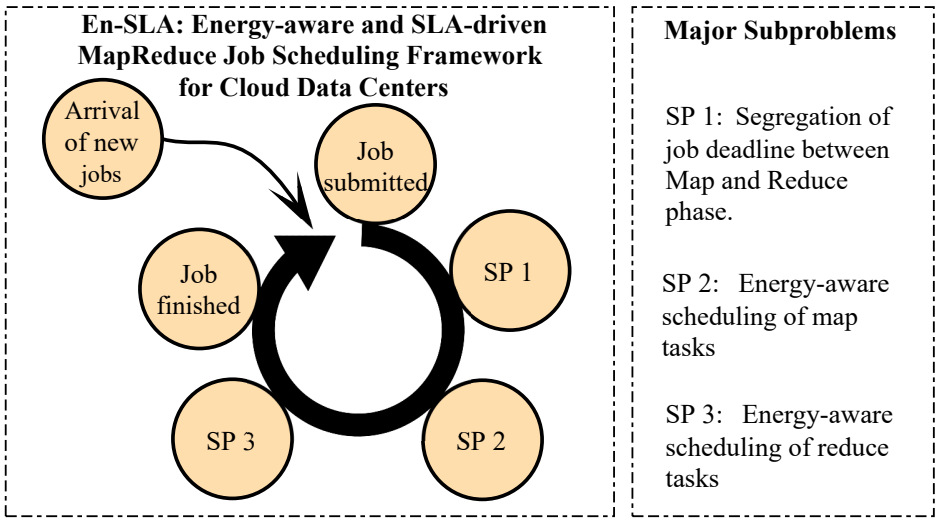

Figure 6.2: Flowchart depicting the working philosophy of the proposed job scheduling framework.

For the purpose of clear understanding, a typical example of a MapReduce job has been depicted in Fig. 6.3. The list of related symbols with their respective meanings are summarized in Table-6.1. The energy consumption and processing deadlines related to task execution on different map and reduce slots (a_k and b_l) is clearly depicted in the figure. For

instance, Fig. 6.3a illustrates the processing and energy consumption statistics of executing map tasks $\mathbb{M} = \{t_1^m, ..., t_i^m, ..., t_s^m\}$ on the available set of map slots, *i.e.*, $A = \{a_1, ..., a_k, ..., a_p\}$. The parameters $p_{i,k}^m$ and $e_{i,k}^m$ depict the processing time and energy consumption statistics corresponding to allocation of the i^{th} map slot on the k^{th} map slot. Similarly, the parameters $p_{j,l}^r$ and $e_{j,l}^r$ represent the respective entities for the reduce phase and the same is depicted using Fig. 6.3b.

Map Tasks

	Processing Time	Energy Consumption
Slots $\longrightarrow$	$a_1 \ ...a_k... \ a_p$	$a_1 \ ...a_k... \ a_p$
Tasks t_1^m	$p_{1,1}^m ... p_{1,k}^m ... \ p_{1,p}^m$	$e_{1,1}^m ... e_{1,k}^m ... \ e_{1,p}^m$
$\downarrow$	...	...
t_i^m	$p_{i,1}^m ... p_{i,k}^m ... \ p_{i,p}^m$	$e_{i,1}^m ... e_{i,k}^m ... \ e_{i,p}^m$
	...	...
t_s^m	$p_{s,1}^m ... p_{s,k}^m ... \ p_{s,p}^m$	$e_{s,1}^m ... e_{s,k}^m ... \ e_{s,p}^m$

6.3(a) Map Phase.

Reduce Tasks

	Processing Time	Energy Consumption
Slots $\longrightarrow$	$b_1 \ ...b_l... \ b_q$	$b_1 \ ...b_l... \ b_q$
Tasks t_1^r	$p_{1,1}^r ... p_{1,l}^r ... \ p_{1,q}^r$	$e_{1,1}^r ... e_{1,l}^r ... \ e_{1,q}^r$
$\downarrow$	...	...
t_j^r	$p_{j,1}^r ... p_{j,l}^r ... \ p_{j,q}^r$	$e_{j,1}^r ... e_{j,l}^r ... \ e_{j,q}^r$
	...	...
t_t^r	$p_{t,1}^r ... p_{t,l}^r ... \ p_{t,q}^r$	$e_{t,1}^r ... e_{t,l}^r ... \ e_{t,q}^r$

6.3(b) Reduce Phase.

Figure 6.3: Typical example of MapReduce job and its corresponding details pertaining to energy consumption and processing time.

6.1.1 Assumptions

The following assumptions have been considered in the proposed work:

1. **The computing infrastructure is assumed to be heterogeneous in nature:** Heterogeneity in the cloud DCs is mainly caused due to regular maintenance, sharing of resources by various cloud tenants and the diversity in the performance needs of

the underlying clusters. Literature suggests that the existing schemes fall short on heterogeneous MapReduce configurations. Hence, it is essential to devise effective job scheduling techniques that scale well with heterogeneous hardware and software configurations in cloud setup.

2. **For the sake of simplicity, the concept of data locality has not been considered in the proposed work:** Ananthanarayanan *et al.* [164] advocated that the concept of data locality will become inconsequential in the near future due to the predominant advances made by the networking community in the last few years. These advances have drastically improved the reading from a disk located in another node (of same or another rack) relative to the local disk. This in turn falsifies the basic data locality assumption, *i.e.*, "disk bandwidths exceed network bandwidths". Apart from this, compression further decreases the size of data to be read from the disk; which invalidates the second data locality assumption, *i.e.*, "disk I/O constitutes a considerable fraction of a task's lifetime."

6.1.2 Subproblem 1: Segregation of job deadline between two phases

This SP is the starting phase for effectively scheduling the map and reduce tasks to different machine slots in accordance with the objective of energy minimization. Hence, the foremost step in this process is to distribute the overall job deadline ($\mathbb{D}$) between the two phases since, the reduce phase operates only after the successful execution of the map phase. In order to achieve this task, we formulate the SP as an ILP and define it as follows:

$$\max\left(\sum_{i=0}^{s}\sum_{k=0}^{p} p_{i,k}^{m}\mathbb{D}_{i,k}^{m} + \sum_{j=0}^{t}\sum_{l=0}^{q} p_{j,l}^{r}\mathbb{D}_{j,l}^{r}\right) \tag{6.1}$$

Table 6.1: List of symbols used with their respective meanings.

Symbols	Meanings
A	Set of available map slots.
$\mathbb{A}$	Assignment matrix.
a_k	k^{th} map slot.
$\mathbb{B}$	Set of available reduce slots.
b_l	l^{th} reduce slot.
C^{HA}	Column optimal values returned using classical HA.
C^{GR}	Column optimal values returned using Greedy approach.
d_1	Difference between the total deadline for Map and Reduce phase respectively.
$\mathbb{D}$	Total deadline for completing the considered MapReduce job.
$\mathbb{D}^m$	Total deadline for completing the map phase of the considered MapReduce job.
$\mathbb{D}^m_{i,k}$	Binary decision variable used to deduce $\mathbb{D}^m$.
$\mathbb{D}^r$	Total deadline for completing the reduce phase of the considered MapReduce job.
$\mathbb{D}^r_{j,l}$	Binary decision variable used to deduce $\mathbb{D}^r$.
$\mathbb{D}'$	Expected job deadline.
$e^m_{i,k}$	Energy consumption of the i^{th} map task on the k^{th} map slot.
$e^r_{j,l}$	Energy consumption of the j^{th} reduce task on the l^{th} reduce slot.
$E^m_{S\times P}$	Energy consumption matrix for map tasks.
$E^r_{T\times Q}$	Energy consumption matrix for reduce tasks.
E^{HA}_{tot}	Optimal energy consumption for Map/Reduce phase computed using classical HA.
E^{GR}_{tot}	Optimal energy consumption for Map/Reduce phase computed using Greedy approach.
i	Index for referring a map task.
j	Index for referring a reduce task.
k	Index for referring a map slot.
l	Index for referring a reduce slot.
$\mathbb{M}$	Set of map tasks.
s	Number of map tasks.
t	Number of reduce tasks.
p	Number of map slots.
$p^m_{i,k}$	Processing time of the i^{th} map task on the k^{th} map slot.
$p^r_{j,l}$	Processing time of the j^{th} reduce task on the l^{th} reduce slot.
P^{HA}_{tot}	Optimal processing time for Map/Reduce phase computed using classical HA.
P^{GR}_{tot}	Optimal processing time for Map/Reduce phase computed using Greedy approach.
$\mathbb{P}^m_{S\times P}$	Processing time matrix for map tasks.
$\mathbb{P}^r_{T\times Q}$	Processing time matrix for reduce tasks.
$\mathbb{PQ}$	Priority queues per map/reduce slot.
q	Number of reduce slots.
$\mathbb{R}$	Set of reduce tasks.
t^m_i	i^{th} map task.
t^r_j	j^{th} reduce task.
$\mathbb{V}$	Largest value of the matrix under consideration.
$X^m_{i,k}$	Binary decision variable to assign i^{th} map task on the k^{th} slot.
$Y^r_{j,l}$	Binary decision variable to assign j^{th} reduce task on the l^{th} slot.

$$st: \quad \sum_{i=1}^{s}\sum_{k=1}^{p} p_{i,k}^{m}\mathbb{D}_{i,k}^{m} + \sum_{j=1}^{t}\sum_{l=1}^{q} p_{j,l}^{r}\mathbb{D}_{j,l}^{r} \leq \mathbb{D} \tag{6.2}$$

$$\sum_{i=1}^{s}\sum_{k=1}^{p} \mathbb{D}_{i,k}^{m} = 1 \tag{6.3}$$

$$\sum_{j=1}^{t}\sum_{l=1}^{q} \mathbb{D}_{j,l}^{r} = 1 \tag{6.4}$$

$$\mathbb{D}_{i,k}^{m} = \{0,1\}; \forall i,k \tag{6.5}$$

$$\mathbb{D}_{j,l}^{r} = \{0,1\}; \forall j,l \tag{6.6}$$

where, $\mathbb{D}_{i,k}^{m}$ and $\mathbb{D}_{j,l}^{r}$ are the binary decision variables and are defined as follows:

$$\mathbb{D}_{i,k}^{m} = \begin{cases} 1, \text{ If } p_{i,k}^{m} \text{ is selected to deduce } \mathbb{D}^{m}, \\ 0, \text{ otherwise.} \end{cases} \tag{6.7}$$

$$\mathbb{D}_{j,l}^{r} = \begin{cases} 1, \text{ If } p_{j,l}^{r} \text{ is selected to deduce } \mathbb{D}^{r}, \\ 0, \text{ otherwise.} \end{cases} \tag{6.8}$$

The overall objective of this SP is selection of the longest and permissible deadlines for the two phases without violating the defined constraints. This is achieved using the maximization function over sum of the decision variables $\mathbb{D}_{i,k}^{m}$ and $\mathbb{D}_{j,l}^{r}$ as illustrated in Eq. (6.1). The maximization function ensures the possibility of exploring all the feasible slots wherein the tasks could be allocated without violating the constraints defined in Eqs. (6.2)-(6.6). Constraint (6.2) ensures that cumulative deadline of map and reduce phase shall not exceed $\mathbb{D}$. In addition to this, the constraints (6.3) and (6.4) ensure that no more than one $p_{i,k}^{m}$ and $p_{j,l}^{r}$ are selected to deduce the optimal values of $\mathbb{D}^{m}$ and $\mathbb{D}^{r}$ respectively. Here, $\mathbb{D}^{m}$ and $\mathbb{D}^{r}$ refer to the corresponding optimal deadlines for the map and reduce phase. Constraints represented using Eq. (6.5) and (6.6) guarantee the integrality requirements of $\mathbb{D}_{i,k}^{m}$ and $\mathbb{D}_{j,l}^{r}$ variables

respectively.

6.1.3 Subproblem 2: Energy-aware scheduling of map tasks

Energy-aware scheduling of the map tasks in the present MapReduce configuration is quite a challenging task. The primary objective of this SP is to schedule the set of map tasks $\mathbb{M} = \{t_1^m, ..., t_i^m, ..., t_s^m\}$ on the available set of map slots, *i.e.*, $A = \{a_1, ..., a_k, ..., a_p\}$. However, the complexity of this problem increases with the inclusion of the following set of the constraints (C):

C.1 The mapping of the map tasks to definite set of map slots should maintain the desired SLA, *i.e.*, $\mathbb{D}^m$ should not be violated.

C.2 The available map slots are non-shareable, *i.e.*, a particular a_k should be allocated to a definite t_i^m.

C.3 A t_i^m should be assigned for execution to at-most one a_k.

Here, ILP has been employed to formulate the above mentioned SP of scheduling map tasks and it's mathematically expressed as follows:

$$\min \left(\sum_{i=1}^{s} \sum_{k=1}^{p} e_{i,k}^m X_{i,k}^m \right) \tag{6.9}$$

subject to:

$$st: \quad \sum_{k=1}^{p} p_{i,k}^{m} X_{i,k}^{m} \leq \mathbb{D}^{m}; \forall i \tag{6.10}$$

$$\sum_{i=1}^{s} X_{i,k}^{m} = 1; \forall k \tag{6.11}$$

$$\sum_{k=1}^{p} X_{i,k}^{m} = 1; \forall i \tag{6.12}$$

$$X_{i,k}^{m} = \{0,1\}; \forall i,k \tag{6.13}$$

where, $X_{i,k}^{m}$ is the binary decision variable as defined below.

$$X_{i,k}^{m} = \begin{cases} 1, \text{ If } i^{th} \text{ map task is mapped to } k^{th} \text{ slot,} \\ 0, \text{ otherwise.} \end{cases} \tag{6.14}$$

Eq. (6.9) expresses energy minimization objective of the proposed ILP problem. Constraints C.1, C.2 and C.3 are mathematically expressed using the Eq. (6.10), (6.11) and (6.12) respectively. The last constraint expressed using Eq. (6.13) is used to represent the integrality constraint of $X_{i,k}^{m}$.

6.1.4 Subproblem 3: Energy-aware scheduling of reduce tasks

Scheduling the reduce tasks $\mathbb{R} = \{t_1^r, ..., t_j^r, ..., t_t^r\}$ on the available reduce slots, *i.e.*, $\mathbb{B} = \{b_1, ..., b_l, ..., b_q\}$; is identical to the above SP and pose the same challenges. Hence, it is formulated alike the previously discussed ILP.

$$\min \left(\sum_{j=1}^{t} \sum_{l=1}^{q} e_{j,l}^{r} Y_{j,l}^{r} \right) \tag{6.15}$$

$$st: \quad \sum_{l=1}^{q} p_{j,l}^{r} Y_{j,l}^{r} \leq \mathbb{D}^{r}; \forall j \tag{6.16}$$

$$\sum_{j=1}^{t} Y_{j,l}^{r} = 1; \forall l \tag{6.17}$$

$$\sum_{l=1}^{q} Y_{j,l}^{r} = 1; \forall j \tag{6.18}$$

$$Y_{j,l}^{r} = \{0,1\}; \forall j,l \tag{6.19}$$

where, the binary decision variable is expressed using $Y_{j,l}^{r}$ and is defined below.

$$Y_{j,l}^{r} = \begin{cases} 1, \text{ If } j^{th} \text{ reduce task is mapped to } l^{th} \text{ slot,} \\ 0, \text{ otherwise.} \end{cases} \tag{6.20}$$

6.1.5 Problem at hand

The above mentioned SPs may become computationally intractable with an increasing number of input variables. Hence, heuristics corresponding to the three SPs have been designed to obtain optimal solutions in polynomial time. The crux of the designed heuristic algorithms lies in extending the concept of Greedy approach and task assignment problem to the considered SPs. The former is an heuristic approach that makes local optimal choices at each stage with the faith of deducing the global optimal solution. The most significant advantage of greedy approach is its ability to estimate an approximate optimal solution in polynomial time. On the contrary, task assignment problem is an integral combinatorial optimization problem which deals with maximum weight matching in a weighted bipartite graph. A task assignment problem with relatively large number of variables is best solved using Hungarian Algorithm (HA) relative to the other approaches such as-enumeration, simplex method and transportation method [165]. A short description of HA and its use in the current context is elaborated as follows.

Classical HA was first proposed by a mathematician named D. Koning in order to solve task assignment problem optimally. It is also referred to as *Kuhn-Munkres* algorithm and solves the classical task assignment problem with polynomial time complexity ($O(mn^2)$ with cost matrix $X \in R^{m \times n}$). Additionally, it's widely accepted for providing the global optimal solutions. Over the years, many variants of HA have been suggested by the researchers and their applications have been utilized in wide variety of fields. Typically, HA is applied to serial systems wherein, the total assignment cost is the sum of the individual costs of the participating tasks. More recently, the authors in [166] have presented a novel approach to deduce the assignment cost of the serial-parallel systems. In such systems, the cumulative cost of the assignment problem involves the sum of the serial tasks and the maximum cost of the parallel tasks [166]. Motivated from these concepts, we extend the applications of HA for the task-to-slot mapping in the considered MapReduce setup.

6.2 En-SLA: Energy-aware and SLA-driven Job Scheduling for MapReduce

This section presents in detail the heuristic algorithms that have been designed to support the proposed job scheduling framework.

6.2.1 Algorithm for Subproblem 1

This SP deals with job deadline segregation amongst the two phases, *i.e.*, Map and Reduce phase. The sequence of the steps to address this problem has been illustrated using Algorithm 6.1. It takes the following parameters as input- $\mathbb{P}^m_{S\times P}, \mathbb{P}^r_{T\times Q}$ and $\mathbb{D}$ (Line 1), where $\mathbb{P}^m_{S\times P}$ and $\mathbb{P}^r_{T\times Q}$ denote the matrices containing the processing time of tasks across map and reduce slots respectively. Using the first two parameters, it instantiates the deadline assignment matrix

($\mathbb{A}_{(S+T)\times(P+Q)}$) (Line 1). In the next step, the parallel tasks are transformed into virtual serial tasks (Line 2). In this scenario, the tasks of the map/reduce phase are treated as parallel tasks since we intend to find the maximum possible value of the deadline as Eq. (6.1). The detailed information pertaining to the transformation of parallel tasks to virtual tasks is mentioned below.

Definition 1: Transformation of parallel tasks to virtual serial tasks

The overall idea of the serial-parallel systems is to visualize the Map and Reduce phases as pure serial tasks, whose individual deadlines contribute to overall job deadline $\mathbb{D}$. Their corresponding tasks on the other hand, can be seen as pure parallel tasks since their contributions are decided based on the maximum processing time of the participating tasks in the respective phases. The same is reflected in Fig. 6.4. Here, the overall idea is to estimate the value of $\mathbb{D}$ by transforming the considered serial-parallel system to serial system. This is achieved by remodeling the parallel tasks into virtual serial tasks using selection of tasks with the maximum processing time. The detailed information about the same can be found in [166].

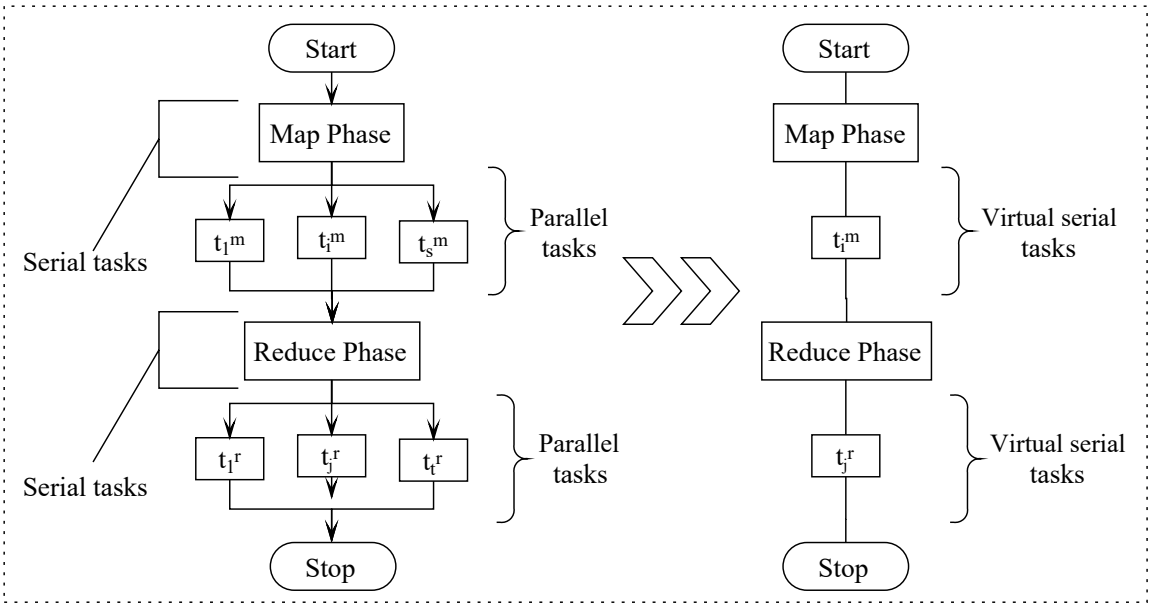

Figure 6.4: Replacing the parallel tasks for SP 1 into virtual serial tasks.

The result of this transformation yields two serial tasks for map and reduce phase respectively and the resultant values are stored in intermediate matrix $\mathbb{A}_{(S+T)\times 2}$ (Line 4). However, this matrix may or may not be square. Thus, $\mathbb{A}_{(S+T)\times 2}$ is then restructured to get a perfectly square matrix $\mathbb{A}$ by padding extra zero columns/rows (Lines 4-8). Now, the problem under consideration is in perfect shape to be represented as a task assignment problem, wherein the objective is to maximize the deadline of the job. For the maximization objective, the intermediate matrix $\mathbb{A}$ needs to be modified by subtracting the largest value ($\mathbb{V}$) of matrix from all the values of $\mathbb{A}$ (Lines 9-10). Now, the classical HA is applied to $\mathbb{A}$ to deduce the optimal values of $\mathbb{D}^m$ and $\mathbb{D}^r$ (Line 11). Using these values, the expected job deadline ($\mathbb{D}^{'}$) is computed (Line 12), which is then compared with the actual job deadline ($\mathbb{D}$). Based on the comparison, the proposed algorithms takes decision to update the values of $\mathbb{D}^m$/$\mathbb{D}^r$ (Lines 13-41). In case the value of $\mathbb{D}^{'}$ exactly matches $\mathbb{D}$, then the algorithm accepts the optimal values as computed by the classical HA (Lines 13-14). On the other hand, if the value of $\mathbb{D}^{'}$ is found to be less than $\mathbb{D}$, then the difference of their values (d_1) is segregated proportionally between map and reduce phase till the two deadlines become equal or d_1 is exhausted (Lines 15-36). In the last scenario, when the value of $\mathbb{D}^{'}$ exceeds the actual deadline $\mathbb{D}$, then the proposed algorithm compares the values of $\mathbb{D}^m$ and $\mathbb{D}^r$ to deduce the phase which requires to process tasks with greater makespan (Lines 37-41). Accordingly, their values are furthered calculated. Finally, the algorithm returns the optimal values of map and reduce phase deadlines, *i.e.*, $\mathbb{D}^m$ and $\mathbb{D}^r$ (Line 42).

6.2.2 Algorithm for Subproblems 2 & 3

The SPs 2 and 3 deal with the energy-aware scheduling of map and reduce tasks to respective slots, while maintaining the desirable SLA. Since, the nature of both the SPs is identical, this section presents an algorithm only for addressing SP 2. However, Algorithm 6.2 is extensible

Algorithm 6.1 Segregating job deadline across Map & Reduce phase.

procedure DEADLINESEGRE($\mathbb{P}^m_{S\times P}, \mathbb{P}^r_{T\times Q}, \mathbb{D}$)
  $\mathbb{A}_{(S+T)\times(P+Q)} \leftarrow$ (Processing time of the tasks across two phases)
  $\mathbb{A}_{(S+T)\times 2} \leftarrow$ (Transform the parallel tasks into virtual serial tasks)
  if $\mathbb{A}_{(S+T)\times 2}$ is unstructured **then**
    if $(S+T) > 2$ **then**
      Pad $(S+T)-2$ extra zero columns
    else
      Pad $2-(S+T)$ extra zero rows
    end if
  end if
  Set $\mathbb{V} = max(\mathbb{A}_{i,j})$
  $\mathbb{A} = \mathbb{V} - \mathbb{A}$
  $[\mathbb{D}^m, \mathbb{D}^r] \leftarrow$ CLASSICALHA($\mathbb{A}$)
  Set $\mathbb{D}^{'} = \mathbb{D}^m + \mathbb{D}^r$
  if $\mathbb{D}^{'} == D$ **then**
    Freeze $\mathbb{D}^m$ and $\mathbb{D}^r$
  else if $\mathbb{D}^{'} < D$ **then** $d_1 = D - \mathbb{D}^{'}$
    while $\mathbb{D}_1 \neq 0$ **do**
      if $\mathbb{D}^m < \mathbb{D}^r$ **then**
        $d_2 = \mathbb{D}^r - \mathbb{D}^m$
        if $d_1 \leq \mathbb{D}_2$ **then**
          $\mathbb{D}^m = \mathbb{D}^m + \mathbb{D}_1$
          $d_1 = 0$
        else
          $\mathbb{D}^m = \mathbb{D}^m + \mathbb{D}_2$
          $d_1 = d_1 - d_2$
        end if
      else if $\mathbb{D}^m > \mathbb{D}^r$ **then**
        $d_2 = \mathbb{D}^m - \mathbb{D}^r$
        if $d_1 \leq \mathbb{D}_2$ **then**
          $\mathbb{D}^r = \mathbb{D}^r + \mathbb{D}_1$
          $d_1 = 0$
        else
          $\mathbb{D}^r = \mathbb{D}^r + \mathbb{D}_2$
          $d_1 = d_1 - d_2$
        end if
      else
        $\mathbb{D}^m = \mathbb{D}^m + \mathbb{D}_1/2$
        $\mathbb{D}^r = \mathbb{D}^r + \mathbb{D}_1/2$
        $d_1 = 0$
      end if
    end while
  else

```
44:         if ( 𝔻^m < 𝔻^r ) then
45:             𝔻^m = D − 𝔻^r
46:         else
47:             𝔻^r = D − 𝔻^m
48:         end if
49:     end if
50:     return 𝔻^m & 𝔻^r
51: end procedure
```

to both the SPs. Its detailed working is illustrated in the following segment.

Algorithm 6.2 accepts three input parameters for execution and these are namely- $E^m_{S\times P}$, $\mathbb{P}^m_{S\times P}$, and $\mathbb{D}$ (Line 1). Here, $E^m_{S\times P}$ represents the matrix containing the energy consumption profiles of map tasks to map slots. Using these values, the proposed algorithm first instantiates a task assignment matix ($\mathbb{A}_{\mathbb{S}\times\mathbb{P}}$) (Line 2). Next, the algorithm modifies the values of $\mathbb{A}_{\mathbb{S}\times\mathbb{P}}$ in accordance with the individual task's makespan. In this step, the tasks with processing time greater than $\mathbb{D}^m$ are eliminated from the considered solution space by assigning them very large energy consumption values (Lines 4-6). After this, the considered matrix is restructured to get a perfectly square matrix ($\mathbb{A}_{\mathbb{S}'\times\mathbb{P}'}$) (Line 7). This is achieved by padding extra zero columns/rows (Lines 8-11). This renders the considered problem suitable for task assignment problem, hence, it is then solved using classical HA (Line 12). This step returns the column (or slot) optimal values (C^{HA}) along with optimized energy consumption value (E^{HA}_{tot}) (Line 12). Using C^{HA}, the proposed algorithm then computes the corresponding total processing time of the map phase (P^{HA}_{tot}) (Line 13).

In next step, the algorithm leverages the advantages of Greedy strategy to verify whether the value of E^{HA}_{tot} is optimal or not (Line 13). This step too return two values, *i.e.*, column (or slot) optimal values (C^{GR}) along with optimized energy consumption value (E^{GR}_{tot}) as per the Greedy strategy. Based on the values of E^{HA}_{tot} and E^{GR}_{tot}, the proposed algorithm decides to split the map phase into different stages (Lines 15-31). In case E^{HA}_{tot} is less than or equal to E^{GR}_{tot}, then algorithm accepts the values provided by classical HA as optimal and does not

Algorithm 6.2 Scheduling of tasks during Map phase.

procedure EnTskSchMap($E^m_{S\times P}$, $\mathbb{P}^m_{S\times P}$, $\mathbb{D}$)
  $\mathbb{A}_{\mathbb{S}\times\mathbb{P}} \leftarrow$ (Energy consumption across Map phase)
  Restructure $\mathbb{A}_{\mathbb{S}\times\mathbb{P}}$ in accordance D^m violation
  $\forall \mathbb{A}_{i,k} \in \mathbb{A}_{\mathbb{S}\times\mathbb{P}}$
  if $\mathbb{A}_{i,j} \geq \mathbb{D}^m$ **then**
    $\mathbb{A}_{i,j} = \mathbb{A}_{i,j} \times max(\mathbb{A}_{i,j}) \times \mu$
  end if
  if $\mathbb{A}_{\mathbb{S}\times\mathbb{P}}$ is unstructured **then**
    if $S \geq P$ **then**
      Pad $(S-P)$ extra zero columns
    else
      Pad $(P-S)$ extra zero rows
    end if
  end if
  $[C^{HA}, E^{HA}_{tot}] \leftarrow$ ClassicalHA($\mathbb{A}$)
  $P^{HA}_{tot} = max\{P[C^{HA}[1,k],k]\}; \forall k$
  $[C^{GR}, E^{GR}_{tot}] \leftarrow$ GreedySt($\mathbb{A}$)
  if $E^{HA}_{tot} \leq E^{GR}_{tot}$ **then**
    Set $NoS \leftarrow 1$
  else
    $\mathbb{PQ} \leftarrow$ ConfTasks($\mathbb{A}, C^{GR}$)
    Set $NoS \leftarrow \max\{length(\mathbb{PQ})\}$
    for $\forall\, NoS$ **do**
      $P^{GR}_{tot} = P^{GR}_{tot} + max\{P[\mathbb{PQ}[stage,k],k]\}$
    end for
  end if
  if $P^{GR}_{tot} \leq \mathbb{D}^m$ **then**
    Set $OptEn = E^{GR}_{tot}$
    Set $OptMs = P^{GR}_{tot}$
  else
    Set $OptEn = E^{HA}_{tot}$
    Set $OptMs = P^{HA}_{tot}$
  end if
  if $OptMs > \mathbb{D}^m$ **then**
    Set $SLAV$ = True
  else
    Set $SLAV$ = True
  end if
  return *NoS, OptEn, OptMs* and *SLAV*
end procedure

split the phases into multiple stages (Line 16). Otherwise, the algorithm tends to explore the possibility of splitting the map phase into different stages. This is further achieved by finding the conflicting tasks per map slot according to task-to-slot mapping using the Greedy strategy (Line 18). For enhanced efficiency, it is assumed that the procedure CONFTASKS returns the list of priority queues (*PQ*) per slot, wherein the tasks with higher makespan are given higher priority. Next, the number of stages (*NoS*) for the map phase are computed using *PQ*s (Line 19). Post this, the algorithm checks the feasibility of considering multiple *NoS* and subsequently computes the total processing time of the map phase (P_{tot}^{GR}) according to the adopted Greedy strategy (Lines 20-21). Following this, the algorithm compares the computed value of P_{tot}^{GR} with the deadline of the map phase $\mathbb{D}^m$. In case, P_{tot}^{GR} is found to be less than $\mathbb{D}^m$, then the algorithm accepts the Greedy strategy for task-to-slot mapping else goes with the results deduced by classical HA (Lines 22-31). Subsequently, the optimal energy consumption (*OptEn*), optimal makespan (*OptMs*) and number of stages (*NoS*) involved in the map phase are updated and returned accordingly by the algorithm along with the indication about SLA violation (*SLAV*) (Line 32).

The above mentioned approach can be easily extended to multiple MapReduce job scenario in the following manner. As soon a job arrives (say J_1), En-SLA starts to execute and maps the available slots/containers to execute the Map and Reduce tasks in accordance with Algorithms 1 and 2. These slots/containers are assigned to the respective tasks for a particular time window and released as soon as the window expires. However, in case another MapReduce Job (J_2) arrives in between, then the allocated slots/containers are marked as

unavailable using the status variable $Unavl_k^{'}$ which is defined as follows:

$$Unavl_k^{'} = \begin{cases} 1, \text{ If } k^{th} \text{ container is unavialable of map/reduce} \\ \quad \text{task execution,} \\ 0, \text{ otherwise.} \end{cases}$$

The available containers then compete for executing rest of the MapReduce Jobs. In this manner, the proposed En-SLA could be extended to the case wherein multiple jobs coexist.

6.2.3 Case Study

Map Tasks

	Processing Time			Energy Consumption		
Slots $\longrightarrow$	a_1	a_2	a_3	a_1	a_2	a_3
Tasks t_1^m	8	4	2	8	12	12
$\downarrow$ t_2^m	3	2	1	3	4	3

6.5(a) Map Phase.

Reduce Tasks

	Processing Time		Energy Consumption	
Slots $\longrightarrow$	b_1	b_2	b_1	b_2
Tasks t_1^r	2	3	6	3
$\downarrow$ t_2^r	2	2	6	4

6.5(b) Reduce Phase.

Figure 6.5: Case study: Typical example of a MapReduce job.

For the purpose of clearly understanding the working of the designed algorithms, let us consider the following case study. The detailed description of the case study is illustrated using Fig. 6.5. As evident from the figure, map phase comprises of two tasks $\mathbb{M} = \{t_1^m, t_2^m\}$ that needs to mapped to three different slots, *i.e.*, $A = \{a_1, a_2, a_3\}$. Similarly, the reduce phase comprises of two tasks $\mathbb{R} = \{t_1^r, t_2^r\}$ and two available slots ($\mathbb{B} = \{b_1, b_2\}$). The related energy consumption profiles along with their processing times are also detailed in the figure. Let us

consider, the overall deadline $\mathbb{D}$ of a job equivalent to 12 milliseconds (ms). Hence, the first task would be to split $\mathbb{D}$ amongst the two phases in accordance with the SLA target and the current processing times of the map and reduce tasks. Hence, $\mathbb{D}^m$ and $\mathbb{D}^r$ were found to be 8 and 4 ms respectively.

Thereafter, the energy-aware scheduling of map and reduce phases are executed using Algorithm 6.2. The related outcomes are elaborated in the following segment. Since, the deadline for the map phase was set as $\mathbb{D}^m = 8$, therefore all the map tasks and the available slots participated in selecting most feasible solution for the problem. The most energy-efficient mapping in the present scenario was found to be equivalent to $\{X^m_{1,1} = 1, X^m_{2,3} = 1\}$, resulting in total energy consumption of 11 Joules (J). On the similar lines, the results of scheduling reduce tasks yield the following output: $\{Y^r_{1,2} = 1, Y^r_{2,1}\}$ with total energy consumption of 9 J.

6.3 Results and Discussions

This section presents the validation of the proposed scheme on real time data traces and its detailed comparison with the existing schemes. The illustrative description about the data traces, case studies considered and obtained results is mentioned as follows.

6.3.1 Data traces used:

In order to validate the efficacy of the proposed scheme, real time data traces has been obtained from OpenCloud Hadoop Cluster [167]. This cluster is based at Carnegie Mellon University (CMU) and is administered by university's parallel data lab. It comprises of a total of 64 nodes and each node is equipped with 2.8 GHz dual quad core CPU (8 cores), 16 GB RAM, 10 Gbps ethernet NIC and 4 Seagate 7200 rpm SATA disk drives. For the purpose of evaluating the proposed En-SLA scheme, we have considered one month data for the period of December

2011. The acquired data has been scaled down with respect to job deadline for simulation purpose.

6.3.2 Details about the existing schemes:

For evaluating the performance of the proposed scheme, three different variations of the proposed scheme have been considered. The first scheme refers to *energy-aware Greedy strategy (En-Gr)* that tends to greedily select and allocate tasks to different slots based on minimum energy consumption. The second scheme is referred to *makespan-aware Greedy strategy (Ms-Gr)* which tends to greedily select the tasks with minimum processing time and allocates them to different slots. The third scheme is also makespan oriented and is based on the proposed En-SLA scheme. If the objective function of the proposed scheme is shifted from energy minimization to makespan minimization, then it acquires the form of the third scheme. We name this scheme as *makespan-aware and SLA-driven job scheduling for MapReduce (Ms-SLA)*.

Apart from this, an existing state-of-the-art scheme suggested in [94] has also been considered for evaluation of the proposed scheme. The scheme proposed in [94] refers to *Energy-aware MapReduce Scheduling Algorithm (EMRSA)*.

6.3.3 Evaluation parameters:

The proposed scheme has been evaluated with respect to the following parameters.

1. ***Number of Stages:*** This parameter represents if a particular phase (either Map or Reduce) has been split into multiple stages or not. It has been considered as an important metric to achieve optimal task-to-slot mapping with respect to energy minimization. The proposed scheduling framework considers to split a particular phase into multiple

stages only if the total energy consumption can be reduced to a next level without violating the job deadline and SLA.

2. ***Total Energy Consumption:*** This is the second metric of evaluating the proposed scheme and is perhaps the most important one. It denotes the total energy consumption in accordance with the task-to-slot mapping for Map and Reduce phase respectively.

3. ***Total Makespan:*** Makespan refers to the sum of the maximum processing times across the selected slots scheduled for task execution involved in different stages of a phase. The selected slots represents the set of the slots that have been optimally selected by the proposed En-SLA scheme.

4. ***SLA Violated:*** It is the forth metric for assessing the efficacy of the proposed scheme. A particular assignment/mapping is considered to be violated if its corresponding makespan exceeds its designated deadline. For instance, in the considered job scheduling framework, the task-to-slot mapping of the Map phase would be attributed as violated if the makespan of the participating tasks outpaces $\mathbb{D}^m$.

6.3.4 Case studies considered:

For demonstrating the competence of the proposed scheme in different scenarios, three distinct case studies have been considered. Case Study I depicts the detailed technical results obtained by simulating the proposed scheme on OpenCloud data traces for December 2011. Following this, the rest of the case studies compare the performance of the proposed scheme with the other existing schemes under different workload scenarios, *i.e.*, small-scale and large-scale. The technical description about these case studies is illustrated in Table-6.2.

Table 6.2: Technical description of different case studies.

Case Study	Range of Map Tasks	Range of Reduce Tasks	Workload Description
Case Study I	0-21500	0-2200	Variable-scale
Case Study II	0-20	0-10	Small-scale
Case Study III	2000-3000	200-500	Large-scale

Case Study I (Variable Workload Traces)

This case study evaluates the performance of the proposed scheme on one month data traces obtained from OpenCloud. The considered case study has been taken into account to reflect the scalability and performance of the proposed scheme across variable workload traces. For instance, Fig. 6.6a depicts the MapReduce workload with respect to total number of map and reduce tasks across the different submitted jobs. It is evident from the figure, that the number of map tasks is comparatively higher than the number of reduce tasks. For example, the job id 53 has comparatively very large number of map (21383) and reduce tasks (100) in comparison with the other jobs. The deadline characteristics of the submitted jobs are also acquired from OpenCloud and the related results have been summarized using Fig. 6.6b. The figure distinctly depicts that the submitted jobs have differing deadlines. The deadline for the job id 53 has been set at 375 ms. Using these data statistics, the proposed En-SLA scheme achieves task-to-slot mapping of the jobs in an energy-efficient manner while maintaining the desirable SLA.

Fig. 6.7 shows the segregation of job deadline into $\mathbb{D}^m$ and $\mathbb{D}^r$ for map and reduce phase respectively. These results are computed using Algorithm 6.1. For instance, overall job deadline $\mathbb{D}$ for job id 53 was approximately 375 ms and it was successfully segregated between the two phases based on the respective values of $\mathbb{P}^m_{S\times P}$ and $\mathbb{P}^r_{T\times Q}$. Here, the values for $\mathbb{D}^m$ and $\mathbb{D}^r$ were found to be 225 and 150 ms respectively. In the next step, scheduling of map and reduce tasks takes place. The related results about the evaluation parameters are depicted using Figs. 6.8-6.10.

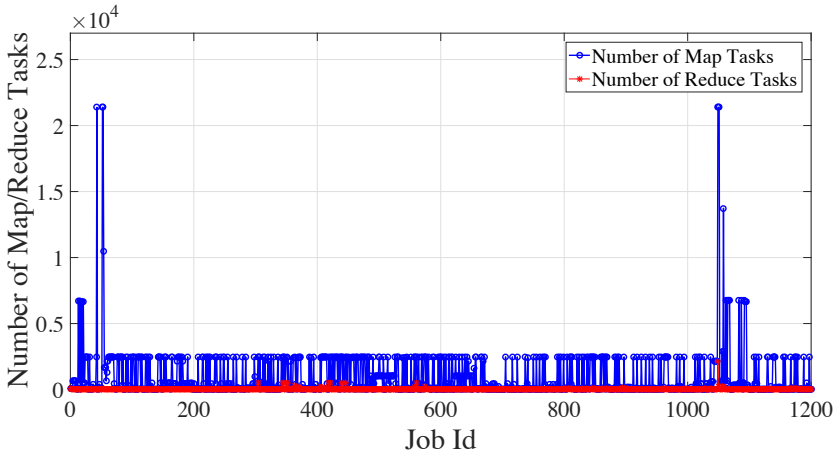

6.6(a) Number of Map and Reduce task acquired from OpenCloud data traces as on December 2011 [167].

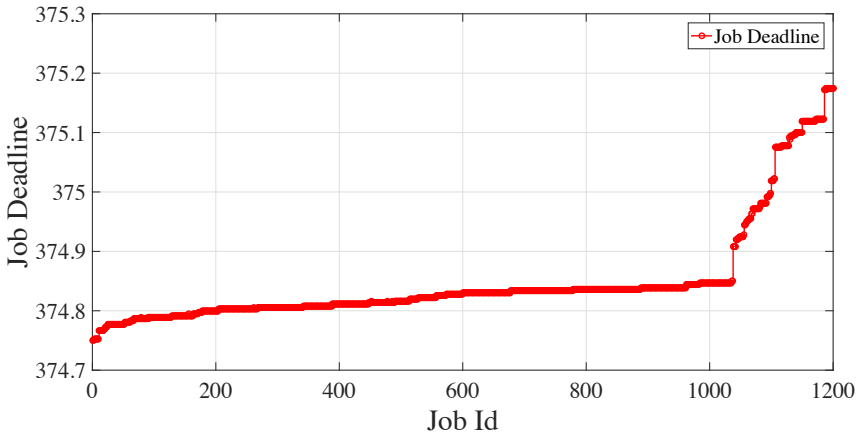

6.6(b) Job deadline data acquired from OpenCloud data traces as on December 2011 [167].

Figure 6.6: Data traces obtained from Open Cloud for December 2011.

The results shown using Fig. 6.8 clearly show that the proposed scheme is capable in splitting map/reduce phase into multiple stages wherever required. This is done in order to achieve higher reduction in energy utilization by the underlying DCs. This is evidently noticeable for jobs with id 40 and 272 whose reduce phases have been split into 2 stages Subsequently, the proposed scheme also computes the total energy consumption across the two phases as depicted in Fig. 6.9. The results clearly indicate that the total energy utilization varies not only with different jobs but also with different workload characteristics. For instance, the total energy utilization with for job id 53 was as high as 2138 and 119 J

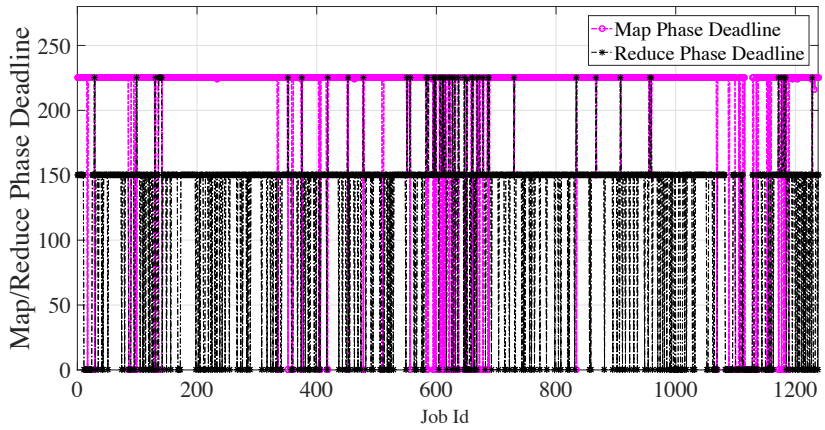

Figure 6.7: Segregation of job deadline between map and reduce phase using the proposed scheme

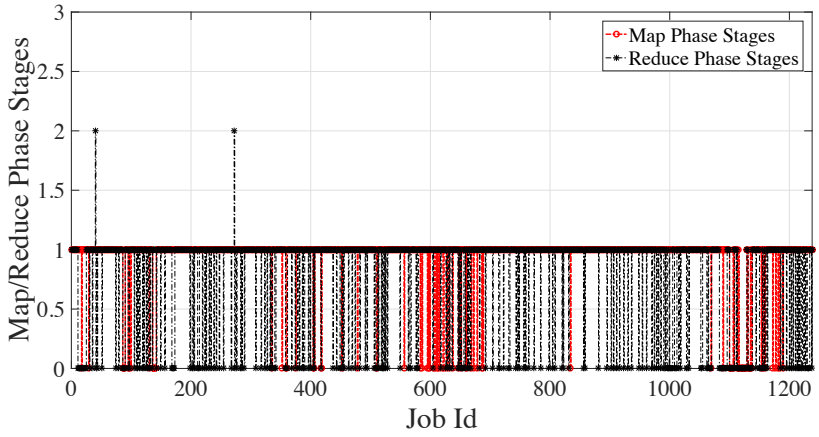

Figure 6.8: Number of stages involved during map and reduce phase.

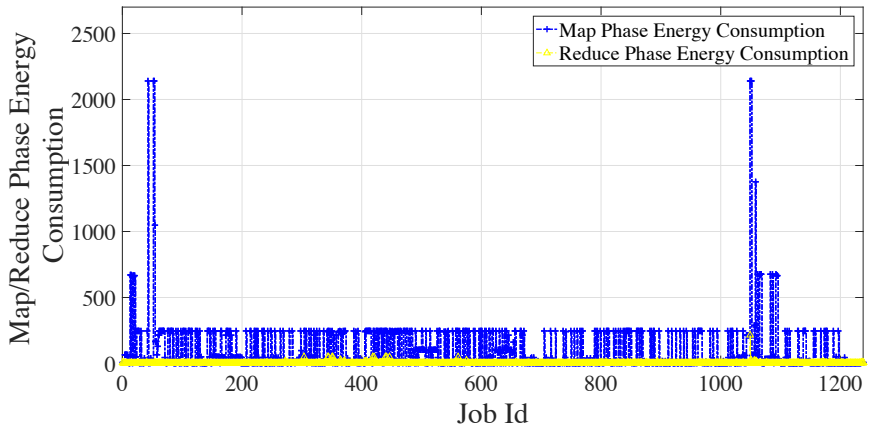

Figure 6.9: Total energy utilization across map and reduce phase.

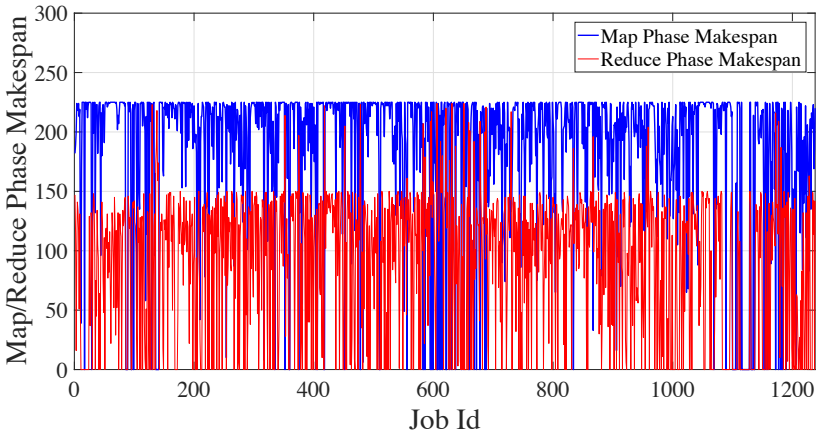

Figure 6.9: Total makespan across map and reduce phase.

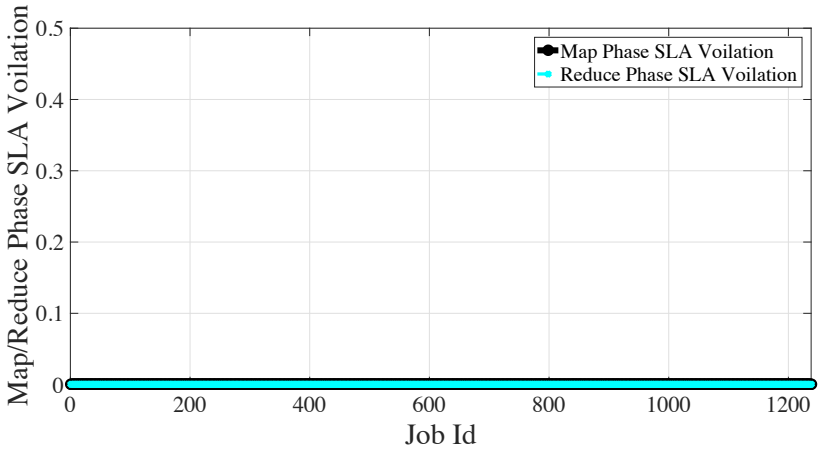

Figure 6.10: SLA violations across map and reduce phase.

Figure 6.11: Case Study I: Energy-aware scheduling using the proposed scheme on one month data traces acquired from OpenCloud.

respectively for map and reduce phase respectively.

The corresponding makespan of both the phases has been calculated using the logic defined in Algorithm 6.2. The related results have been highlighted using Fig. 6.9 and the corresponding SLA violations have been depicted using Fig. 6.10. For instance, the makespan for job id 53 was found to be 225 ms for map phase and the same did not exceed its respective $\mathbb{D}^m$. As a result, the corresponding SLA was not breached as depicted in Fig. 6.10. It is also noticeable from the figure, that the average number of SLA violations are almost zero across

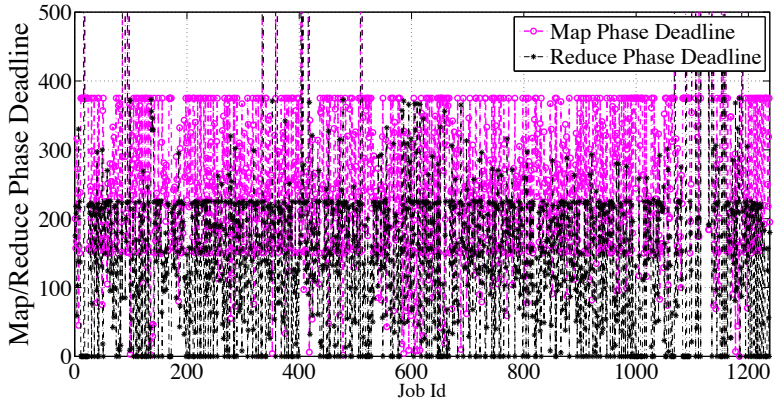

Figure 6.12: Segregation of job deadline between map and reduce phase using the proposed scheme

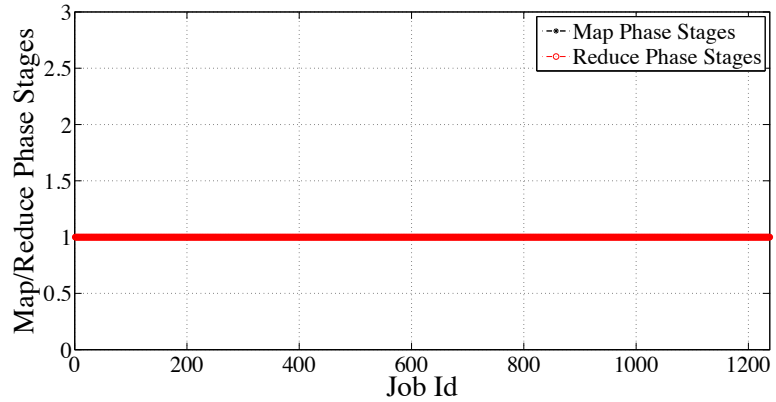

Figure 6.13: Number of stages involved during map and reduce phase.

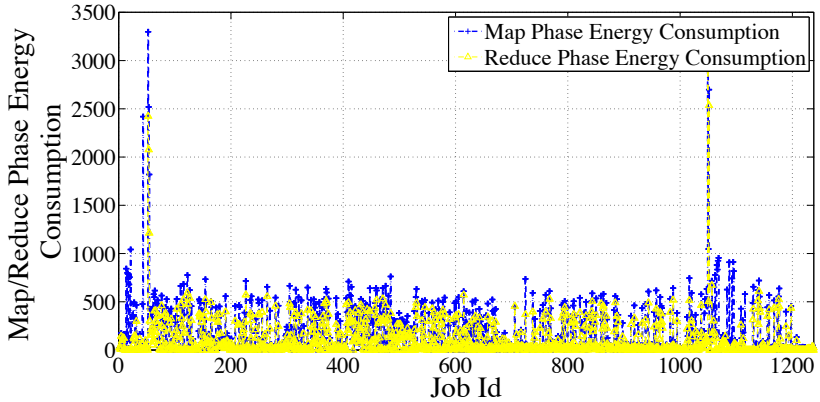

Figure 6.14: Total energy utilization across map and reduce phase.

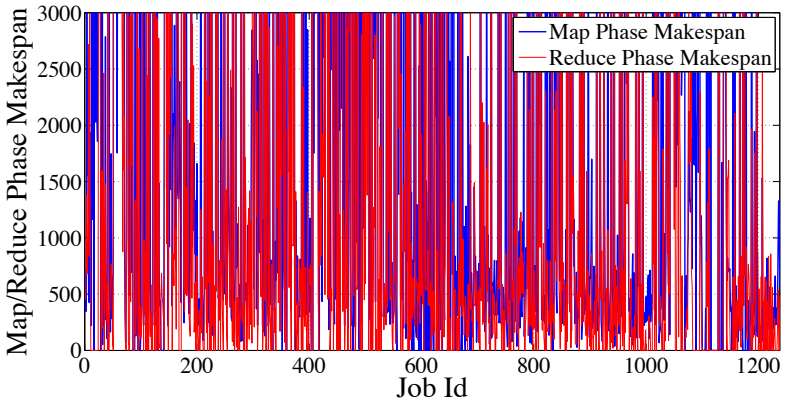

Figure 6.14: Total makespan across map and reduce phase.

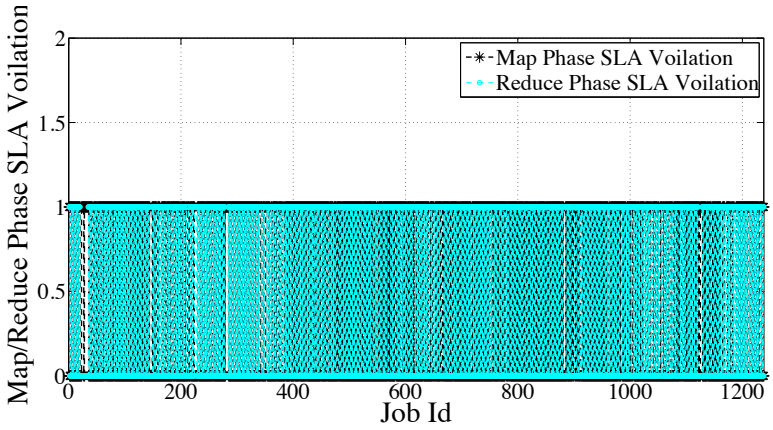

Figure 6.15: SLA violations across map and reduce phase.

Figure 6.16: Case Study I: Energy-aware scheduling using EMRSA on one month data traces acquired from OpenCloud.

all the jobs of variable workload capacity using the proposed job scheduling framework.

In contrast to EMRSA, the proposed En-SLA scheme achieves superior results in terms of trade-off between energy utilization and SLA adherence; as evident from Figs. 6.11 and 6.16. En-SLA achieves 59.80% and 52.05% better energy efficiency and SLA assurance respectively; relative to EMRSA.

Case Study II (Small-scale Workload Traces)

The small-scale workload traces depict the selective real-time data traces taken from Open-Cloud wherein the number of map and reduce tasks is relatively very less. In this considered case study, the jobs having map and reduce tasks in the range of 0 to 20 and 0 to 10 respectively have been taken into account. The detailed comparison of the proposed scheme with the other schemes have been done and the related results have been illustrated using Fig. 6.17.

Fig. 6.17a depicts the number of stages across the two phases. It is clearly evident from the figure, that the number of stages across the two phases is maintained at 1 by the proposed En-SLA scheme to achieve optimal task-to-slot mapping. On the other hand, other schemes tend to divide the map phase in multiple stages as seen for job id 6, 16, 17 and 20. Additionally, it can observed the number of stages across the reduce phase is maintained exactly the same by all the schemes. It is also noticeable that the proposed scheme leads to optimal energy consumption in comparison with the other schemes as seen from Fig. 6.17b. However, for jobs with ids 6 and 8, Ms-SLA achieves far more optimal energy utilization for the map phase in comparison with the proposed scheme. Nevertheless, Ms-SLA violates the respective SLA as evident from the results illustrated in Fig. 6.17d. It is also observed that makespan of the map and reduce tasks is maintained in a reasonable limit by the proposed scheme in comparison with the existing schemes. The related results have been drawn in Fig. 6.17c.

Case Study III (Large-scale Workload Traces)

This case study deals the detailed comparison of the proposed scheme with the existing schemes on large-scale workload data traces acquired from OpenCloud. The technical details about the number of tasks considered in this case study are highlighted in Table-6.2.

The detailed comparison of all the schemes based on the considered set of evaluation

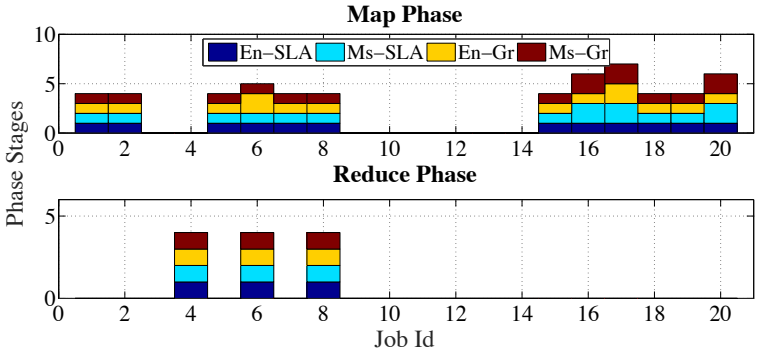

6.17(a) Comparison of number of stages involved during map and reduce phase.

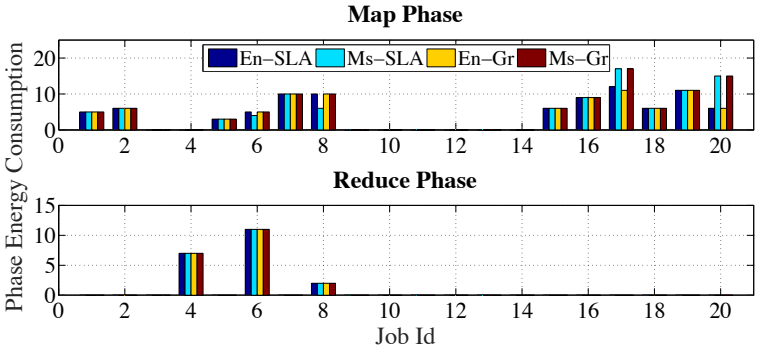

6.17(b) Comparison of energy utilization across map and reduce phase.

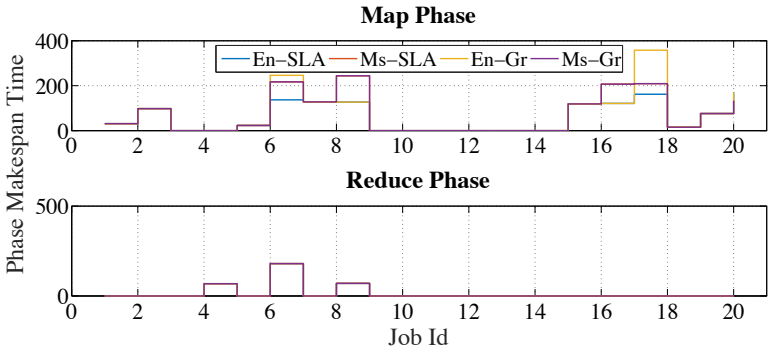

6.17(c) Comparison of task makespan across map and reduce phase.

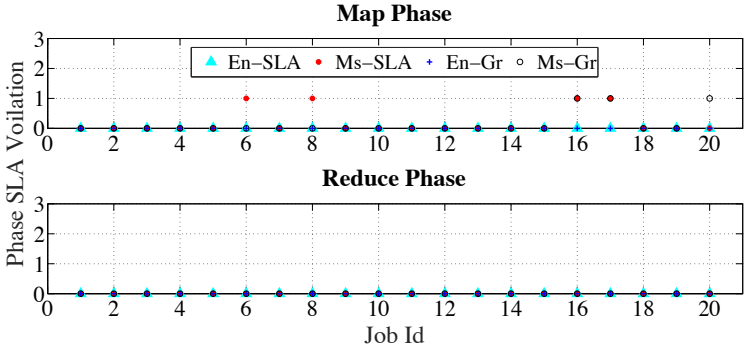

6.17(d) Comparison of SLA violations across map and reduce phase.

Figure 6.17: Case Study II: Comparison of the proposed scheme against the existing schemes for small-scale data.

parameters is depicted using Fig. 6.18. The proposed scheme along with En-Gr maintains the number of stages to 1 across both the phases as evident from Fig. 6.18a. The other two schemes, on the other hand have variable number of stages in range of 1-4. The second evaluation parameter is total energy consumption in accordance with task-to-slot mapping. The related results are highlighted using Fig. 6.18b. It is distinctly visible from the figure that the most optimal energy utilization across the map phase is parallelly achieved by the proposed scheme along with En-Gr. Nevertheless, a different trend is observed for the reduce phase, wherein Ms-SLA achieves the most optimal energy utilization results followed by the proposed scheme in conjugation with En-Gr. On the contrary, the Ms-SLA experiences maximum level of SLA violations as seen from Fig. 6.18d. In addition to this, Fig. 6.18c depicts the task's makespan, wherein the proposed scheme and Ms-Gr achieves the most optimal makespan results across the map and reduce phase respectively.

The results discussed above distinctly highlight the efficacy of the proposed scheme over the existing schemes-Ms-SLA, En-Gr and Ms-Gr. The proposed scheme is found to be the most suitable scheme which achieves optimal energy consumption while achieving desirable SLA and maintaining the job deadline at all times.

6.3.5 Comparison summary

The relative comparison of the proposed En-SLA scheme against the existing schemes is illustrated in Table 6.3. From the table, it can be concluded that En-SLA performs better than the existing schemes across all case studies.

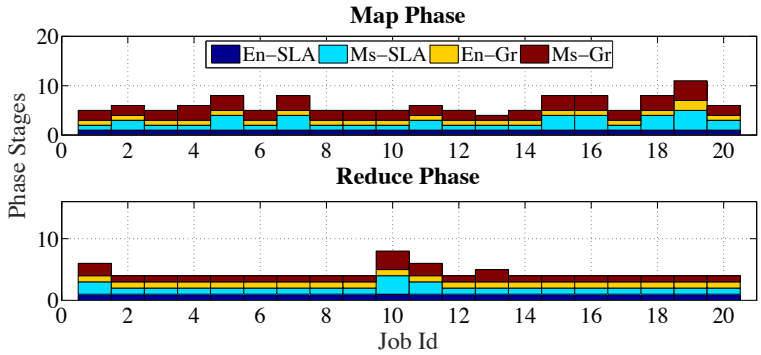

6.18(a) Comparison of number of stages involved during map and reduce phase.

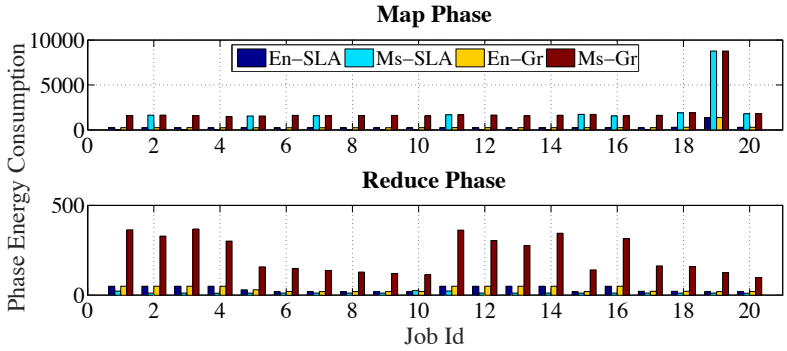

6.18(b) Comparison of energy utilization across map and reduce phase.

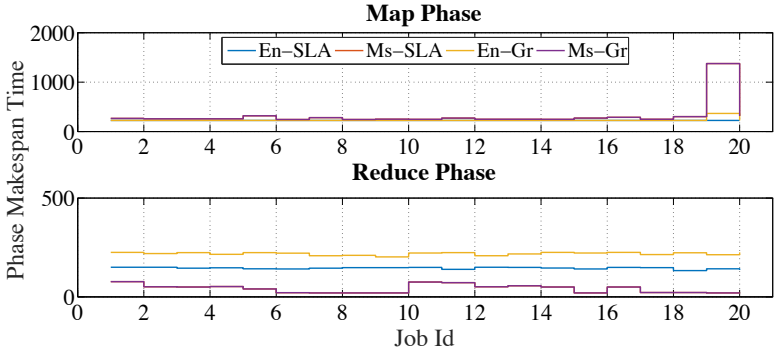

6.18(c) Comparison of task makespan across map and reduce phase.

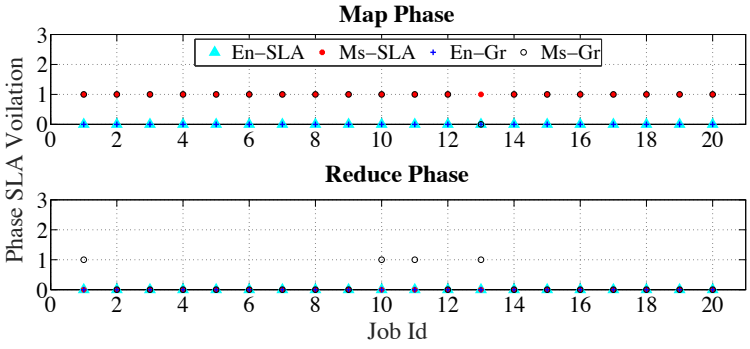

6.18(d) Comparison of SLA violations across map and reduce phase.

Figure 6.18: Case Study III: Comparison of the proposed scheme against the existing schemes for large-scale data.

Table 6.3: Comparison of En-SLA with the existing schemes.

Case Study-I

Metric	**EMRSA**
Energy efficiency	59.80%
SLA guarantee	52.05%

Case Study-II

Metric	**Ms-SLA**	**En-Gr**	**Ms-Gr**
Energy efficiency	1.63%	$\approx$	4.47%
SLA guarantee	20%	10%	15%

Case Study-III

Metric	**Ms-SLA**	**En-Gr**	**Ms-Gr**
Energy efficiency	-	$\approx$	84.62%
SLA guarantee	100%	15%	100%

6.4 Concluding Remarks

An energy proportional and SLA driven job scheduling strategy has been designed in this chapter particularly for cloud DCs equipped with MapReduce framework. The designed solution operates in three phases, *i.e.*, job deadline segregation, scheduling of map tasks followed by scheduling of reduce tasks. In the next chapter, conclusions are drawn along with future directions.

Chapter 7

Conclusion and Future Scope

7.1 Conclusion

Increasing dependence on electricity by every strata of modern life and global environmental concerns have raised the significance of modern frequency regulation agents to maintain grid's stability. Towards this end, Electric Vehicles and Data Centers (DCs) have emerged as promising candidates. Thus, different frequency support techniques have been proposed in this thesis. The proposed schemes demonstrated promising results which authorize their future investigations and incorporation in real-time environment. The following segment sheds some lights on the working of the proposed schemes and the conclusions drawn from their implementation on different datasets.

The first scheme proposed an efficient means for grid frequency support by leveraging the joint participation of EVs. In the proposed scheme, AGs have been modeled using CPN based controller which regulate the charging and discharging rates of EVs in accordance with the regulation signal. The scheme also handles the dynamics associated with the mobility of participating EVs, during the regulation process. The effectiveness of the proposed scheme has been studied by extensive simulation performed on the real-time data obtained from PJM

and ERCOT. Moreover, in comparison with an existing scheme, the proposed scheme was found to be more effective in managing the frequency imbalances by involving fleet of EVs.

The second scheme proposed a V2G-based frequency support scheme using an *"Aggregator-based Hierarchical Control Mechanism"*. The designed scheme not only helps in providing effective frequency regulation services, but also caters the challenging issue of bi-directional V2G support. Additionally, it exploits the benefits of conventional droop mechanism in the V2G setup for optimal regulation signal dispatch across aggregators and charging stations. This is done in accordance with their respective frequency regulation capacities, so as to avoid their over/under utilization. EV's battery degradation issues are also taken into account, while providing the necessary ancillary services. The above mentioned objectives have been supported by the decomposition of the complex multi-objective primal problem into simpler sub-problems; which are then solved by using the interior point method. Further, the designed solution have been verified with extensive simulation performed on real-time PJM and ERCOT regulation data. The obtained results clearly indicate that the proposed scheme gives superior results under different conditions and is feasible to be adopted in real-time scenarios, in comparison with an existing scheme.

The third scheme presented a *"MILP-based Hierarchical Control Design"* for frequency regulation using integrated fleet of EVs. The proposed work explored the potential of incorporating EVs in frequency regulation in a centralized mode wherein primary focus was to minimize grid frequency deviations. Moreover, the proposed scheme also concentrated on maximal V2G support, optimal dispatch of reference signals, reduced battery degradation and increased incentives to EVs for participating in the regulation market. This complex problem was addressed using *'Mixed Integer linear programming (MILP)'* which in-turn formed the control layer of the designed hierarchical control scheme. The proposed work has been experimentally validated using real-time traces acquired from *PJM* and *CAISO*. Also,

the proposed scheme has been compared with an existing scheme and the obtained results indicate superior performance of the proposed scheme.

Energy utilization by the cloud DCs has rapidly increased with the growing popularity of big data applications. Hence, to address this problem, the fourth scheme presented an efficient job scheduling framework particularly for MapReduce. The primary agenda of the framework is to achieve task-to-slot mapping in an energy-efficient manner while maintaining the desirable SLA targets. This entire problem can be viewed as a multi-objective optimization problem under multi-constraint environment. Hence, the nature of this complex optimization problem was reduced by segregating it into three SPs and then mathematically expressing them using ILP. Additionally, the work also presented different algorithms based on heuristics to achieve the desirable results optimally and in reasonable time. Finally, the efficacy of the proposed framework was evaluated on real-time data traces acquired from OpenCloud and compared with the existing schemes. The obtained results prove the effectiveness of the proposed scheme.

7.2 Future Scope

Though, the proposed schemes demonstrated good performance relative to the current state-of-the-art techniques, but there is always a scope for improvement. This section elaborates some of the future directions in context of the proposed work.

In the near future, we would extend the proposed work with respect to various aspects as mentioned as follows. For instance, the schemes proposed for grid frequency support using the fleet of EVs can be extended by achieving their distributed control for effective frequency regulation. Additionally, the economic benefits of V2G interactions can also be explored. Further, the proposed CPN controller for frequency regulation can be researched further using

communication and control flow in high-level Petri Nets. Most importantly, the proposed control schemes can be refined to yield higher efficiencies in terms of better optimal solutions and faster convergence. In this direction, the role of evolutionary optimization can be the next vital step.

On the similar lines, En-SLA can be extended in the direction of maximal data locality. This would help to reduce the network and data migration cost to a great extent; which in turn would substantially reduce the energy utilization of the cloud DCs. Further, the potential of Software Defined Networks in the context of communication (within or between DCs) can be explored to find its impact in reducing DC's total operational cost.

Bibliography

[1] S. K. Singh, K. Khanna, R. Bose, B. K. Panigrahi, and A. Joshi, "Joint-transformation-based detection of false data injection attacks in smart grid," *IEEE Transactions on Industrial Informatics*, vol. 14, no. 1, pp. 89–97, Jan. 2018.

[2] M. L. Das, "Grids security without public key settings," in *International Conference on Distributed Computing and Internet Technology*. Springer, 2012, pp. 253–254.

[3] V. Odelu, A. K. Das, M. Wazid, and M. Conti, "Provably secure authenticated key agreement scheme for smart grid," *IEEE Transactions on Smart Grid*, vol. 9, no. 3, pp. 1900–1910, May 2018.

[4] R. Jiang, R. Lu, Y. Wang, J. Luo, C. Shen, and X. S. Shen, "Energy-theft detection issues for advanced metering infrastructure in smart grid," *Tsinghua Science and Technology*, vol. 19, no. 2, pp. 105–120, Apr. 2014.

[5] M. H. Bollen, "The smart grid: Adapting the power system to new challenges," *Synthesis Lectures on Power Electronics*, vol. 2, no. 1, pp. 1–180, 2011.

[6] H. Gharavi and R. Ghafurian, "Smart grid: The electric energy system of the future," *Proceedings of the IEEE*, vol. 99, no. 6, pp. 917–921, 2011.

[7] W. Li, T. Logenthiran, V. Phan, and W. L. Woo, "Proposed optimised smart grid system using multi-agent system," in *2018 IEEE Innovative Smart Grid Technologies - Asia (ISGT Asia)*, May 2018, pp. 528–533.

[8] K. Yang and A. Walid, "Outage-storage tradeoff in frequency regulation for smart grid with renewables," *IEEE Transactions on Smart Grid*, vol. 4, no. 1, pp. 245–252, Mar. 2013.

[9] S. V. Chakraborty, S. K. Shukla, and J. Thorp, "A hierarchical networked micro-simulator to study grid-integration of renewables and electric vehicles," in *2013 Workshop on Modeling and Simulation of Cyber-Physical Energy Systems (MSCPES)*, May 2013, pp. 1–6.

[10] ——, "Computing optimal solar penetration in the presence of plug-in electric vehicles," in *2012 IEEE Energytech*, May 2012, pp. 1–6.

[11] M. Wazid, A. K. Das, N. Kumar, and J. J. P. C. Rodrigues, "Secure three-factor user authentication scheme for renewable-energy-based smart grid environment," *IEEE Transactions on Industrial Informatics*, vol. 13, no. 6, pp. 3144–3153, Dec. 2017.

[12] F. Sanchez, F. Gonzalez-Longatt, and D. Bogdanov, "Impact assessment of frequency support by electric vehicles: Great britain scenario 2025," 2018.

[13] T. Masuta and A. Yokoyama, "Supplementary load frequency control by use of a number of both electric vehicles and heat pump water heaters," *IEEE Transactions on Smart Grid*, vol. 3, no. 3, pp. 1253–1262, Sep. 2012.

[14] N. B. Arias, S. Hashemi, P. Bach, C. T. Andersen, and R. Romero, "V2g enabled evs providing frequency containment reserves: Field results," in *Proceedings of 2018 IEEE International Conference on Industrial Technology*, 2018, doi: 10.1109/ICIT.2018.8352459.

[15] O. Elgerd, *Electric energy systems theory: an introduction*, 2nd ed., ser. McGraw-Hill Series in Electrical Engineering. McGraw-Hill, 1983, ch. The Energy System in Steady State-The Control Problem.

[16] F. Zhang, M. Tokombayev, Y. Song, and G. Gross, "Effective flywheel energy storage (FES) offer strategies for frequency regulation service provision," in *IEEE Power Systems Computation Conference (PSCC)*, 2014, pp. 1–7.

[17] J. Eyer and G. Corey, "Energy storage for the electricity grid: Benefits and market potential assessment guide," *Sandia National Laboratories*, vol. 20, no. 10, 2010.

[18] H. Hao, T. Middelkoop, P. Barooah, and S. Meyn, "How demand response from commercial buildings will provide the regulation needs of the grid," in *IEEE 50th Annual Allerton Conference on Communication, Control, and Computing (Allerton)*, 2012, pp. 1908–1913.

[19] E. Romero-Cadaval, F. Barrero-González, E. González-Romera, and M.-I. Milanés-Montero, "Using plug-in electric vehicles to implement ancillary services in smart distribution grids," in *Plug In Electric Vehicles in Smart Grids*. Springer, 2015, pp. 309–349.

[20] Final report system disturbance on 4 november 2006. Union for the coordination of transmission of electricity. [Accessed: Mar. 2016]. [Online]. Available: https://www.entsoe.eu/fileadmin/user_upload/_library/publications/ce/otherreports/Final-Report-20070130.pdf

[21] U. Bhaskar. CERC plans to further narrow frequency band for national grid. Live Mint. [Accessed: Jun. 2015]. [Online]. Available: http://www.livemint.com/Industry/3HIYmLsbcM47fsaCUyK7DI/CERC-plans-to-further-narrow-frequency-band-for-national-gri.html

[22] "Report of the enquiry committee on grid disturbance in northern region on 30th july, 2012 and in northern, eastern & north-eastern region on 31st july," [Accessed: Oct. 2015]. [Online]. Available: http://www.powermin.nic.in/pdf/GRID_ENQ_REP_16_8_12.pdf

[23] Power blackout risks, risk management options, emerging risk initiative position paper. CRO Forum, Texas Energy Storage Alliance. [Accessed: Jan. 2016]. [Online]. Available: https://www.allianz.com/v_1339677769000/media/responsibility/documents/position_paper_power_blackout_risks.pdf

[24] G. Cook and J. Van Horn, "How dirty is your data? A look at the energy choices that power cloud computing," *Greenpeace International*, 2011.

[25] Gartner says data center capacity in India to surpass 5 million square feet by 2012. Gartner. [Accessed: Mar. 2016]. [Online]. Available: http://www.gartner.com/newsroom/id/808212

[26] K. Wang, L. Gu, X. He, S. Guo, Y. Sun, A. Vinel, and J. Shen, "Distributed energy management for vehicle-to-grid networks," *IEEE Network*, vol. 31, no. 2, pp. 22–28, March 2017.

[27] I. E. Agency, "Global ev outlook 2017: two million and counting," *IEA Publ*, pp. 1–71, 2017.

[28] D. Hurst and J. Gartner. Electric vehicles: 10 predictions. Pike Research Report. [Accessed: Aug. 2016]. [Online]. Available: http://www.cars21.com/web/assets/link/PikeResearch-EV-10-predictions.pdf

[29] N. Grid, "Future energy scenarios," [Accessed: Mar. 2017]. [Online]. Available: http://fes.nationalgrid.com/fes-document/

[30] F. Mwasilu, J. J. Justo, E.-K. Kim, T. D. Do, and J.-W. Jung, "Electric vehicles and smart grid interaction: A review on vehicle to grid and renewable energy sources integration," *Renewable and Sustainable Energy Reviews*, vol. 34, pp. 501–516, 2014.

[31] "National electric mobility mission plan 2020," Department of Heavy Industries, Government of India, Tech. Rep., 2012.

[32] E. Yao, V. W. Wong, and R. Schober, "Optimization of aggregate capacity of PEVs for frequency regulation service in day-ahead market," *IEEE Transactions on Smart Grid*, 2016, doi: 10.1109/TSG.2016.2633873.

[33] N. Rotering and M. Ilic, "Optimal charge control of plug-in hybrid electric vehicles in deregulated electricity markets," *IEEE Transactions on Power Systems*, vol. 26, no. 3, pp. 1021–1029, 2011.

[34] S. V. Chakraborty, S. K. Shukla, and J. Thorp, "Evaluating the grid impact of plug-in electric vehicles using dynamic commuting profiles," in *2013 IEEE Grenoble Conference*, June 2013, pp. 1–6.

[35] Y. Wang, W. Saad, Z. Han, H. V. Poor, and T. Başar, "A game-theoretic approach to energy trading in the smart grid," *IEEE Transactions on Smart Grid*, vol. 5, no. 3, pp. 1439–1450, May 2014.

[36] T. Masuta and A. Yokoyama, "Supplementary load frequency control by use of a number of both electric vehicles and heat pump water heaters," *IEEE Transactions on Smart Grid*, vol. 3, no. 3, pp. 1253–1262, 2012.

[37] K. Shimizu, T. Masuta, Y. Ota, and A. Yokoyama, "Load frequency control in power system using vehicle-to-grid system considering the customer convenience of electric vehicles," in *International Conference on Power System Technology (POWERCON)*. IEEE, 2010, pp. 1–8.

[38] M. D. Galus, M. G. Vayá, T. Krause, and G. Andersson, "The role of electric vehicles in smart grids," *Wiley Interdisciplinary Reviews: Energy and Environment*, vol. 2, no. 4, pp. 384–400, 2013.

[39] M. Yilmaz and P. T. Krein, "Review of the impact of vehicle-to-grid technologies on distribution systems and utility interfaces," *IEEE Transactions on Power Electronics*, vol. 28, no. 12, pp. 5673–5689, 2013.

[40] "Global EV outlook 2015," International Energy Agency (IEA), Tech. Rep., 2015, [Accessed: Oct. 2015].

[41] Global EV outlook 2016 Beyond one million electric cars. International Energy Agency. [Accessed: Apr 2017]. [Online]. Available: https://www.iea.org/publications/freepublications/publication/Global_EV_Outlook_2016.pdf

[42] W. Kempton and J. Tomić, "Vehicle-to-grid power fundamentals: Calculating capacity and net revenue," *Journal of Power Sources*, vol. 144, no. 1, pp. 268–279, 2005.

[43] J. Tomic and W. Kempton, "Using fleets of electric-drive vehicles for grid support," *Journal of Power Sources*, vol. 168, no. 2, pp. 459 – 468, 2007.

[44] W. Kempton and J. Tomic, "Vehicle-to-grid power implementation: From stabilizing the grid to supporting large-scale renewable energy," *Journal of Power Sources*, vol. 144, no. 1, pp. 280 – 294, 2005.

[45] H. Ni, "PJM advanced technology pilots for system frequency control," in *2012 IEEE PES Innovative Smart Grid Technologies (ISGT)*, 2012, pp. 1–6.

[46] W. Kempton, V. Udo, K. Huber, K. Komara, S. Letendre, S. Baker, D. Brunner, and N. Pearre, "A test of vehicle-to-grid (V2G) for energy storage and frequency regulation in the PJM system," *Results from an Industry-University Research Partnership*, vol. 32, 2008.

[47] C. Peng, J. Zou, and L. Lian, "Dispatching strategies of electric vehicles participating in frequency regulation on power grid: A review," *Renewable and Sustainable Energy Reviews*, vol. 68, pp. 147–152, 2017.

[48] H. Liu, J. Qi, J. Wang, P. Li, C. Li, and H. Wei, "EV Dispatch Control for Supplementary Frequency Regulation Considering the Expectation of EV Owners," *IEEE Transactions on Smart Grid*, 2016, doi: 10.1109/TSG.2016.2641481s.

[49] Y. Ota, H. Taniguchi, T. Nakajima, K. M. Liyanage, J. Baba, and A. Yokoyama, "Autonomous distributed V2G (vehicle-to-grid) satisfying scheduled charging," *IEEE Transactions on Smart Grid*, vol. 3, no. 1, pp. 559–564, 2012.

[50] S. Kamboj, N. Pearre, W. Kempton, K. Decker, K. Trnka, and C. Kern, "Exploring the formation of electric vehicle coalitions for vehicle-to-grid power regulation," in *AAMAS Workshop on Agent Technologies for Energy Systems*, 2010.

[51] H. Liu, Z. Hu, Y. Song, and J. Lin, "Decentralized vehicle-to-grid control for primary frequency regulation considering charging demands," *IEEE Transactions on Power Systems*, vol. 28, no. 3, pp. 3480–3489, 2013.

[52] E. Yao, V. W. Wong, and R. Schober, "Robust frequency regulation capacity scheduling algorithm for electric vehicles," *IEEE Transactions on Smart Grid*, vol. 8, no. 2, pp. 984–997, 2017.

[53] S. Han, S. Han, and H. Aki, "A practical battery wear model for electric vehicle charging applications," *Applied Energy*, vol. 113, pp. 1100–1108, 2014.

[54] M. Bayat, K. Sheshyekani, and A. Rezazadeh, "A unified framework for participation of responsive end-user devices in voltage and frequency control of the smart grid," *IEEE Transactions on Power Systems*, vol. 30, no. 3, pp. 1369–1379, 2015.

[55] M. Amini and A. Islam, "Allocation of electric vehicles' parking lots in distribution network," in *2014 IEEE PES Innovative Smart Grid Technologies Conference (ISGT)*. IEEE, 2014, pp. 1–5.

[56] S. Hajforoosh, M. A. Masoum, and S. M. Islam, "Real-time charging coordination of plug-in electric vehicles based on hybrid fuzzy discrete particle swarm optimization," *Electric Power Systems Research*, vol. 128, pp. 19–29, 2015.

[57] M. R. Mozafar, M. H. Moradi, and M. H. Amini, "A Simultaneous Approach for Optimal Allocation of Renewable Energy Sources and Electric Vehicle Charging Stations in Smart Grids based on Improved GA-PSO Algorithm," *Sustainable Cities and Society*, 2017, doi: 10.1016/j.scs.2017.05.007.

[58] S. Li, M. Brocanelli, W. Zhang, and X. Wang, "Integrated power management of data centers and electric vehicles for energy and regulation market participation," *IEEE Transactions on Smart Grid*, vol. 5, no. 5, pp. 2283–2294, 2014.

[59] M. Datta and T. Senjyu, "Fuzzy control of distributed PV inverters/energy storage systems/electric vehicles for frequency regulation in a large power system," *IEEE Transactions on Smart Grid*, vol. 4, no. 1, pp. 479–488, 2013.

[60] E. Sortomme and M. El-Sharkawi, "Optimal combined bidding of vehicle-to-grid ancillary services," *IEEE Transactions on Smart Grid*, vol. 3, no. 1, pp. 70–79, 2012.

[61] ——, "Optimal charging strategies for unidirectional vehicle-to-grid," *IEEE Transactions on Smart Grid*, vol. 2, no. 1, pp. 131–138, 2011.

[62] S. Izadkhast, P. Garcia-Gonzalez, and P. Frias, "An aggregate model of plug-in electric vehicles for primary frequency control," 2015.

[63] T. Ma and O. Mohammed, "Real-time plug-in electric vehicles charging control for V2G frequency regulation," in *IEEE 39th Annual Conference of Industrial Electronics Society, IECON*, 2013, pp. 1197–1202.

[64] K. Janfeshan, M. Masoum, and S. Deilami, "V2G application to frequency regulation in a microgrid using decentralized fuzzy controller," in *2014 Proceedings of the 6th International Conference on Modelling, Identification Control (ICMIC)*, Dec. 2014, pp. 361–364.

[65] A. Oudalov, D. Chartouni, and C. Ohler, "Optimizing a battery energy storage system for primary frequency control," *IEEE Transactions on Power Systems*, vol. 22, no. 3, pp. 1259–1266, 2007.

[66] P. Mercier, R. Cherkaoui, and A. Oudalov, "Optimizing a battery energy storage system for frequency control application in an isolated power system," *IEEE Transactions on Power Systems*, vol. 24, no. 3, pp. 1469–1477, 2009.

[67] S. Han, S. Han, and K. Sezaki, "Development of an optimal vehicle-to-grid aggregator for frequency regulation," *IEEE Transactions on Smart Grid*, vol. 1, no. 1, pp. 65–72, Jun. 2010.

[68] C. Wu, H. Mohsenian-Rad, and J. Huang, "Vehicle-to-aggregator interaction game," *IEEE Transactions on Smart Grid*, vol. 3, no. 1, pp. 434–442, Mar. 2012.

[69] J. Pillai and B. Bak-Jensen, "Integration of vehicle-to-grid in the western danish power system," *IEEE Transactions on Sustainable Energy*, vol. 2, no. 1, pp. 12–19, Jan. 2011.

[70] P. Baboli, M. Moghaddam, and F. Fallahi, "Utilizing electric vehicles on primary frequency control in smart power grids," in *International Conference on Petroleum and Sustainable Development*, vol. vol. 26, 2011.

[71] A. Zarogiannis, M. Marinelli, C. Traholt, K. Knezovic, and P. B. Andersen, "A dynamic behaviour analysis on the frequency control capability of electric vehicles," in *IEEE 49th International Universities Power Engineering Conference (UPEC)*, 2014, pp. 1–6.

[72] Y. Mu, J. Wu, J. Ekanayake, N. Jenkins, and H. Jia, "Primary frequency response from electric vehicles in the Great Britain power system," *IEEE Transactions on Smart Grid*, vol. 4, no. 2, pp. 1142–1150, 2013.

[73] H. Yang, C. Chung, and J. Zhao, "Application of plug-in electric vehicles to frequency regulation based on distributed signal acquisition via limited communication," *IEEE Transactions on Power Systems*, vol. 28, no. 2, pp. 1017–1026, May 2013.

[74] H. Liu, Z. Hu, Y. Song, J. Wang, and X. Xie, "Vehicle-to-grid control for supplementary frequency regulation considering charging demands," *IEEE Transactions on Power Systems*, vol. 30, no. 6, pp. 3110–3119, Nov. 2015.

[75] S. Kamboj, W. Kempton, and K. S. Decker, "Deploying power grid-integrated electric vehicles as a multi-agent system," in *10th International Conference on Autonomous Agents and Multiagent Systems*, 2011, pp. 13–20.

[76] S. W. Kim, Y. G. Jin, Y. H. Song, and Y. T. Yoon, "Decentralized vehicle-to-grid design for frequency regulation within price-based operation," *Journal of Electrical Engineering & Technology*, vol. 10, no. 3, pp. 1335–1341, 2015.

[77] G. S. Aujla, R. Chaudhary, N. Kumar, J. Rodrigues, and A. Vinel, "SDN-Based Data Center Energy Management System Using RES and Electric Vehicles," in *2016 IEEE Global Communications Conference (GLOBECOM)*, 2016, pp. 1–6.

[78] G. S. Aujla, M. Singh, N. Kumar, and A. Zomaya, "Stackelberg Game for Energy-aware Resource Allocation to Sustain Data Centers Using RES," *IEEE Transactions on Cloud Computing*, 2017, doi: 10.1109/TCC.2017.2715817.

[79] A. C. L. Hernández, N. L. D. Aldana, M. Graells, J. C. V. Quintero, and J. M. Guerrero, "Mixed-Integer-Linear-Programming-Based Energy Management System for Hybrid PV-Wind-Battery Microgrids: Modeling, Design, and Experimental Verification," *IEEE Transactions on Power Electronics*, vol. 32, no. 4, pp. 2769–2783, 2017.

[80] P. Malysz, S. Sirouspour, and A. Emadi, "An optimal energy storage control strategy for grid-connected microgrids," *IEEE Transactions on Smart Grid*, vol. 5, no. 4, pp. 1785–1796, 2014.

[81] I. Sengor, H. C. Kilickiran, H. Akdemir, B. Kekezoglu, O. Erdinc, and J. P. Catalão, "Energy Management of A Smart Railway Station Considering Regenerative Braking and Stochastic Behaviour of ESS and PV Generation," *IEEE Transactions on Sustainable Energy*, 2017.

[82] L. Yao, J.-Y. Shen, and W. H. Lim, "Real-time energy management optimization for smart household," in *2016 IEEE International Conference on Internet of Things (iThings) and IEEE Green Computing and Communications (GreenCom) and IEEE Cyber, Physical and Social Computing (CPSCom) and IEEE Smart Data (SmartData)*. IEEE, 2016, pp. 20–26.

[83] O. Erdinc, N. G. Paterakis, T. D. Mendes, A. G. Bakirtzis, and J. P. Catalão, "Smart household operation considering bi-directional EV and ESS utilization by real-time pricing-based DR," *IEEE Transactions on Smart Grid*, vol. 6, no. 3, pp. 1281–1291, 2015.

[84] Y. Wang, B. Wang, T. Zhang, H. Nazaripouya, C.-C. Chu, and R. Gadh, "Optimal energy management for Microgrid with stationary and mobile storages," in *Transmission and Distribution Conference and Exposition (T&D), 2016 IEEE/PES*. IEEE, 2016, pp. 1–5.

[85] D. Thomas, C. S. Ioakimidis, V. Klonari, F. Vallée, and O. Deblecker, "Effect of electric vehicles' optimal charging-discharging schedule on a building's electricity cost demand

considering low voltage network constraints," in *2016 IEEE PES Innovative Smart Grid Technologies Conference Europe (ISGT-Europe)*. IEEE, 2016, pp. 1–6.

[86] S. Han and S. Han, "Economic Feasibility of V2G Frequency Regulation in Consideration of Battery Wear," *Energies*, vol. 6, no. 2, pp. 748–765, 2013.

[87] A. Brooks, *Vehicle-to-grid Demonstration Project: Grid Regulation Ancillary Service with a Battery Electric Vehicle*. California Environmental Protection Agency, Air Resources Board, Research Division, Dec. 2002. [Online]. Available: http://www.udel.edu/V2G/docs/V2G-Demo-Brooks-02-R5.pdf

[88] D. Dallinger, D. Krampe, and M. Wietschel, "Vehicle-to-grid regulation reserves based on a dynamic simulation of mobility behavior," *IEEE Transactions on Smart Grid*, vol. 2, no. 2, pp. 302–313, Jun. 2011.

[89] E. Yao, V. W. Wong, and R. Schober, "Optimization of aggregate capacity of PEVs for frequency regulation service in day-ahead market," *IEEE Transactions on Smart Grid*, vol. 9, no. 4, pp. 3519–3529, 2016.

[90] E. Sortomme and M. El-Sharkawi, "Optimal charging strategies for unidirectional vehicle-to-grid," *IEEE Transactions on Smart Grid*, vol. 2, no. 1, pp. 131–138, Mar. 2011.

[91] J. Tan and L. Wang, "Coordinated optimization of PHEVs for frequency regulation capacity bids using hierarchical game," in *IEEE Power & Energy Society General Meeting*, 2015, pp. 1–5.

[92] T. N. Pham, H. Trinh, and L. V. Hien, "Load frequency control of power systems with electric vehicles and diverse transmission links using distributed functional observers," *Smart Grid, IEEE Transactions on*, vol. 7, no. 1, pp. 238–252, 2016.

[93] T. Zhang, W. Chen, Z. Han, and Z. Cao, "Charging scheduling of electric vehicles with local renewable energy under uncertain electric vehicle arrival and grid power price," *IEEE Transactions on Vehicular Technology*, vol. 63, no. 6, pp. 2600–2612, July 2014.

[94] L. Mashayekhy, M. M. Nejad, D. Grosu, Q. Zhang, and W. Shi, "Energy-aware scheduling of mapreduce jobs for big data applications," *IEEE Transactions on Parallel and Distributed systems*, vol. 26, no. 10, pp. 2720–2733, 2015.

[95] C.-T. Chen, L.-J. Hung, S.-Y. Hsieh, R. Buyya, and A. Y. Zomaya, "Heterogeneous job allocation scheduler for hadoop mapreduce using dynamic grouping integrated neighboring search," *IEEE Transactions on Cloud Computing*, 2017.

[96] L. Mashayekhy, M. M. Nejad, D. Grosu, D. Lu, and W. Shi, "Energy-aware scheduling of mapreduce jobs," in *2014 IEEE International Congress on Big Data (BigData Congress)*. IEEE, 2014, pp. 32–39.

[97] Y. Shao, C. Li, W. Dong, and Y. Liu, "Energy-aware dynamic resource allocation on hadoop yarn cluster," in *IEEE 18th International Conference on High Performance Computing and Communications; IEEE 14th International Conference on Smart City; IEEE 2nd International Conference on Data Science and Systems (HPCC/SmartCity/DSS)*. IEEE, 2016, pp. 364–371.

[98] M. Dayarathna, Y. Wen, and R. Fan, "Data center energy consumption modeling: A survey," *IEEE Communications Surveys & Tutorials*, vol. 18, no. 1, pp. 732–794, 2016.

[99] M. I. Green, "Cloud computing and its contribution to climate change," *Greenpeace International*, 2010.

[100] G. Cook, "How clean is your cloud? catalysing an energy revolution," *Greenpeace International*, 2012.

[101] N. Y. I. S. O. (NYISO), "Federal Energy Regulatory Commission, 2010 ISO/RTO Metrics Report Appendix G, 2010," [Accessed: Mar. 2017]. [Online]. Available: http://www.ferc.gov/industries/electric/indus-act/rto/metrics/nyiso-rto-metrics.pdf

[102] A. Mittal, C. Kundu, R. Bose, and R. K. Shevgaonkar, "Entropy based image segmentation for energy efficient lte system with cloud," *Wireless Personal Communications*, vol. 92, no. 3, p. 1145—1162, Feb 2017.

[103] S. Li, M. Brocanelli, W. Zhang, and X. Wang, "Data center power control for frequency regulation," in *2013 IEEE Power and Energy Society General Meeting (PES)*. IEEE, 2013, pp. 1–5.

[104] D. Aikema, R. Simmonds, and H. Zareipour, "Data centres in the ancillary services market," in *IEEE International Green Computing Conference (IGCC)*, 2012, pp. 1–10.

[105] A. Qureshi, R. Weber, H. Balakrishnan, J. Guttag, and B. Maggs, "Cutting the electric bill for internet-scale systems," in *ACM SIGCOMM computer communication review*, vol. 39, no. 4, 2009, pp. 123–134.

[106] M. Ghamkhari and H. Mohsenian-Rad, "Data centers to offer ancillary services," in *IEEE Third International Conference on Smart Grid Communications*, 2012, pp. 436–441.

[107] H. Chen, A. K. Coskun, and M. C. Caramanis, "Real-time power control of data centers for providing regulation service," in *IEEE 52nd Annual Conference on Decision and Control (CDC)*, 2013, pp. 4314–4321.

[108] L. Rao, X. Liu, L. Xie, and W. Liu, "Minimizing electricity cost: Optimization of distributed internet data centers in a multi-electricity-market environment," in *INFOCOM*, Mar. 2010, pp. 1–9.

[109] J. Li, Z. Li, K. Ren, and X. Liu, "Towards optimal electric demand management for internet data centers," *IEEE Transactions on Smart Grid*, vol. 3, no. 1, pp. 183–192, Mar. 2012.

[110] M. Brocanelli, S. Li, X. Wang, and W. Zhang, "Joint management of data centers and electric vehicles for maximized regulation profits," in *IEEE International Green Computing Conference (IGCC)*, 2013, pp. 1–10.

[111] ——, "Maximizing the revenues of data centers in regulation market by coordinating with electric vehicles," *Sustainable Computing: Informatics and Systems*, vol. 6, pp. 26–38, 2015.

[112] S. S. A. AlAnazi, M. Dabbagh, B. Hamdaoui, M. Guizani, and N. Zorba, "Joint Resource Scheduling and Peak Power Shaving for Cloud Data Centers with Distributed Uninterruptible Power Supply," Ph.D. dissertation, 2016.

[113] Energy logic: Reducing data center energy consumption by creating savings that cascade across systems. Emerson Network Power. A White Paper from the Experts in Business-Critical Continuity.

[114] J. Hamilton, "Cooperative expendable micro-slice servers (cems): low cost, low power servers for internet-scale services," in *Conference on Innovative Data Systems Research (CIDR'09)(January 2009)*. Citeseer, 2009.

[115] D. Wang, C. Ren, A. Sivasubramaniam, B. Urgaonkar, and H. Fathy, "Energy storage in datacenters: what, where, and how much?" in *ACM SIGMETRICS Performance Evaluation Review*, vol. 40, no. 1. ACM, 2012, pp. 187–198.

[116] J. Song, X. Liu, Z. Zhu, D. Zhao, and G. Yu, "A novel task scheduling approach for reducing energy consumption of mapreduce cluster," *IETE Technical Review*, vol. 31, no. 1, pp. 65–74, 2014.

[117] M. Zapater, J. L. Risco-Martín, P. Arroba, J. L. Ayala, J. M. Moya, and R. Hermida, "Runtime data center temperature prediction using grammatical evolution techniques," *Applied Soft Computing*, vol. 49, pp. 94–107, 2016.

[118] M. Tatchell-Evans, N. Kapur, J. Summers, H. Thompson, and D. Oldham, "An experimental and theoretical investigation of the extent of bypass air within data centres employing aisle containment, and its impact on power consumption," *Applied Energy*, vol. 186, pp. 457–469, 2017.

[119] M. L. Das, "Privacy and accountability concerns in the age of big data," *Big Data: Storage, Sharing, and Security*, p. 341, 2016.

[120] J. Dean and S. Ghemawat, "Mapreduce: simplified data processing on large clusters," *Communications of the ACM*, vol. 51, no. 1, pp. 107–113, 2008.

[121] T. White, *Hadoop: The definitive guide*. " O'Reilly Media, Inc.", 2012.

[122] D. Cheng, J. Rao, Y. Guo, C. Jiang, and X. Zhou, "Improving performance of heterogeneous mapreduce clusters with adaptive task tuning," *IEEE Transactions on Parallel and Distributed Systems*, vol. 28, no. 3, pp. 774–786, 2017.

[123] B. Moseley, A. Dasgupta, R. Kumar, and T. Sarlós, "On scheduling in map-reduce and flow-shops," in *Proceedings of the twenty-third annual ACM symposium on Parallelism in algorithms and architectures*. ACM, 2011, pp. 289–298.

[124] J. Wolf, D. Rajan, K. Hildrum, R. Khandekar, V. Kumar, S. Parekh, K.-L. Wu, and A. Balmin, "Flex: A slot allocation scheduling optimizer for mapreduce workloads," in *ACM/IFIP/USENIX International Conference on Distributed Systems Platforms and Open Distributed Processing*. Springer, 2010, pp. 1–20.

[125] A. Verma, L. Cherkasova, and R. H. Campbell, "Two sides of a coin: Optimizing the schedule of mapreduce jobs to minimize their makespan and improve cluster performance," in *2012 IEEE 20th International Symposium on Modeling, Analysis and Simulation of Computer and Telecommunication Systems*. IEEE, 2012, pp. 11–18.

[126] R. Nanduri, N. Maheshwari, A. Reddyraja, and V. Varma, "Job aware scheduling algorithm for mapreduce framework," in *2011 IEEE Third International Conference on Cloud Computing Technology and Science (CloudCom)*. IEEE, 2011, pp. 724–729.

[127] Z. Ren, J. Wan, W. Shi, X. Xu, and M. Zhou, "Workload analysis, implications, and optimization on a production hadoop cluster: A case study on taobao," *IEEE Transactions on Services Computing*, vol. 7, no. 2, pp. 307–321, 2014.

[128] H. Chang, M. Kodialam, R. R. Kompella, T. Lakshman, M. Lee, and S. Mukherjee, "Scheduling in mapreduce-like systems for fast completion time," in *2011 Proceedings IEEE INFOCOM*. IEEE, 2011, pp. 3074–3082.

[129] M. Zaharia, A. Konwinski, A. D. Joseph, R. H. Katz, and I. Stoica, "Improving mapreduce performance in heterogeneous environments." in *OSDI*, vol. 8, no. 4, 2008, p. 7.

[130] S. Ibrahim, H. Jin, L. Lu, B. He, G. Antoniu, and S. Wu, "Maestro: Replica-aware map scheduling for mapreduce," in *2012 12th IEEE/ACM International Symposium on Cluster, Cloud and Grid Computing (CCGrid)*. IEEE, 2012, pp. 435–442.

[131] X. Bu, J. Rao, and C.-z. Xu, "Interference and locality-aware task scheduling for mapreduce applications in virtual clusters," in *Proceedings of the 22nd international symposium on High-performance parallel and distributed computing*. ACM, 2013, pp. 227–238.

[132] X. Wang, D. Shen, G. Yu, T. Nie, and Y. Kou, "A throughput driven task scheduler for improving mapreduce performance in job-intensive environments," in *2013 IEEE International Congress on Big Data*. IEEE, 2013, pp. 211–218.

[133] T. Sandholm and K. Lai, "Dynamic proportional share scheduling in hadoop," in *Workshop on Job Scheduling Strategies for Parallel Processing*. Springer, 2010, pp. 110–131.

[134] M. Pastorelli, A. Barbuzzi, D. Carra, M. Dell'Amico, and P. Michiardi, "Hfsp: size-based scheduling for hadoop," in *Big Data, 2013 IEEE International Conference on*. IEEE, 2013, pp. 51–59.

[135] X. Wang, Y. Wang, and Y. Cui, "An energy-aware bi-level optimization model for multi-job scheduling problems under cloud computing," *Soft Computing*, vol. 20, no. 1, pp. 303–317, 2016.

[136] M. Zaharia, D. Borthakur, J. S. Sarma, K. Elmeleegy, S. Shenker, and I. Stoica, "Job scheduling for multi-user mapreduce clusters," *EECS Department, University of California, Berkeley, Tech. Rep. UCB/EECS-2009-55*, 2009.

[137] Í. Goiri, K. Le, T. D. Nguyen, J. Guitart, J. Torres, and R. Bianchini, "GreenHadoop: leveraging green energy in data-processing frameworks," in *Proceedings of the 7th ACM european conference on Computer Systems*. ACM, 2012, pp. 57–70.

[138] J. Leverich and C. Kozyrakis, "On the energy (in) efficiency of hadoop clusters," *ACM SIGOPS Operating Systems Review*, vol. 44, no. 1, pp. 61–65, 2010.

[139] Y. Chen, S. Alspaugh, D. Borthakur, and R. Katz, "Energy efficiency for large-scale mapreduce workloads with significant interactive analysis," in *Proceedings of the 7th ACM european conference on Computer Systems*. ACM, 2012, pp. 43–56.

[140] W. Lang and J. M. Patel, "Energy management for mapreduce clusters," *Proc. VLDB Endow.*, vol. 3, no. 1-2, pp. 129–139, Sep. 2010. [Online]. Available: http://dx.doi.org/10.14778/1920841.1920862

[141] F. R. Yu, P. Zhang, W. Xiao, and P. Choudhury, "Communication systems for grid integration of renewable energy resources," *IEEE Network*, vol. 25, no. 5, pp. 22–29, Sep. 2011.

[142] L. Zhu, F. R. Yu, B. Ning, and T. Tang, "Optimal charging control for plug-in electric vehicles in smart microgrids fueled by renewable energy sources," *International Journal of Green Energy*, vol. 10, no. 9, pp. 924–943, 2013. [Online]. Available: https://doi.org/10.1080/15435075.2012.727364

[143] PJM, "Regulation signal data - june 2014 xls," [Accessed: Mar. 2015]. [Online]. Available: http://www.pjm.com/markets-and-operations/ancillary-services.aspx

[144] ERCOT, "Storage participation in ercot," Texas Energy Storage Alliance, [Accessed: Mar. 2015]. [Online]. Available: http://www.ercot.com

[145] R. Rana, M. Singh, and S. Mishra, "Design of Modified Droop Controller for Frequency Support in Microgrid using Fleet of Electric Vehicles," *IEEE Transactions on Power Systems*, vol. 32, no. 5, pp. 3627 – 3636, 2017.

[146] W. Wang, Y. Xu, and M. Khanna, "A survey on the communication architectures in smart grid," *Computer Networks*, vol. 55, no. 15, pp. 3604–3629, 2011.

[147] V. C. Güngör, D. Sahin, T. Kocak, S. Ergüt, C. Buccella, C. Cecati, and G. P. Hancke, "Smart grid technologies: communication technologies and standards," *IEEE transactions on Industrial Informatics*, vol. 7, no. 4, pp. 529–539, 2011.

[148] S. Bu, F. R. Yu, Y. Cai, and X. P. Liu, "When the smart grid meets energy-efficient communications: Green wireless cellular networks powered by the smart grid," *IEEE Transactions on Wireless Communications*, vol. 11, no. 8, pp. 3014–3024, August 2012.

[149] K. Kaur, R. Rana, N. Kumar, M. Singh, and S. Mishra, "A colored petri net based frequency support scheme using fleet of electric vehicles in smart grid environment," *IEEE Transactions on Power Systems*, vol. 31, no. 6, pp. 4638–4649, 2016.

[150] A. C. L. Hernández, N. L. D. Aldana, M. Graells, J. C. V. Quintero, and J. M. Guerrero, "Mixed-Integer-Linear-Programming Based Energy Management System for Hybrid PV-wind-battery Microgrids: Modelling, Design and Experimental Verification," *IEEE Transactions on Power Electronics*, 2016, doi: 10.1109/TPEL.2016.2581021s.

[151] M. Wright, "The interior-point revolution in optimization: history, recent developments, and lasting consequences," *Bulletin of the American mathematical society*, vol. 42, no. 1, pp. 39–56, 2005.

[152] J. Tan and L. Wang, "Integration of plug-in hybrid electric vehicles into residential distribution grid based on two-layer intelligent optimization," *IEEE Transactions on Smart Grid*, vol. 5, no. 4, pp. 1774–1784, 2014.

[153] H. Fan, L. Jiang, C.-K. Zhang, and C. Mao, "Frequency regulation of multi-area power systems with plug-in electric vehicles considering communication delays," *IET Generation, Transmission & Distribution*, vol. 10, no. 14, pp. 3481–3491, 2016.

[154] J. Tan and Y. Zhang, "Coordinated Control Strategy of a Battery Energy Storage System to Support a Wind Power Plant Providing Multi-Timescale Frequency Ancillary Services," *IEEE Transactions on Sustainable Energy*, 2017, doi: 10.1109/TSTE.2017.2663334.

[155] G. T. . V. (2012-09), "3rd Generation Partnership Project; Technical Specification Group Services and System Aspects; System improvements for Machine-Type Communications (MTC) (Release 11)," Tech. Rep.

[156] M. B. Shahab, A. Hussain, and M. Shoaib, "Smart grid traffic modeling and scheduling using 3gpp lte for efficient communication with reduced ran delays," in *Telecommunications and Signal Processing (TSP), 2013 36th International Conference on*. IEEE, 2013, pp. 263–267.

[157] G. D. Yalcin and N. Erginel, "Determining weights in multi-objective linear programming under fuzziness," in *Proceedings of the World Congress on Engineering*, vol. 2, 2011, pp. 6–8.

[158] X.-q. Li, B. Zhang, and H. Li, "Computing efficient solutions to fuzzy multiple objective linear programming problems," *Fuzzy sets and systems*, vol. 157, no. 10, pp. 1328–1332, 2006.

[159] I. Duggal and B. Venkatesh, "Short-term scheduling of thermal generators and battery storage with depth of discharge-based cost model," *IEEE Transactions on Power Systems*, vol. 30, no. 4, pp. 2110–2118, 2015.

[160] R. S. Zebulum, M. A. Pacheco, and M. M. B. Vellasco, *Evolutionary electronics: automatic design of electronic circuits and systems by genetic algorithms*. CRC press, 2001, vol. 22.

[161] "Mosek," [Accessed: Apr. 2017]. [Online]. Available: https://www.mosek.com/resources/downloads

[162] K. Kaur, M. Singh, and N. Kumar, "Fleet of electric vehicles for frequency support in Smart Grid using 2-layer hierarchical control mechanism," in *2016 IEEE Power and Energy Society General Meeting (PESGM)*, 2016, pp. 1–5.

[163] (2015, Jun.) 2014 annual report on market issues & performance. Department of Market Monitoring. California ISO. [Accessed: Mar. 2017].

[164] G. Ananthanarayanan, A. Ghodsi, S. Shenker, and I. Stoica, "Disk-locality in datacenter computing considered irrelevant." in *HotOS*, vol. 13, 2011, pp. 12–12.

[165] M. S. Gaglani, "A study on transportation problem, transshipment problem, assignment problem and supply chain management," Ph.D. dissertation, Saurashtra University, 2011.

[166] T. Li, Y. Li, and Y. Qian, "Improved hungarian algorithm for assignment problems of serial-parallel systems," *Journal of Systems Engineering and Electronics*, vol. 27, no. 4, pp. 858–870, 2016.

[167] Opencloud hadoop cluster trace : format and schema. Carnegie Mellon University Parallel Data Lab. [Accessed: Jan. 2017]. [Online]. Available: http://ftp.pdl.cmu.edu/pub/datasets/hla/dataset.html